Analysis of Exposure to EMF Time-Dependence in 5G Base Stations Deployment

Bernardo Salgueiro de Almeida Grilo Galego

Thesis to obtain the Master of Science Degree in

Telecommunications and Informatics Engineering

Supervisor: Prof. Luís Manuel de Jesus Sousa Correia

Examination Committee

Chairperson: Prof. Ricardo Jorge Fernandes Chaves

Supervisor: Prof. Luís Manuel de Jesus Sousa Correia

Members of Committee: Prof. Custódio José de Oliveira Peixeiro

Eng. Fernando Manuel dos Santos Sousa

June 2024

I declare that this document is an original work of my own authorship and that it fulfils all the requirements of the Code of Conduct and Good Practices of the Universidade de Lisboa.

To the student in me

Acknowledgements

First and foremost, I would like to express my gratitude and respect to Professor Luís Correia, whose guidance, experience and endless support were crucial in helping me write this work. Without his foresight, much of this thesis would not be as well presented and clear as it is. Thank you for all your wisdom, for pushing me to perfection and for forging me academically.

I would like to give a word of appreciation to my GROW colleagues - Ana, Francisco, José and Pedro - for helping me feel like I was not alone in this confusing forest that is writing a thesis. I probably could have done it without you, but with a lot less laughter along the way.

A thank you to Sofía Patrício, for not only providing a great starting point for this work, but also for accompanying me for several months, patiently answering all my questions and providing useful information.

To Fernando Sousa, from Huawei, for all the necessary information he provided, for the opportunity to have his feedback and good humor on a bi-weekly basis and for facilitating access to base stations in Lisbon. Thank you for all the time dedicated to helping me.

Lastly, I must also thank the many friends that I made along the years in IST - from Tagus, N3E, ISTSat. I feel that college is a place where you grow, both academically and personally, and you certainly made sure of the latter.

”Experience is simply the name we give our mistakes.” - Oscar Wilde

Abstract

This thesis aims to develop a model capable of analysing the behaviour of the electromagnetic field around a 3.6 GHz band 5G active antenna, over time. The model allows for the computation of the transmission power of each individual beam in an active antenna, and from this, making use of established guidelines, it allows for the calculation of the exclusion zone around it. To achieve realistic results, real-life scenarios were created, along with several common mobile services. With the aim of maintaining the realism of the simulation, various sub-models were designed, which realistically and dynamically adjust the antenna's environment to better simulate everyday usage. This thesis was made in collaboration with Huawei, which have relayed real data from base stations using their antennas. Furthermore, in order to compare with the results from the model and with previous work, on-site measurements were performed. The procedure for these, and the discussion of results, both simulated and measured, are presented in this work. This thesis finds a conservative value for the exclusion zone of 6.6 m, which is considered safe in this work's created scenarios.

Keywords

5G, Electromagnetic field, Exclusion zone, Active antennas, 3.6 GHz band

Resumo

Esta tese tem como objetivo o desenvolvimento de um modelo capaz de analisar o comportamento do campo eletromagnético em redor de uma antena ativa 5G na banda dos 3.6 GHz, ao longo do tempo. O modelo permite a computação da potência transmitida por cada lobo numa antena ativa, tornando possível, com o auxílio de procedimentos pré-establecidos, calcular a zona de exclusão. Para alcançar resultados realistas, cenários reais foram criados, juntamente com vários serviços móveis comuns. Com o objetivo de manter o realismo da simulaçáo, vários sub-modelos foram criados, que realisticamente e dinamicamente ajustam o ambiente da antena para melhor simular utilização quotidiana da mesma. Esta tese foi feita em colaboração com a Huawei, que forneceu informação real das estações base que utilizam as suas antenas. Adicionalmente, para comparar com os resultados do modelo e com trabalho prévio, medições foram realizadas em estações base. O procedimento para estas, bem como a discussão de resultados simulados e medidos, são apresentados neste trabalho. Esta tese encontra um valor conservativo da zona de exclusão igual a 6.6 m, que é considerado seguro nos cenários criados neste trabalho.

Palavras-chave

5G, Campo eletromagnético, Zona de exclusão, Antenas ativas, Banda dos 3.6 GHz

Table of contents

Acknowledgements vii

Abstract ix

Resumo x

List of figures xiii

List of tables xv

List of abbreviations xvi

List of symbols xviii

List of software xxi

1 Introduction 1
- 1.1 Overview and motivation . . . 2
- 1.2 Objective and contents . . . 4

2 Fundamental concepts and state of the art 7
- 2.1 Radio interface . . . 8
  - 2.1.1 GSM . . . 8
  - 2.1.2 UMTS . . . 8
  - 2.1.3 LTE . . . 9
  - 2.1.4 NR . . . 10
- 2.2 Services and applications . . . 11
- 2.3 Coverage, capacity and interference . . . 13
- 2.4 Electromagnetic field radiation . . . 15
  - 2.4.1 Antennas in 5G . . . 15
  - 2.4.2 Radiation regions . . . 16
  - 2.4.3 EMF radiation exposure . . . 18
- 2.5 Exclusion zone . . . 21
- 2.6 State of the art . . . 23

3 Model description and assessment 25
- 3.1 Model configuration . . . 26
- 3.2 Scenarios' description . . . 28
  - 3.2.1 Street and bus stop . . . 28
  - 3.2.2 Residential building . . . 31
  - 3.2.3 Demonstration . . . 33
- 3.3 Services description . . . 35
- 3.4 Transmission power . . . 39
- 3.5 Compliance distance and exclusion zone . . . 44
- 3.6 Model assessment . . . 49

4 On-site measurements 53

4.1 On-site measurements procedure . . . 54
4.2 On-site measurements results and discussion . . . 55

5 Model results **59**
5.1 Scenarios' parameters . . . 60
5.2 Beam transmission power over time . . . 62
5.3 Service distribution, number of users and RB usage . . . 63
5.4 Broadside compliance distance over time . . . 67
5.5 Exclusion zone distance . . . 70

6 Conclusions **75**

Annex A - Supplementary equations **79**

Annex B - Download throughput and session duration for mobile streaming services **81**

Annex C - Antennas description **82**
C.1 Huawei AAUxxxx . . . 82
C.2 NOKIA AirScalexxxx . . . 83

Annex D - Description of base stations **84**
D.1 NOS base station . . . 84
D.2 MEO base station . . . 85

References **87**

List of figures

1.1 An active antenna (extracted from [1]). . . . 3
2.1 Services and applications in NR (extracted from [7]). . . . 12
2.2 Key requirements in the three main usage scenarios in NR (extracted from [5]). . . . 12
2.3 Beam configuration depending on the number of antenna elements in the phased-array (extracted from [6]). . . . 16
2.4 MU beamforming with null steering (extracted from [6]). . . . 16
2.5 EMF regions around an antenna (extracted from [30]). . . . 17
2.6 Evolution of the radiation pattern of an antenna with respect to distance (extracted from [30]). . . . 18
2.7 EMF radiation effects on human body [10]. . . . 19
2.8 Steady-state temperature rise reference levels for time-averaged exposures of ≥ 6 min (extracted from [10]). . . . 20
2.9 Generic directional antenna EZ (extracted from [33]). . . . 22
3.1 Model configuration. . . . 26
3.2 Flowchart representation of a run of the developed model. . . . 27
3.3 Plot examples of the UDS (adapted from [39]). . . . 29
3.4 BS vertical sketch in the street and bus stop scenarios. . . . 30
3.5 BS horizontal sketch in the street and bus stop scenarios. . . . 30
3.6 User elevation with respect to the street width, for various values of building height ($h_a = 5.5$ m, $h_{user} = 1.8$ m, $\gamma = -13°$). . . . 31
3.7 Residential building scenario (uniform plane). . . . 32
3.8 BS vertical sketch in the uniform plane scenario. . . . 32
3.9 BS horizontal sketch in the uniform plane scenario. . . . 33
3.10 Demonstration scenario (Gaussian plane). . . . 34
3.11 BS horizontal sketch in the uniform Gaussian scenario. . . . 34
3.12 BS vertical sketch in the uniform Gaussian scenario. . . . 35
3.13 User generation. . . . 37
3.14 Temporal behaviour of the simulation. . . . 38
3.15 Beams' spatial location. . . . 40
3.16 Flowchart representation of the creation of beams. . . . 41
3.17 RB throughput as a function of SNR, for 4x4 MIMO and $\mu = 1$, with average coding rate values. . . . 43
3.18 Flowchart representation of the steps to calculate any user's throughput, required RBs and power from the BS. . . . 45
3.19 Flowchart of the physical layer verifications. . . . 46
3.20 Flowchart representation of the EZ calculation. . . . 48
3.21 System in an over usage situation. . . . 50
3.22 EZ distance with respect to the transmission power, along the direction of maximum gain. 50
3.23 System in a worst case situation. . . . 51
4.1 NOS BS horizontal sketch, along with the measurement points. . . . 54
4.2 MEO BS horizontal sketch, along with the measurement points. . . . 55
4.3 Vertical BS sketch with a straight line across the terrace. . . . 56
4.4 Horizontal BS sketch with straight lines across the terrace. . . . 56
4.5 Measurement point examples. . . . 57
4.6 SSB beams spatial distribution (extracted from [64]). . . . 57

4.7 NOS BS electric field strength over distance. 58
4.8 MEO BS electric field strength over distance. 58
5.1 Beam transmission power over time in the different scenarios. 63
5.2 User received power density over time in the different scenarios. 64
5.3 Power density with respect to distance, with $f_{\phi\psi} = 1$. 65
5.4 Number of real-time services over time in the different scenarios. 65
5.5 Number of non real-time services over time in the different scenarios. 66
5.6 Number of users over time in the different scenarios. 67
5.7 Used RB share over time in the different scenarios. 68
5.8 Broadside compliance distance over time in the different scenarios. 69
5.9 Compliance distance over an entire beam. 70
5.10 PDF of the absolute maximum and maximum average broadside compliance distance in the different scenarios. 71
5.11 CDF of the absolute maximum and maximum average broadside compliance distance in the different scenarios. 72
C.1 Huawei AAUxxxx radiation patterns (extracted from [71]). 83
D.1 NOS BS view of the measured sector (rightmost). 84
D.2 NOS BS view of the rooftop in front of the measured sector. 85
D.3 MEO BS views of the measured sector. 86
D.4 MEO BS view of the rooftop in front of the measured sector. 86

List of tables

2.1 GSM assigned nominal frequency bands in Portugal [1, 15, 16]. 8
2.2 GSM power output limits per BS class and per frequency band [17]. 8
2.3 UMTS assigned nominal frequency bands in Portugal [1, 15, 16]. 9
2.4 UMTS mean power level per carrier per BS class [19]. 9
2.5 LTE assigned nominal frequency bands in Portugal [1, 15, 16]. 9
2.6 LTE mean power level per carrier per BS class [21]. 10
2.7 NR assigned nominal frequency bands in Portugal [1, 25]. 11
2.8 NR rated carrier output power per BS class [24]. 11
2.9 QoS parameters for each described category [1]. 13
2.10 Differences between BS classes [1]. 14
2.11 Steady-state body core temperature rise reference levels for time-averaged exposures of ≥ 30 min (adapted from [10]). 20
2.12 Validity range of each propagation model [33]. 22
3.1 Created mobile services. 36
3.2 Average coding rate for each studied modulation scheme [68]. 42
3.3 Validation tests. 49
5.1 Statistics on the number of active DL UEs in one sector of the BS, over four days [77]. . . 60
5.2 Services' utilisation share in different scenarios. 60
5.3 Default input parameters. 61
5.4 Created scenarios and the real locations they simulate. 61
5.5 Number of runs and run duration in each scenario's simulation. 62
5.6 Minimum and maximum user distance to the Base Station (BS) in each scenario. 64
5.7 Average and standard deviations of the absolute maximum and maximum average broadside compliance distance in the different scenarios, with their relative difference. 70
5.8 Various p-percentile of the obtained maximum average broadside compliance distance CDFs, in the different scenarios. 73
B.1 Required download throughput and average session duration for mobile streaming services. 81
C.1 Huawei AAUxxxx technical specifications [71, 64]. 82
C.2 NOKIA AirScalexxxx technical specifications [72]. 83

List of abbreviations

$\pi/2$**-BPSK**	$\pi/2$ Binary Phase Shift Keying
1024-QAM	1024 Quadrature Amplitude Modulation
16-QAM	16 Quadrature Amplitude Modulation
256-QAM	256 Quadrature Amplitude Modulation
2G	2nd Generation
32-QAM	32 Quadrature Amplitude Modulation
3G	3rd Generation
3GPP	3rd Generation Partnership Project
4-PAM	4 Pulse Amplitude Modulation
4G	4th Generation
5G	5th Generation
64-QAM	64 Quadrature Amplitude Modulation
8-PAM	8 Pulse Amplitude Modulation
8-PSK	8 Phase Shift Keying
AQPSK	Asymmetric Quadrature Phase Shift Keying
AR	Augmented Reality
BPSK	Binary Phase Shift Keying
BS	Base Station
CDF	Cumulative Distribution Function
CDMA	Code Division Multiple Access
CP	Cyclic Prefix
CQI	Channel Quality Indicator
CS	Circuit Switched
DL	Downlink
EDGE	Enhanced Data rates for Global Evolution
EIRP	Equivalent Isotropic Radiated Power
eMBB	Enhanced Mobile Broadband
EMF	Electromagnetic Field
ETSI	European Telecommunications Standards Institute
EZ	Exclusion Zone
FDD	Frequency Division Duplexing
GBR	Guaranteed Bit Rate
GMSK	Gaussian Minimum Shift Keying
GPRS	General Packet Radio Service
GSM	Global System for Mobile Communications
HSCSD	High Speed Circuit Switched Data
HSDPA	High-Speed Download Packet Access
HSUPA	High Speed Uplink Packet Access
ICI	Inter Cell Interference
ICNIRP	International Commission on Non-Ionising Radiation Protection
IEEE	Institute of Electrical and Electronics Engineers
IoT	Internet of Things
IR	Ionising Radiation
LOS	Line of Sight

LTE	Long Term Evolution
LTE-A Pro	Long Term Evolution - Advanced Pro
LTE-A	Long Term Evolution - Advanced
MaMIMO	Massive Multiple Input Multiple Output
MEO	MEO Telecomunicações
MIMO	Multiple Input Multiple Output
MMS	Multimedia Message Service
mMTC	Massive Machine Type Communications
MU	Multi User
nGBR	Non Guaranteed Bit Rate
NLOS	Non Line of Sight
NOS	NOS Telecomunicações
NR	New Radio
NSA	Non-Standalone
OFDMA	Orthogonal Frequency Division Multiple Access
PDF	Probability Distribution Function
PER	Packet Error Loss Ratio
PS	Packet Switched
QoS	Quality of Service
QPSK	Quadrature Phase Shift Keying
RB	Resource Block
RF	Radio Frequency
RX	Reception
SA	Standalone
SAR	Specific Energy Absorption Rate
SC	Subcarrier
SC-FDMA	Single Carrier - Frequency Division Multiple Access
SCS	Subcarrier Spacing
SMS	Short Message Service
SNR	Signal to Noise Ratio
SSB	Synchronisation Signal Block
SSS	Secondary Synchronisation Signal
TDD	Time Division Duplexing
TDMA	Time Division Multiple Access
TRX	Transmitter-receiver
TX	Transmission
UDS	User Distribution Scenario
UE	User Equipment
UL	Uplink
UMTS	Universal Mobile Telecommunications System
uRLLC	Ultra-reliable and Low Latency Communications
V2V	Vehicle to Vehicle
VoIP	Voice over Internet Protocol
VR	Virtual Reality
WHO	World Health Organisation

List of symbols

α_{pd}	Average power decay
δ	Dirac pulse
γ	Elevation tilt
λ	Wavelength
μ	Numerology configuration integer
ϕ	Azimuth angle
ϕ_0	Beam centre azimuth angle
ϕ_{max}	Maximum azimuth angle
ϕ_{user}	Azimuth angle of user
ψ	Elevation angle
ψ_0	Beam centre elevation angle
ψ_{max}	Maximum elevation angle
ψ_{min}	Minimum elevation angle
ψ_{user}^{demo}	Elevation angle of a user in the Gaussian plane scenario
ψ_{user}^{line}	Elevation angle of a user in the line scenarios
ψ_{user}^{uni}	Elevation angle of a user in the uniform plane scenario
ρ_N	Signal to Noise ratio
θ_{3dB}	Circular half power beam width
θ_{3dB}^{h}	Horizontal half power beam width
θ_{3dB}^{v}	Vertical half power beam width
B_W	Bandwidth
c_ϕ	Azimuth coefficient
c_ψ	Elevation coefficient
D	Depth
D_L	Largest dimension of the transmitting area of the antenna
d_{cell}	Base station coverage radius
d_{comp}	Compliance distance
d_{comp}^{abs}	Absolute maximum compliance distance
d_{comp}^{avg}	Maximum average compliance distance
d_{comp}^{beams}	Compliance distance of every beam
d_{comp}^{max}	Maximum compliance distance
d_{ff}	Radius of the radiating near-field region
d	Distance
d_{EZ}	Exclusion zone distance
d_{fp}	Distance to the focal point of the Gaussian waveform
d_{max}	Maximum user distance
d_{max}^{demo}	Maximum user distance in the Gaussian plane scenario
d_{min}^{demo}	Minimum user distance in the Gaussian plane scenario
d_{street}	Street width in the created scenarios
d_{user}	Distance from the antenna to a user
d_{user}^{demo}	Distance from the antenna to a user in the Gaussian plane scenario
d_{user}^{line}	Distance from the antenna to a user in the line scenarios
d_{user}^{uni}	Distance from the antenna to a user in the uniform plane scenario
d_{nf}	Radius of the reactive near-field region

E	Electric field strength
E_{inc}	Incident electric field strength
E_{inc}^{RL}	Reference level of the incident electric field strength
E_{lim}	Electric field strength limit
E_{max}	Maximum electric field strength
f_E	Electric field strength dependence with distance
F	Noise figure
$f_{\phi\psi}$	Normalised antenna rafiation pattern
f	Frequency
f_Δ	Frequency interval
f_{SCS}	Subcarrier spacing frequency
G	Gain
G_{RX}	Receiver antenna gain
G_{TX}	Transmitter antenna gain
G_{TX}^{max}	Maximum transmitter antenna gain
H_{inc}	Incident magnetic field strength
H_{inc}^{RL}	Reference level of the incident magnetic field strength
h	Height
h_a	Antenna's height
h_b	Base station building's height
h_{rb}	Residential building's height
h_{user}	User's height
I	Interference power
L_0	Path loss in free space propagation
L_C	Cable losses between the transmitter and the antenna
L_{max}	Maximum allowed path losses
L_p	Average path losses
L_{ref}	Reference path losses
L_{user}	User absorption losses
M	Modulation order
N	Noise power
N_{ele}	Number of antenna elements
N_{ele}^{beam}	Number of antenna elements in a beam
N_{MIMO}	Massive Input Massive Output order
N_{RB}	Number of resource blocks
N_{RB}^{min}	Minimum number of resource blocks
N_{RB}^{user}	Number of resource blocks per user
N_{SC}^{RB}	Number of subcarriers per resource block
N_{serv}	Number of different telecommunication services
N_{SF}^{frame}	Number of subframes per frame
N_{slot}^{SF}	Number of slots per subframe
N_{symb}^{frame}	Number of symbols per frame
N_{symb}^{slot}	Number of symbols per slot
N_{users}	Number of users
N_{users}^{max}	Maximum number of users
N_{users}^{min}	Minimum number of users
P_{EIRP}	Equivalent isotropic radiated power

P_{ele}	Transmission power per element
P_r^{min}	Minimum accepted power level at the receiver antenna
P_{RX}	Received power
P_{RX}^{max}	Maximum received power
P_{TX}	Transmitter output power
P_{beam}	Power transmitted per beam
P_{beam}^{max}	Maximum transmission power per beam
P_{TX}^{max}	Maximum antenna transmission power
P_{TX}^{min}	Minimum antenna output power
P_{TX}^{lim}	Antenna output power limit to calculate an exclusion zone
P_{SC}	Power transmitted per subcarrier
P_{SC}^{max}	Maximum power transmitted per subcarrier
P_{user}	Power transmitted per user
R_{user}	Required throughput per user
R_{RB}	Throughput per Resource Block
R_{RB}^{QPSK}	Throughput per Resource Block with QPSK modulation
R_{RB}^{16-QAM}	Throughput per Resource Block with 16-QAM modulation
R_{RB}^{64-QAM}	Throughput per Resource Block with 64-QAM modulation
$R_{RB}^{256-QAM}$	Throughput per Resource Block with 256-QAM modulation
R_{RB}^{M-QAM}	Throughput per Resource Block with M-QAM modulation
R_{RB}^{max}	Maximum throughput per Resource Block
R_{TX}	Transmission throughput
S	Power density
S_n	Share of service *n* in a specific scenario
S_{inc}	Incident power density
S_{inc}^{RL}	Reference level of the incident power density
S_{lim}	Power density limit
S_{user}	User’s incident power density
t	Time
t_{sim}	Simulation time
t_{frame}	Frame period
t_{user}	New user period
U_{inc}	Incident energy density
U_{inc}^{RL}	Reference level of the incident energy density
V_M	Maximum voltage
W	Width
w	User spatial probability
Z_0	Free space impedance

List of software

Microsoft Visual Studio Code 1.72.2	Text editor
LaTeX	Document formatting tool
Python 3.11.8	Programming language
SRM-3006 Tools	Program to read measurement data
draw.io	Vectorial drawing program

Chapter 1

Introduction

This chapter provides an overview of the work that is done on the thesis. A brief history of mobile communications is given, followed by a description of the problem under study and the motivation for a solution. At the end of the chapter, the thesis' objective is stated and its contents are presented.

1.1 Overview and motivation

In the early 1980s, the first generation of mobile communications emerged, which used analogue technology and only permitted voice communications [1]. Over the next four decades, four new generations of mobile communications would be developed, each with more capabilities, features and techniques than the previous one. These would be developed to meet the increasing demands of mobile communications, not to solely make voice communications, as in the first generation, but to use a widespread and ever increasing array of technology at the disposal of the public.

In the beginning of the 1990s, the 2nd Generation (2G) technology was launched, and with it, the first digital systems for mobile communications were introduced. For this generation, European Telecommunications Standards Institute (ETSI) developed the Global System for Mobile Communications (GSM) standard which, besides supporting voice communications (as did the first generation), supports other services such as Short Message Service (SMS) and Multimedia Message Service (MMS) [1]. Over time, GSM was further improved upon, and evolved into High Speed Circuit Switched Data (HSCSD), General Packet Radio Service (GPRS) and finally Enhanced Data rates for Global Evolution (EDGE), upgrading the network from a purely Circuit Switched (CS) one to a mixture of CS and Packet Switched (PS), with a maximum throughput of nearly 100 kbps [1]. These improvements laid the foundations for what would become, in the beginning of the 2000s, the 3rd Generation (3G) technology [1, 2].

The early 2000s brought with it the introduction of smartphones, which offered the public widespread access to the internet. As such, 3G technology was built with data communications in mind, allowing for easier and faster mobile internet access from any location in the world. For that reason, 3rd Generation Partnership Project (3GPP) developed Universal Mobile Telecommunications System (UMTS), which would later be improved with High-Speed Download Packet Access (HSDPA) and High Speed Uplink Packet Access (HSUPA), capable of throughputing to a user close to 30 Mbps [1]. Multiple Input Multiple Output (MIMO) was developed in this technology [3], allowing for increased data rates.

The evolution from 3G to the 4th Generation (4G) technology was not like the previous generation evolution. While UMTS was built upon GSM's network, and because of that uses a mixture of CS and PS network, Long Term Evolution (LTE), introduced in 2010, has a purely PS network while still maintaining interoperability with older generations [1, 4]. Along the decade, it was further improved into Long Term Evolution - Advanced (LTE-A) and then into Long Term Evolution - Advanced Pro (LTE-A Pro), with a maximum throughput of around 300 Mbps [1].

During the last decade, mobile data traffic has been exponentially rising due to easier access to user equipment, a growing number of Internet of Things (IoT) devices and an increase in mobile data use cases, among other factors. For this reason, and although 4G will remain competitive for several years, ETSI developed New Radio (NR), the base technology for the 5th Generation (5G) technnology [5]. It allows for massive and near-instantaneous connectivity among humans, among machines, and between humans and machines, as well as providing the means for new use cases and services, which were impossible to accomplish with 4G [6]. In order to build upon LTE's network, 5G is being released in two major steps - the Non-Standalone (NSA) architecture, which adds NR BSs to the LTE-A Pro network, and the Standalone (SA) architecture, which connects the NR BSs to the 5G core network [5]. 5G not only brings about a network change, it also introduces the use of active antennas [6], which unlike passive antennas, employ multiple high-gain focused beams to communicate with users (an active antenna is

shown in Figure 1.1). This allows for much higher data rates than the previous generation, unlocking several new use cases for mobile telecommunications. Active antennas also introduce Massive Multiple Input Multiple Output (MaMIMO) - a higher number of transmitters, further increasing the data rate to a maximum of 10 Gbps, 1 to 2 orders of magnitude greater than LTE. Although in the future 5G will make use of a new band in mobile communications - the millimeter band (above 6 GHz) - early deployment networks will make use of the 700 MHz and 3.6 GHz bands, which are the bands studied in the thesis.

Figure 1.1: An active antenna (extracted from [1]).

Despite all the benefits that 5G offers, concerns have been raised regarding the safety of humans due to the exposure to Electromagnetic Field (EMF) radiation. These concerns are aggravated when it is put into account that NR uses previously unused frequency bands, particularly the millimeter wave band, and the aforementioned new technologies, such as active antennas (with beamforming and MaMIMO). Furthermore, as higher frequencies have shorter range, the NR network will be denser than previous ones, decreasing the distance between the user and the BS, and therefore increasing the chance of human exposure to EMF radiation [8, 9].

To ensure that any user of any mobile communications system is not harmed while doing so, worldwide organisations established entities in charge of defining guidelines to limit exposure to EMF, such as the International Commission on Non-Ionising Radiation Protection (ICNIRP) [10], whose guidelines are followed in this thesis. These guidelines stipulate that there should be a zone surrounding any antenna wherein people should not be present - the Exclusion Zone (EZ), inside which EMF radiation could be harmful to humans. These guidelines must be followed by telecommunications operators.

The radical changes put forward by the introduction of 5G, particularly the introduction of active anten-

nas, put in question the applicability of the regular methods and models used to estimate the EZ of older generation BSs. These assume a constant maximum transmission power and a time-constant radiation pattern [11], which is not adequate when discussing active antennas (because of beamforming and MaMIMO). Therefore, there is a need to develop a model suitable for the estimation of the EZ around 5G NR antennas, otherwise a BS deployment can be overly restricted (possibly lowering performance) or not restricted enough (possibly harming users). This thesis proposes a statistical approach when defining the EZ of a BS, based on user behaviour and time-dependent parameters.

1.2 Objective and contents

This thesis was developed in collaboration with Huawei [12], and its aim is to develop a model capable of simulating EMF in the vicinity of 3.6 GHz band 5G active antennas BS deployments and determine their EZ, for various realistic scenarios. For this, realistic telecommunication services and realistic spatial user distributions were created, and an analysis of their usage of the 5G BS was performed in order to define the EZ. As an additional objective, this thesis also checks if the results obtained in [13] are realistic, using on-site measurements on BSs around Lisbon.

This thesis is composed of 6 chapters including the present one. Furthermore, annexes containing additional information and all references made throughout the thesis can be found at the end of the document.

Chapter 2 contains the fundamental concepts required to develop the model, from the radio interface to the services and applications that are used in 5G; from a discussion on active antennas to a theoretical description of EMF around the BS. The guidelines established by ICNIRP are presented, as well as the methods that define compliance. Besides this, the chapter explores current methods and models to estimate an EZ and a discussion on the current state of the art, containing relevant published works related to the topic of this thesis.

Chapter 3 presents the developed model, defining its inputs, sub-models and required outputs. Realistic scenarios with realistic user distributions are created and throughouly detailed. In addition to this, realistic mobile communications services are created and defined. The model's inner workings, such as user generation, its temporal behaviour, the calculation of the transmission power and the estimation of the EZ, are presented and explored. At the end of the chapter, the model goes through some assessment tests to validate its results.

In Chapter 4, on-site measurements, along with their procedure, are shown. These were performed in order to compare with the results from the developed model and to compare with the work done in [13]. The visited BSs are described, as are the studied antennas. A discussion on the obtained results is performed in this chapter.

In Chapter 5, each created scenario is assigned a real location in Lisbon, and they are described in terms of input parameters for the model. In order to further differentiate the scenarios, each of them presents a different services' utilisation share. This chapter also presents and discusses the results obtained with the model for the different scenarios, from beam transmission power over time to the

service distribution among users. At the end of this chapter, the value of the EZ in each scenario is estimated and considerations about its value are done.

Lastly, Chapter 6 presents a summary of the thesis, along with the final conclusions taken from it, and showcases some suggestions that could be looked into in future work.

At the end of the main body of the thesis, a set of annexes are presented. Annex A contains some supplementary equations that are referenced throughout the main body of the thesis, Annex B presents a table with the average download size and required download throughput of some mobile communications services, Annex C displays the technical specifications of the studied antennas and Annex D showcases a physical description of the BSs wherein the measurements were conducted.

Chapter 2

Fundamental concepts and state of the art

This chapter provides the fundamental concepts required to develop the model. It presents a technical description of all generations of telecommunications, along with the current radio interface state in Portugal. It explores possible services and applications for 5G, together with key parameters for its BSs deployment and a brief comparison between passive and active antennas. This chapter also presents and explains the limits and guidelines set by ICNIRP with regard to EMF radiation exposure, while also discussing the concept of an exclusion zone. In the end of the chapter, the current state of the art is presented.

2.1 Radio interface

This section explores the radio interface of GSM, UMTS, LTE and NR, analysing the employed frequency bands for each techonology as well as discussing its multiple access techniques, duplexing modes and BS maximum output power.

2.1.1 GSM

Regarding multiple access techniques, GSM employs Time Division Multiple Access (TDMA) with Frequency Division Duplexing (FDD) for the duplexing scheme [2]. The modulation technique used by GSM can be Gaussian Minimum Shift Keying (GMSK) or 8 Phase Shift Keying (8-PSK) [14]. The assigned nominal frequency bands in Portugal for GSM are shown in Table 2.1, where each Radio Frequency (RF) channel is spaced by 200 kHz [2].

Table 2.1: GSM assigned nominal frequency bands in Portugal [1, 15, 16].

Frequency band [MHz]	Uplink frequency [MHz]	Downlink frequency [MHz]	Total frequency bandwidth [MHz]
900	[885, 915]	[930, 960]	60
1800	[1710, 1770]	[1805, 1865]	120

According to [17], GSM BSs can be divided into three classes: Normal BS, Micro BS and Pico BS. Power classes are attributed to each BS class, limiting their maximum and minimum output power. These limits, per BS class and per frequency band, are shown in Table 2.2.

Table 2.2: GSM power output limits per BS class and per frequency band [17].

Frequency band [MHz]	Normal BS power output [dBm]	Micro BS power output [dBm]	Pico BS power output [dBm]
900	[33.98, 58.06]	[9, 24]	[13, 20]
1800	[33.98, 46.02]	[17, 32]	[16, 23]

2.1.2 UMTS

The 3G technology, UMTS, uses Code Division Multiple Access (CDMA) as a multiple access technique and FDD as the duplexing method. CDMA allows multiple users to simultaneously share the same channel with the use of coding schemes. While in Downlink (DL), 3G technology employs Quadrature Phase Shift Keying (QPSK), 16 Quadrature Amplitude Modulation (16-QAM) or 64 Quadrature Amplitude Modulation (64-QAM), in Uplink (UL) it makes use of Binary Phase Shift Keying (BPSK), 4 Pulse Amplitude Modulation (4-PAM) or 8 Pulse Amplitude Modulation (8-PAM) [18].

The assigned nominal frequency bands in Portugal for UMTS are shown in Table 2.3, where each RF

channel is spaced by 5 MHz [3].

Table 2.3: UMTS assigned nominal frequency bands in Portugal [1, 15, 16].

Frequency band [MHz]	Uplink frequency [MHz]	Downlink frequency [MHz]	Total frequency bandwidth [MHz]
900	[885, 915]	[930, 960]	60
1800	[1710, 1770]	[1805, 1865]	120
2100	[1920, 1980]	[2110, 2170]	120

The mean power level per carrier per BS class is shown in Table 2.4 (BS classes are further discussed in Section 2.3). Note that there is no value for Macro Cell power output - this is because there is no upper limit required for its rated output power. In normal conditions, all values present in Table 2.4 can fluctuate but remain within an interval from -2 dB to 2 dB from the shown value [19].

Table 2.4: UMTS mean power level per carrier per BS class [19].

Macro cell power output [dBm]	Micro cell power output [dBm]	Pico cell power output [dBm]	Femto cell power output [dBm]	
			With MIMO	Without MIMO
-	38	24	17	20

2.1.3 LTE

Unlike previous generations, LTE does not use the same multiple access technique in both UL and DL. For DL, it makes use of Orthogonal Frequency Division Multiple Access (OFDMA), while in UL it uses Single Carrier - Frequency Division Multiple Access (SC-FDMA). This distinction is necessary because SC-FDMA has a lower peak-to-average power ratio than OFDMA, which improves the efficiency of the transmission and decreases power consumption in end devices [4].

LTE can use BPSK, QPSK, 16-QAM, 64-QAM, 256 Quadrature Amplitude Modulation (256-QAM) or 1024 Quadrature Amplitude Modulation (1024-QAM) [20]. The duplexing method is again FDD. The assigned nominal frequency bands in Portugal for LTE are shown in Table 2.5.

Table 2.5: LTE assigned nominal frequency bands in Portugal [1, 15, 16].

Frequency band [MHz]	Uplink frequency [MHz]	Downlink frequency [MHz]	Total frequency bandwidth [MHz]
800	[832, 862]	[791, 821]	60
2600	[2510, 2570]	[2630, 2690]	120

To allow multiple users to access the available bandwidth, each user is allocated a set of orthogonal Subcarriers (SCs) with a fixed Subcarrier Spacing (SCS) between them (in the case of LTE with a normal

Cyclic Prefix (CP), that spacing is 15 kHz), called a Resource Block (RB). A single RB consists of 12 SCs in the frequency domain and 7 symbols in the time domain (in normal CP configuration) [20].

While UMTS used a fixed channel bandwidth of 5 MHz, LTE allows for 6 different channel bandwidths ([1.4, 3, 5, 10, 15, 20] MHz), which allows for flexible bandwidth allocation depending on the number of users and the services they are using (each different channel bandwidth allocates a different number of RBs to each user) [4].

The mean power level per carrier per BS class is shown in Table 2.6. Note that there is no value for a Macro Cell - this is because there is no upper limit required for its rated output power. In normal conditions, all values present in Table 2.6 can fluctuate but remain within an interval from -2 dB to 2 dB from the shown value [21].

Table 2.6: LTE mean power level per carrier per BS class [21].

Macro cell power output [dBm]	Micro cell power output [dBm]	Pico cell power output [dBm]	Femto cell power output [dBm]	
			With MIMO	Without MIMO
-	38	24	17	20

2.1.4 NR

This technology uses the same DL multiple access technique that LTE uses: OFDMA. However, for UL, while LTE makes the sole use of SC-FDMA, NR can use both SC-FDMA and OFDMA [22]. Contrary to 4G, NR supports a variable SCS which is given by

$$f_{SCS\,[\text{kHz}]} = 15 \cdot 2^{\mu}, \tag{2.1}$$

where μ is the numerology configuration integer, ranging from 0 to 6. In NR, again contrary to 4G, a RB is expressed only in the frequency domain, being composed of 12 consecutive SCs, independently of the SCS [23].

In addition to all modulation schemes that LTE supports, NR can use $\pi/2$ Binary Phase Shift Keying ($\pi/2$-BPSK) (only in UL and only if transform precoding is enabled in the transmitter) [23]. The assigned nominal frequency bands in Portugal for NR are shown in Table 2.7. Note that the 3.6 GHz band makes no distinction between DL and UL - this is because this band uses Time Division Duplexing (TDD) as a duplexing method, and as such, does not require a paired band. For the 700 MHz band, the duplexing method is again FDD [1].

The rated carrier output power per BS class is shown in Table 2.8. In normal conditions, all values present in Table 2.8 can fluctuate but remain within an interval from -2 dB to 2 dB from the shown value. Note that there is no value for a Macro Cell - this is because there is no upper limit required for its rated output power. Femto Cells are not used in the technology [24].

Table 2.7: NR assigned nominal frequency bands in Portugal [1, 25].

Frequency band [MHz]	Uplink frequency [MHz]	Downlink frequency [MHz]	Total frequency bandwidth [MHz]
700	[703, 733]	[758, 788]	60
3600	[3400, 3800]		400

Table 2.8: NR rated carrier output power per BS class [24].

Macro cell power output [dBm]	Micro cell power output [dBm]	Pico cell power output [dBm]
-	38	24

2.2 Services and applications

The goal of this section is to identify and explore the main services and applications in NR. This technology allows for new services and use cases, which can be classified into three main usage scenarios [7]:

- **Enhanced Mobile Broadband (eMBB)** - Mobile broadband addresses the human-centric use cases for access to services and data. eMBB is an upgrade to the 4G network that provides higher data rates, higher user mobility and higher traffic capacity. eMBB allows mobile broadband to be enabled in moving vehicles, allowing for a seamless user experience, and allows it to be enabled in areas with high user density. This in turn enables new applications such as real-time interactions and seamless Augmented Reality (AR) / Virtual Reality (VR) experience.
- **Ultra-reliable and Low Latency Communications (uRLLC)** - This scenario is characterised by stringent requirements for throughput, latency and availability, for it enables time-sensitive applications such as autonomous driving (Vehicle to Vehicle (V2V) communication), factory automation and remote robotic medical surgeries.
- **Massive Machine Type Communications (mMTC)** - This usage scenario is characterised by a very large number of interconnected devices over a network, with little to no human interaction. These devices typically transmit small volumes of data and usually have a long battery lifespan. This includes IoT services such as smart cities or smart homes.

These use cases are displayed in Figure 2.1. As additional use cases are sure to emerge in the near future, the technology must have flexibility to adapt. Figure 2.2 maps the key requirements in each discussed usage scenario. It can be seen that while eMBB presents a vast array of requirements, uRLLC and mMTC present more specific needs.

In order to measure the overall performance of a particular service, Quality of Service (QoS) parameters can be quantified, and Table 2.9 describes the mentioned services in terms of these. Four service categories are defined for previous technologies, and NR still supports them [1]:

- **Conversational services** - Real-time voice service between two or more humans (for example, Voice over Internet Protocol (VoIP)). They are very time-sensitive due to human perception.
- **Streaming services** - Unidirectional real-time data service (for example, video streaming). Also time-sensitive, though not as much as conversational services.

- **Interactive services** - These are characterised by requested bidirectional data flow, usually between a human and a machine. These can be time continuous or not (for example, web browsing).
- **Background services** - These are the least time-sensitive services, for they are characterised by unrequested bidirectional data flow, usually between two machines (for example, reception of e-mails).

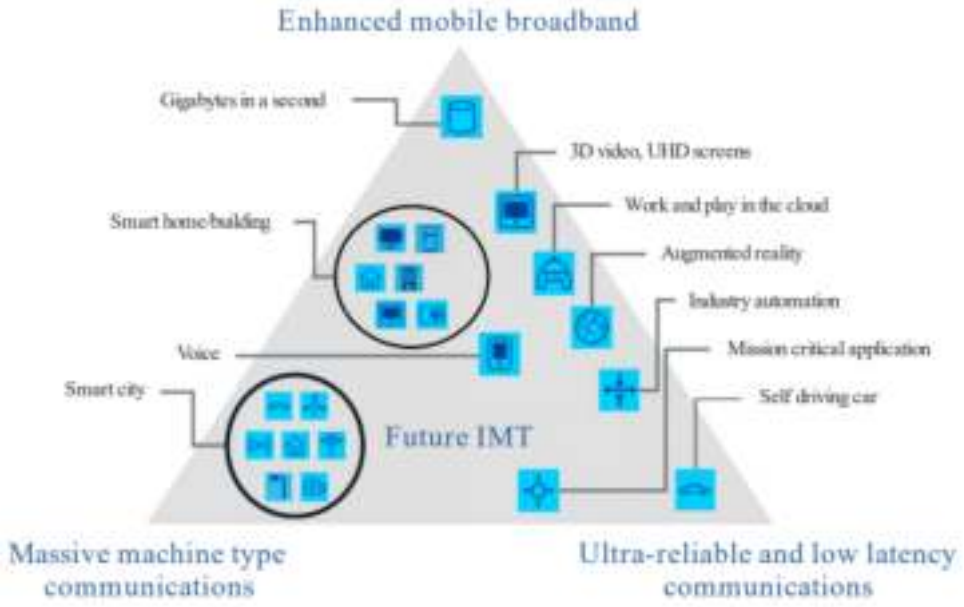

Figure 2.1: Services and applications in NR (extracted from [7]).

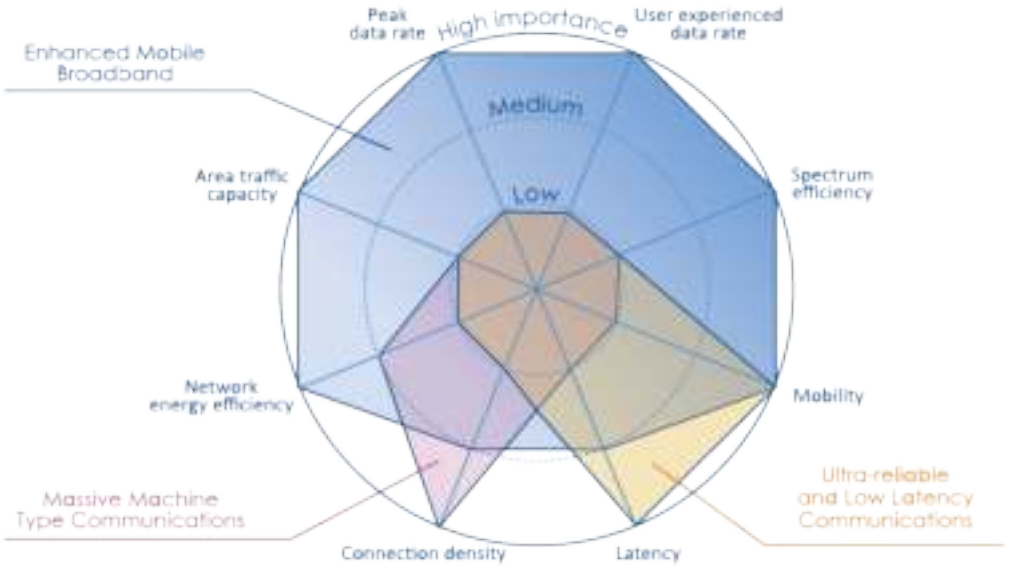

Figure 2.2: Key requirements in the three main usage scenarios in NR (extracted from [5]).

Table 2.9: QoS parameters for each described category [1].

Parameter	Service category			
	Conversational	Streaming	Interactive	Background
Real-time	Yes	Yes	No	No
Symmetric	Yes	No	No	No
Guaranteed rate	Yes	Yes	No	No
Delay	Minimum / Fixed	Minimum / Variable	Moderate / Variable	High / Variable
Buffer	No	Yes	Yes	Yes
Bursty	No	No	Yes	Yes

Furthermore, both LTE and NR define several priority classes [1]. Each is defined by a unique Channel Quality Indicator (CQI), which is a measure sent from the User Equipment (UE) to the network, quantifying the channel's quality. It states the maximum expected delay and the Packet Error Loss Ratio (PER) of the channel. Each priority class can be assigned a Guaranteed Bit Rate (GBR) or a Non Guaranteed Bit Rate (nGBR) bearer, depending on its QoS parameters.

2.3 Coverage, capacity and interference

This section addresses the coverage and capacity of a BS, as well as the interference caused by the surrounding environment and other BSs. These three concepts are the main ones to consider when planning a BS deployment.

The coverage of a BS can be defined as the geographical area wherein it can communicate with users. Assuming an antenna with an omnidirectional radiation pattern in the azimuthal plane, the coverage of a BS (in the same plane) is approximately a circle. As per [1], its radius, for a given minimum power level at the receiver, is given by, using (A.1) and (A.2),

$$d_{cell\,[\text{km}]} = 10^{\frac{P_{EIRP}\,[\text{dBm}] - P_r^{min}\,[\text{dBm}] + G_{RX}\,[\text{dBi}] - L_{ref}\,[\text{dB}]}{10\alpha_{pd}}}, \tag{2.2}$$

where

- P_{EIRP} is the Equivalent Isotropic Radiated Power (EIRP) of the transmitter antenna, given by (A.3);
- P_r^{min} is the minimum power level at the receiver antenna;
- G_{RX} is the gain of the receiving antenna;
- L_{ref} are the reference path losses (propagation model dependent);
- α_{pd} is the average power decay (propagation model dependent).

As is stated in Section 2.1, there are four types of BS classes considered from UMTS forwards. From [1], the main differences between these can be found in Table 2.10.

Table 2.10: Differences between BS classes [1].

BS class	Cell type		Cell radius [km]	P_{EIRP}[dBm]	Example of location
Wide area BS	Macro	Large	> 3	[45, 60]	Top of building
		Small	[1, 3]	[40, 50]	
Medium range BS	Micro		[0.1, 1.0]	[30, 45]	Mall
Local area BS	Pico		< 0.1	[22, 33]	Office
Home BS	Femto		< 0.05	[0, 25]	Home

The capacity of a BS is defined as the number of users that it can serve with a given QoS (with a given minimum bit rate). By combining (A.4), (A.5) and (A.6), it is possible to write that the number of users that can all be served with the same bit rate is given by

$$N_{users} = \left\lfloor \frac{N_{RB} N_{SC}^{RB} N_{symb}^{frame} N_{MIMO} \log_2 (M)_{[\text{bit}]}}{R_{user[\text{bit}\cdot\text{s}^{-1}]} t_{frame[\text{s}]}} \right\rfloor, \tag{2.3}$$

where

- N_{RB} is the number of available RBs;
- N_{SC}^{RB} is the number of SCs per RB (always 12);
- N_{symb}^{frame} is the number of symbols per OFDMA frame (numerology dependent);
- N_{MIMO} is the MIMO order;
- M is the modulation order;
- t_{frame} is the OFDMA frame period (always 10 ms);
- R_{user} is the bit rate per user.

The propagation of the signal from transmitter to receiver degrades the signal quality due to two main factors: attenuation and interference. While attenuation comes from the environment in which the signal propagates and reduces the received signal power, interference comes from other BSs and is responsible for signal distortion, hampering capacity and limiting coverage [26]. Two different interference sources are considered: co-channel interference, which is generated by equipment using the same frequency band, and adjacent channel interference, which is generated by equipment using frequency bands adjacent to the signal frequency [26].

Network operators split up their entire coverage area into several smaller regions (cells), each covered by a different BS. Operators allocate different frequency bands to adjacent cells so that adjacent channel interference is close to zero. In this way, cells can be grouped together in a cluster. Although this frequency distribution lowers Inter Cell Interference (ICI), it does not eliminate it. This problem aggravates near each cell's edge, where the received signal power is at its lowest and interference at its highest. Interference can be reduced by downtilting the BS antenna, using power control and optimising BS deployment sites.

As the noise power and the adjacent channel interference are usually orders of magnitude lower than co-channel interference, they are assumed to be 0. Interference can then be expressed as the division

between the power received from the expected BS over the power received from all other BSs [27],

$$I_{i,j[\text{dB}]} = 10\log_{10}\left[\frac{P_{TX,i[\text{W}]}G_{RX}G_{TX,i}\left(\frac{\lambda_{i[\text{m}]}}{4\pi}\right)^2 d_{i[\text{m}]}^{-\alpha_{pd}}}{\sum_{j=1}^{N} P_{TX,j[\text{W}]}G_{RX}G_{TX,j}\left(\frac{\lambda_{j[\text{m}]}}{4\pi}\right)^2 d_{j[\text{m}]}^{-\alpha_{pd}}}\right], j \neq i, \tag{2.4}$$

where

- N is the number of BSs;
- i is the BS from which the expected transmission comes;
- j represents all other BSs;
- P_{TX} is the transmitter output power;
- G_{TX} is the transmitter antenna gain;
- λ is the received transmission wavelength;
- d is the distance from the transmitter to the receiver.

2.4 Electromagnetic field radiation

This section addresses EMF behaviour around antennas and presents international safety recommendations in regard to its exposure levels. It also presents active antennas which are used in 5G and compares them to passive antennas.

2.4.1 Antennas in 5G

Antennas can be divided into two distinct groups: passive antennas and active antennas, with the main difference between them being that active antennas have the capability to enable scenario-specific beam management, radiating a focused beam on a UE, while passive antennas have a fixed beam pattern, statically radiating energy to a large area. Up until LTE, only passive antennas were used in mobile networks. From 5G onwards, active antennas are being used because 5G services have higher requirements in terms of data rates, precise coverage, spectral and power efficiency (among others) [6]. UMTS introduced MIMO technology, which uses multiple transmitters in the transmitting and/or receiving antenna, exploiting spacial diversity and multiplexing to improve data rates [28]. NR further improves this technology with MaMIMO, using more transmitters per antenna [29]. With the use of active antennas, NR also introduces beamforming and beamsteering [6]. Active antennas can generate narrow beams (beamforming) with varied directivity (beamsteering), as shown in Figure 2.3. Active antennas are merely phased-array antennas, used to concentrate beam energy on desired coverage areas and minimise interference to non-desired coverage areas, resulting in a more efficient transmission than passive antennas [6].

To maximise time and spectral efficiency, Multi User (MU) beamforming is used, which allows a BS to aim multiple beams simultaneously, increasing each user's received power compared to passive antennas [6]. This requires accurate null-steering control on antennas to suppress the interference caused by resource sharing, as shown in Figure 2.4.

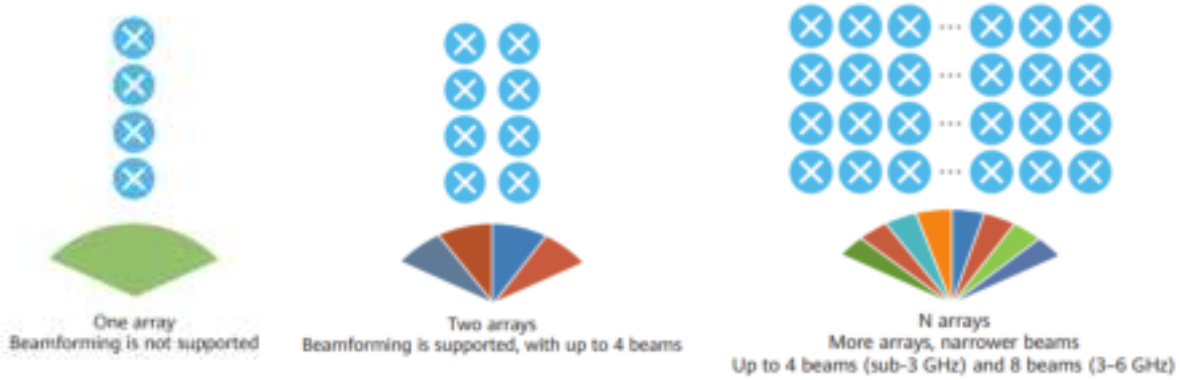

(a) One array. (b) Two arrays. (c) N arrays.

Figure 2.3: Beam configuration depending on the number of antenna elements in the phased-array (extracted from [6]).

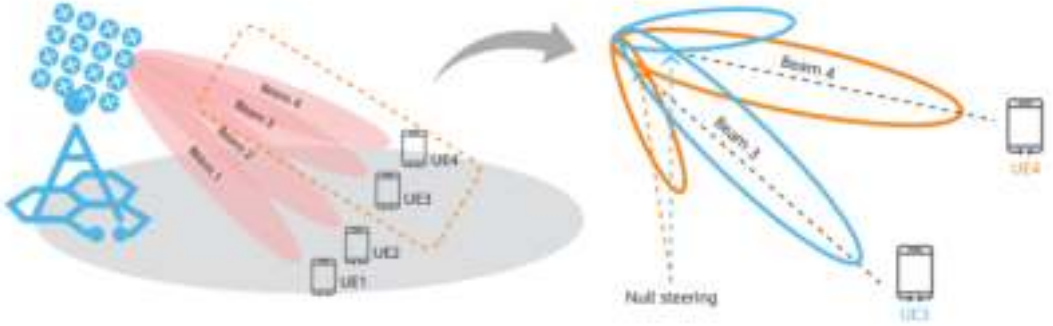

Figure 2.4: MU beamforming with null steering (extracted from [6]).

2.4.2 Radiation regions

The EMF around an antenna has a complex and non-homogenous behaviour. It is divided into three regions, represented in Figure 2.5: reactive near-field, radiating near-field (Fresnel region) and far-field (Fraunhofer region) [30]. No abrupt changes are noted as the boundaries between these regions is crossed, but there are distinct differences among them.

The reactive near-field region is defined as the region immediately surrounding the antenna from which the EMF is radiated. In this region, there is a reactive component to the EMF (mainly the antenna itself), and so the angular field distribution is not known. This implies that there is no way of calculating the relationship between the electric and magnetic fields in this region. From [30], it can be stated that the limit of this region is given by

$$d_{nf\,[\mathrm{m}]} = \begin{cases} 0.62\sqrt{\dfrac{D_{L\,[\mathrm{m}]}^{3}}{\lambda_{[\mathrm{m}]}}} & , D_{L\,[\mathrm{m}]} >> \lambda_{[\mathrm{m}]} \\ \dfrac{\lambda_{[\mathrm{m}]}}{2\pi} & , \text{o.w.} \end{cases}, \tag{2.5}$$

where

- D_L is the largest dimension of the transmitting area of the antenna;
- λ is the wavelength of the transmission signal.

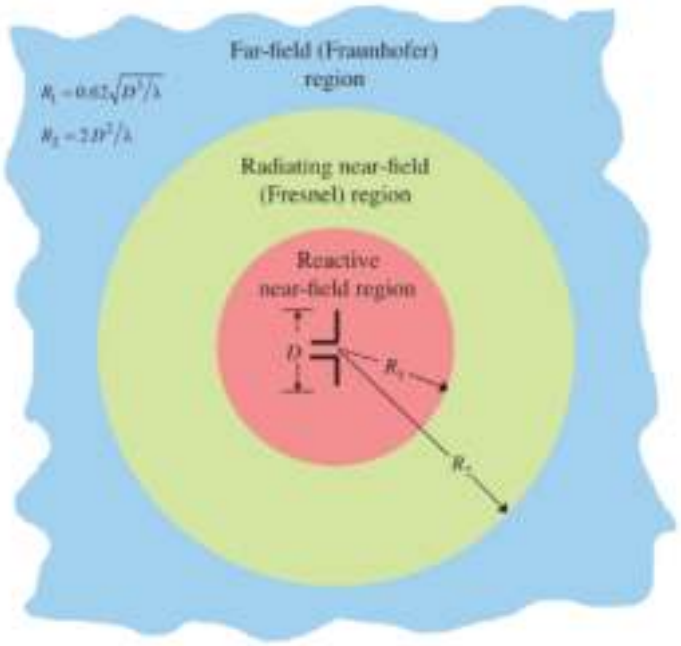

Figure 2.5: EMF regions around an antenna (extracted from [30]).

The radiating near-field region is defined as the region between the reactive near-field region and the far-field region. Here, a reactive component to the EMF may no longer exist (depends on the BS), so the electric and magnetic fields are not necessarily in phase. For antennas where $D_L < 0.086\lambda$, this field does not exist. Its upper limit, according to [30], can be defined by

$$d_{ff[\mathrm{m}]} = 2\frac{D_{L[\mathrm{m}]}^2}{\lambda_{[\mathrm{m}]}}. \tag{2.6}$$

In the far-field region there are no reactive components to the EMF, and the angular field distribution is known; it can be approximated as a spherical wave-front. The electric and magnetic fields are in phase, perpendicular to each other and to the direction of propagation, which extends to infinity [30].

As the observation distance increases from the reactive near-field region up to the far-field region, the radiation pattern of an antenna changes in shape because of the variation in both magnitude and phase of the fields. In the reactive near-field region, the radiation pattern is spread out and nearly uniform because of the reactive component, whereas in the radiating near-field region the pattern begins to form lobes. Finally, in the far-field region, the radiation pattern has its major and minor lobes well-defined [30], as can be seen in Figure 2.6.

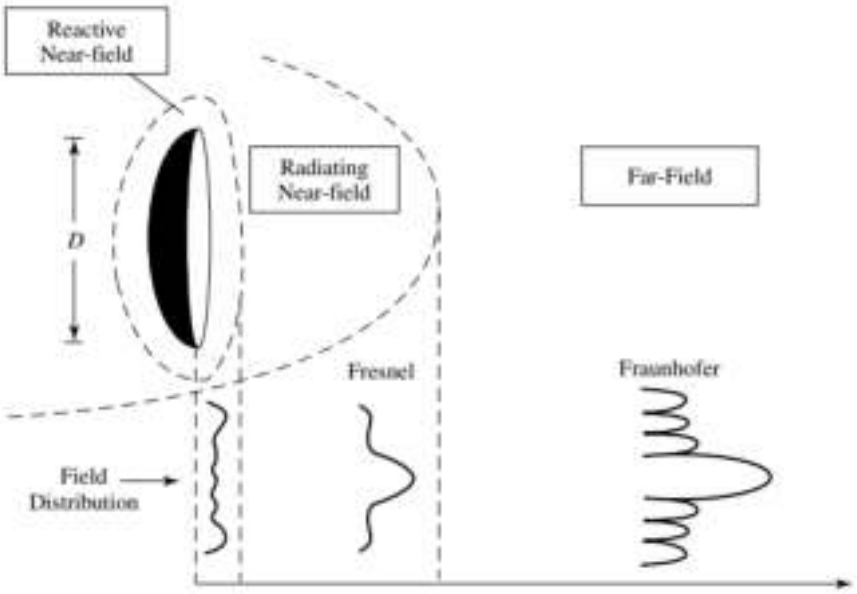

Figure 2.6: Evolution of the radiation pattern of an antenna with respect to distance (extracted from [30]).

2.4.3 EMF radiation exposure

With advancements in technology came an increasing concern about the health effects that exposure to EMF radiation can have on organic matter - more specifically, the human body. Although a lot of studies have been conducted in this area, experimental studies lack the ability to be compared to realistic EMF exposure environments. Besides, research on the subject is mostly observational and thus, depending on the type of study, can be victim to various types of errors and bias [10].

To tackle these concerns, several organisations have established committees (such as the World Health Organisation (WHO)'s International EMF Project [31]) and defined exposure limits and guidelines (such as Institute of Electrical and Electronics Engineers (IEEE) [32] and ICNIRP [10]). Throughout this thesis, the guidelines set by ICNIRP are adopted as EMF radiation exposure limits. These guidelines are limited in scope from 100 kHz to 300 GHz but as mobile telecommunications do not employ frequencies below the lower or above the upper limits, the document is apt to be a reference for this thesis. All information presented in this section is based on [10].

Although radiofrequency EMF radiation is not Ionising Radiation (IR), it can still affect the human body via three effects: nerve stimulation, changes in the permeability of membranes and temperature rise, as is broken down in Figure 2.7.

Exposure to an EMF can induce electric fields within the body, which in turn can stimulate nerves. This stimulation is typically reported as a ”tingling” sensation, not a hurting one. As this is not concerning to human health, and as evidence from neural behaviour research is not sufficiently reliable, exposure limits are not set with nerve stimulation in mind. This effect only happens with frequencies until around 10 MHz, after which heating effects predominate and nerve stimulation decreases.

EMF exposure may also cause cell membranes to become permeable, which in turn can lead to other

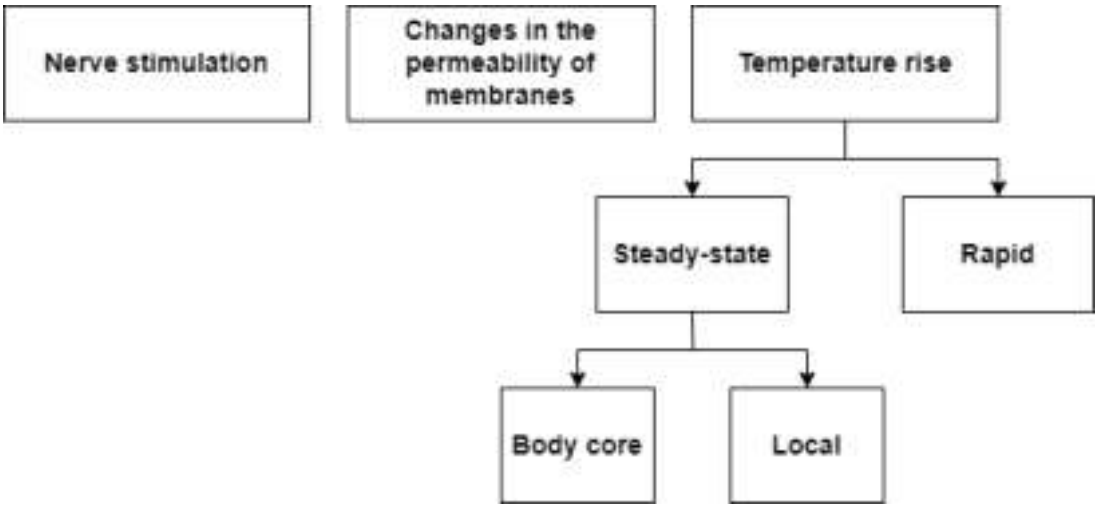

Figure 2.7: EMF radiation effects on human body [10].

undesirable cellular changes. However, this effect only occurs with radiation levels far exceeding the thresholds set for the third effect: temperature rise. As such, there is no need to set restrictions against changes in the permeability of membranes, as the restrictions set to protect against temperature rise already protect against this effect.

The main component of an EMF that affects the human body is the electric field. It interacts with polar molecules, electrons and ions on the human body, generating heat and causing temperature rise. Biological damage occurs when the level of heating exceeds the body's capacity to dissipate excessive energy.

To be able to set restrictions, it is necessary to know how much of the EMF's power is absorbed by biological tissues. The guidelines defined by ICNIRP differentiate temperature rise between steady-state temperature rise (which in turn is subdivided into body core and local temperature), where temperature increases at a slow rate, allowing heat to dissipate over a larger mass, and rapid temperature rise, where there may not be sufficient time for heat to dissipate, resulting in larger temperature rises in small regions of mass. As this thesis is focused on studying the EMF radiation transmited by BSs, rapid temperature rise is not discussed, as the transmissions from these do not present a heterogeneous temperature distribution over tissue mass.

Body core temperature rise due to EMF exposure results in harm only when the increase in temperature is higher than $1\,^{\circ}$C. Radiation with frequency below 6 GHz penetrates biological tissue, and so, this exposure is described in terms of power absorbed per unit mass - Specific Energy Absorption Rate (SAR). Exposure resulting in a whole-body average SAR of approximately $6\,\mathrm{W}\cdot\mathrm{kg}^{-1}$, within the 100 kHz to 6 GHz range, over at least 1 hour, is required to induce a $1\,^{\circ}$C body core temperature rise in human adults. A conservative position is adopted - it is set that $4\,\mathrm{W}\cdot\mathrm{kg}^{-1}$ averaged over 30 min is the radiofrequency EMF exposure level corresponding to a body core temperature rise of $1\,^{\circ}$C. Radiation above 6 GHz is absorbed mostly superficially, and as such, body core temperature cannot be affected by it. Nevertheless, the same $4\,\mathrm{W}\cdot\mathrm{kg}^{-1}$ averaged over 30 min restriction is used in frequencies from 6 to 300 GHz.

SAR can be difficult to measure. For this reason, entities that are more easily evaluated are used, such

as incident electric field strength (E_{inc}), incident magnetic field strength (H_{inc}), incident power density (S_{inc}) and incident energy density (U_{inc}), measured outside the body. Reference levels that provide an equivalent level of protection to the exposure restriction levels discussed above (basic restriction levels) are set in these more accessible units. The reference levels for steady-state temperature rise for time-averaged exposures of ≥ 6 min are shown in Figure 2.8. Table 2.11 shows the same information but for time-averaged exposures of ≥ 30 min, where the absence of a value signifies that it does not need to be taken into account when determining compliance.

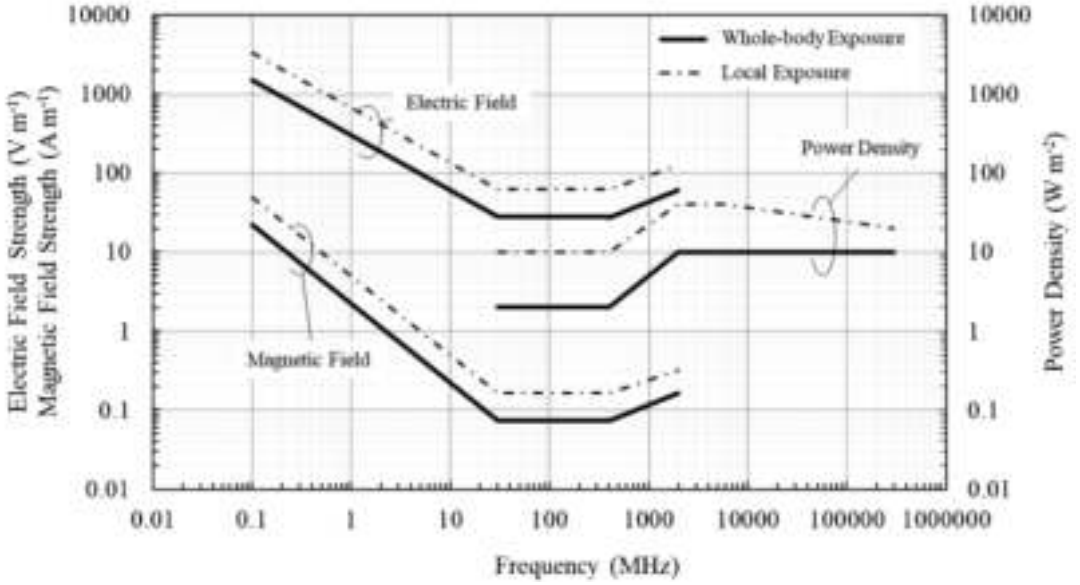

Figure 2.8: Steady-state temperature rise reference levels for time-averaged exposures of ≥ 6 min (extracted from [10]).

Table 2.11: Steady-state body core temperature rise reference levels for time-averaged exposures of ≥ 30 min (adapted from [10]).

Frequency range	$\mathbf{E_{inc}}$[V·m⁻¹]	$\mathbf{H_{inc}}$[A·m⁻¹]	$\mathbf{S_{inc}}$[W·m⁻²]
]400, 2000] MHz	$1.375 f_{[\text{MHz}]}^{0.5}$	$0.0037 f_{[\text{MHz}]}^{0.5}$	$f_{[\text{MHz}]}/200$
]2, 300] GHz	–	–	10

Regarding exposure limits, ICNIRP guidelines divide the human population into two categories: occupationally exposed individuals and general public. Occupationally-exposed individuals are defined as adults who are exposed under controlled conditions associated with their occupational duties. The rest of the human population is defined as general public. Only the values for the general public are presented in this thesis.

The degree of adequacy of the imposed reference levels depends on whether the measured EMF is within the far-field, radiative near-field or reactive near-field regions (Section 2.4.2). As power decays over distance, the guidelines have more conservative rules for exposure in the near-field region than in the far-field region. In order to be compliant with the guidelines, from 400 MHz to 2 GHz, compliance depends on whether the measurement is made in the far-field region. If it is, only one of the entities

between incident electric field strength, incident magnetic field strength and incident power density has to be below the given reference level. If it is not, both the electric and magnetic field strength must be below the reference levels. From 2 to 300 GHz, compliance depends on whether the measurement is made in the reactive near-field region. If it is, reference levels are treated as inadequate, and in this case, compliance with the basic restriction levels must be proved. If the measurement is made in the radiative near-field or far-field regions, compliance is proven if the incident power density is below the given reference level.

There might be cases in which a person is subjected to an EMF with different radiation frequencies, such as being served by BSs from different generations of telecommunications. In this case, exposure effects are additive, and in order to prove compliance with the reference levels for steady-state body core temperature rise effects, the incident electric and magnetic fields strength and the incident power density should follow

$$\begin{aligned}&\sum_{i=0.1\,\text{MHz}}^{30\,\text{MHz}}\left[\left(\frac{E_{inc,i[\text{V·m}^{-1}]}}{E^{RL}_{inc,i[\text{V·m}^{-1}]}}\right)^2+\left(\frac{H_{inc,i[\text{A·m}^{-1}]}}{H^{RL}_{inc,i[\text{A·m}^{-1}]}}\right)^2\right]\\&+\sum_{i>30\,\text{MHz}}^{2\,\text{GHz}}\max\left\{\left(\frac{E_{inc,i[\text{V·m}^{-1}]}}{E^{RL}_{inc,i[\text{V·m}^{-1}]}}\right)^2,\left(\frac{H_{inc,i[\text{A·m}^{-1}]}}{H^{RL}_{inc,i[\text{A·m}^{-1}]}}\right)^2,\frac{S_{inc,i[\text{W·m}^{-2}]}}{S^{RL}_{inc,i[\text{W·m}^{-2}]}}\right\}+\sum_{i>2\,\text{GHz}}^{300\,\text{GHz}}\frac{S_{inc,i[\text{W·m}^{-2}]}}{S^{RL}_{inc,i[\text{W·m}^{-2}]}}\leq 1,\end{aligned}\tag{2.7}$$

where

- $E_{inc,i}$ is the incident electric field strength at frequency i;
- $H_{inc,i}$ is the incident magnetic field strength at frequency i;
- $S_{inc,i}$ is the incident power density at frequency i;
- $E^{RL}_{inc,i}$ is the incident electric field strength reference level for frequency i, given in Table 2.11;
- $H^{RL}_{inc,i}$ is the incident magnetic field strength reference level for frequency i, given in Table 2.11;
- $S^{RL}_{inc,i}$ is the incident power density reference level for frequency i, given in Table 2.11.

2.5 Exclusion zone

Electromagnetic radiating elements, such as antennas, may sometimes form regions around them in which the established EMF human exposure thresholds, discussed in Section 2.4.3, are exceeded. These zones form an EZ and they should be physically delimited to protect the general public from EMF. Some relevant parameters, such as the characteristics of BS installation and of the antenna itself, are essential for the estimation of an EZ and specific procedures are required for the evaluation of EMF around BSs. As discussed in Section 2.4.2, EMF behaviour is not the same in each radiation region. Hence, having an accurate propagation model is necessary to accurately estimate the EZ around a BS.

The range of an EZ may be obtained through measurements, by running complex simulations or by applying propagation models [33]. As measurements and simulations are time-consuming and BS dependent, applying a selection of adequate propagation models is the most practical solution. 7 models are mentioned in [33], with their respective validity ranges shown in Table 2.12. In order to calculate the

EZ range, the model with the highest validity range should be used first. If the calculated power density at that range is below the threshold value, a model with a smaller validity range must be used.

Table 2.12: Validity range of each propagation model [33].

	Validity range [m]							
Propagation model	0	$\frac{\lambda}{2}$	λ	2λ	3λ	$\frac{D_L^2}{4\lambda}$	$\frac{\theta_{3dB} G(\theta,\phi) D_L}{4\pi}$	$\frac{2D_L^2}{\lambda}$
Far-field	X	X	X	X	X	X	X	✓
Far-field approximation	X	X	X	X	X	✓	✓	✓
Far-field gain based	X	X	X	X	✓	✓	✓	✓
Gain based	X	X	X	✓	✓	✓	✓	✓
Synthetic based	X	X	✓	✓	✓	✓	✓	✓
Cylindrical EZ	X	✓	✓	✓	✓	✓	✓	✓
Hybrid	✓	✓	✓	✓	✓	✓	✓	✓

If an antenna is omnidirectional, its radiation regions are considered to be spherical. Otherwise, the direction of the lobe with the highest gain is used as reference, while in the other directions, a correction factor depending on the radiation pattern of the antenna in study is applied [33]. Figure 2.9 represents a generic directional antenna EZ.

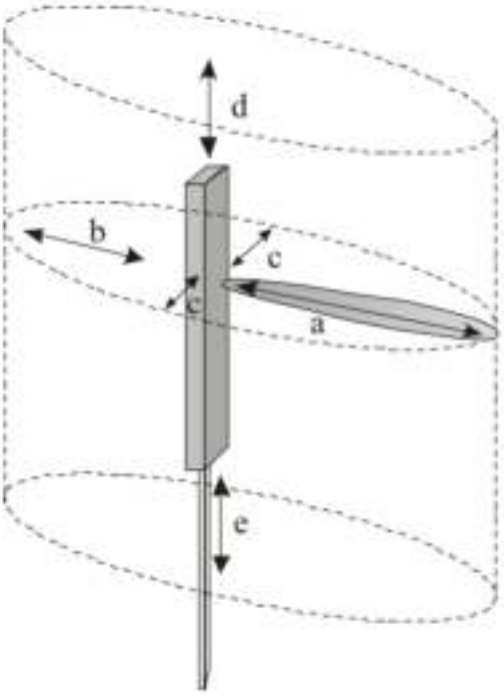

$a = D_{front}$
$b = D_{back}$
$c = D_{side}$
$d = D_{top}$
$e = D_{bottom}$

Figure 2.9: Generic directional antenna EZ (extracted from [33]).

2.6 State of the art

As 5G introduces active antennas with new technology, namely MaMIMO and beamforming (Section 2.4.1), existing EMF measuring methods used in previous technologies may not be suitable anymore. In [11], two methods for exposure measurement are presented, however, both these measurements methods are performed in the far-field region only. As higher frequencies have shorter range, the NR network will be denser (it will have more BSs per unit area) than the previous technologies' networks. This may intensify the level of EMF radiation, possibly surpassing the restriction levels discussed in Section 2.4.3 [8, 9]; it will also reduce the distance between BSs and users, making it necessary to develop a method to estimate the behaviour of EMF in the near-field. In [34], a discussion of 5G technology and the consequent human exposure to EMF radiation is made, although no model for measuring it is provided.

Beamforming allows for very high-gain directional beams, leading to an increase in amount of EMF in a specific direction, something that did not happen previously. MaMIMO systems are also capable of delivering more energy that the previous MIMO systems [9].

Up until NR, the traditional approach in designing an EZ was conservatively assuming the same power in all directions and averaging the measurements of EMF radiation over several minutes (this is the case in [35]). Because of these two reasons, [36] puts forward the idea that this approach is over-conservative, and presents a statistical approach to determine an EZ, stating that, even with MaMIMO, the obtained EZ is smaller compared to the traditionally-obtained one. These results are corroborated in [37] and [38], where the EMF exposure found in BSs with MaMIMO is much below the value assuming a constant maximum power transmission with a fixed beam. The authors of [37] reached this conclusion by evaluating network based measurements in addition to on-site field strength measurements. The authors of [38] found that in an interval over 24 h, the maximum time-averaged power per beam was found to be below the theoretical maximum and lower than what was predicted by the existing statistical models.

Another method of determining an EZ is presented in [39], considering factors such as usage of TDD and spatial distribution of users. Its results show that the time-averaged realistic maximum power is just 7 - 22 % of the theoretical maximum power, which in turn leads to a smaller EZ than the ones calculated through other models.

In [40], it is shown that some existing BSs may be unable to accommodate 5G technology since they are already transmitting enough EMF radiation (with other telecommunications technologies) to be over or very close to the restrictions set in [10].

It is noteworthy to refer that there is literature focused on studying 5G EMF exposure from UEs and their compliance with restrictions, such as [41, 42, 43]. In [44], a method for measuring power density in an antenna's near-field is presented, and in [45], a system for measuring a 5G mobile terminal near-field in the 18 - 50 GHz range is presented, along with obtained results. Contrary to this thesis, these studies only take frequencies above 6 GHz into consideration.

In [46], a model for estimating the EZ of a 5G BS is proposed, although it considers that the antennas are continuously radiating at maximum power, which, as previously discussed, leads to over-conservative results. The objective of this thesis is specifically addressed in [13], but the author could not compare the obtained simulated results with on-site measurements, in order to validate the model. Furthermore,

the simulation was performed with the antenna transmitting at full power. Nevertheless, it found that NR deployment can increase the EZ of existing BSs up to $170\,\%$ of its original diameter.

Chapter 3

Model description and assessment

This chapter presents the developed model and sub-models to calculate the EZ, along with the creation of realistic scenarios and 5G services. It details how the model obtains the transmission power of each beam and the compliance distance over time, and how from these the EZ is obtained. The model is also validated through assessment tests.

3.1 Model configuration

In this section, the model developed to estimate the EZ around 5G BSs is presented with its inputs and required outputs, along with their description. This information is consolidated in Figure 3.1, which also presents the various sub-models. A flowchart detailling a single run of the model is shown in Figure 3.2, where the displayed blocks are further explained along this chapter.

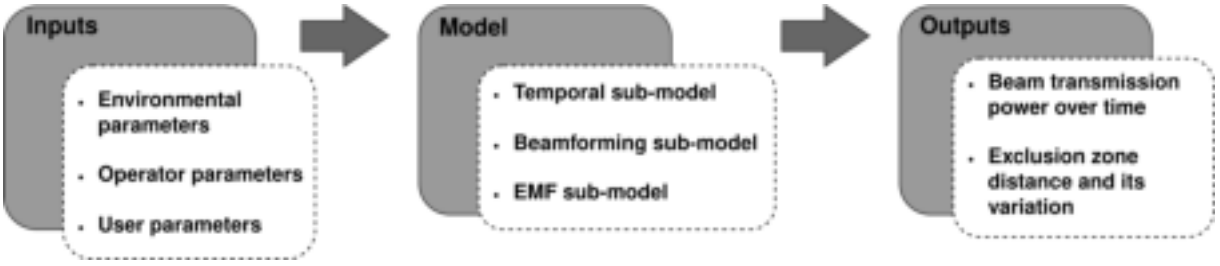

Figure 3.1: Model configuration.

The inputs required by the model can be divided into three categories:

- **Environmental parameters**, which represent the characteristics of the environment in which the BS is inserted, such as its installation height and the height of its building;
- **Operator parameters**, refering the specifications of the BS, including transmiting parameters (gain, radiation pattern, numerology value, ...) and the antenna's physical characteristics (number of elements, azimuth and elevation range, mechanical tilt, ...);
- **User parameters** characterise user-related parameters (number of users, user height and losses, reception gain) and service-related parameters (number of services, their download size and usage duration, ...), as well as additional parameters to simulate realistic scenarios.

As the active antennas used in 5G BSs have beamforming capabilities, their maximum EIRP can be significantly higher compared to passive antennas. However, since these beams are not always on nor always at their maximum transmission power, using the maximum EIRP to estimate the EZ, as is made with passive antennas, leads to over-estimated values [36]. As such, the estimation of the EZ must be made on a timed-averaged EIRP, taking into account the mobility of users as well as the characteristics of the provided service. For these reasons, a temporal sub-model and a beamforming sub-model are required. In order to verify compliance with restrictions, the EMF behaviour around the antenna must be known, and for that, an EMF sub-model, which includes a propagation model, is also required.

The required output from the model is the beam transmission power over time, which allows one to calculate the time-variant compliance distance, and from there estimate the EZ distance around the BS. As additional outputs, the model can also show the power density received by each user, the RB usage, distribution of services and number of users over time, which yield further information that can be used to better estimate the EZ value.

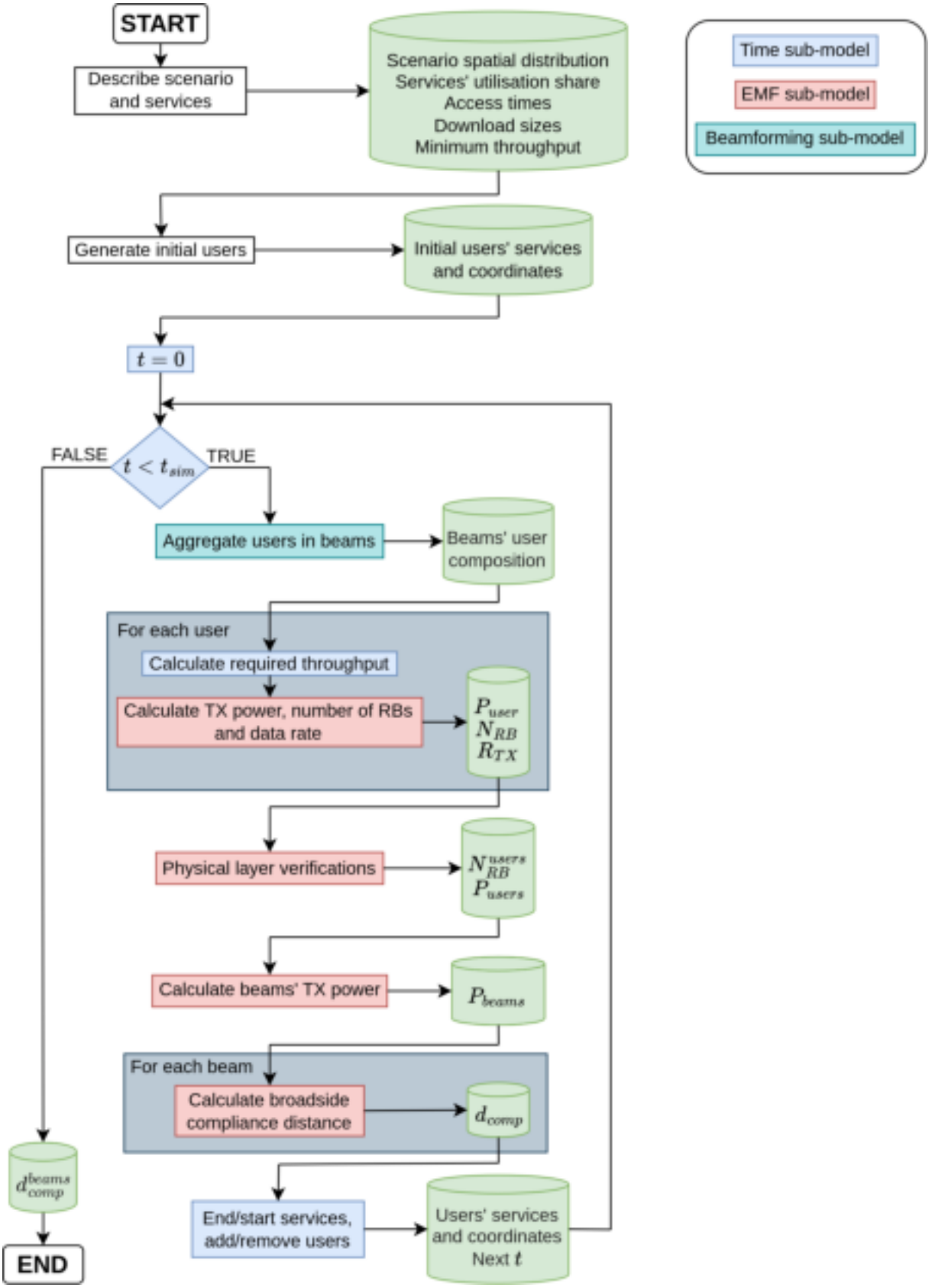

Figure 3.2: Flowchart representation of a run of the developed model.

3.2 Scenarios' description

To simulate realistic usage of a 5G BS, realistic usage scenarios need to be created. These contain fictitious users, distributed in Line of Sight (LOS) to the antenna and making use of various services. If a user is in LOS to the BS, a focused beam is employed. If the user is not in LOS, the BS may transmit simultaneously using multiple beams. Maximum exposure is caused by the focused beams, and so, users in this simulation are always within LOS to the BS. Four User Distribution Scenario (UDS) are defined in [39], which spatially distributes users in elevation and azimuth. This thesis adapts these UDS, as they are necessary to realistically simulate beamforming and the energy distribution behaviour of the antenna. Each of the four adapted UDS represents a realistic user spatial distribution, and all have the property that the integral of their spatial probability density function (w) over the scan range is equal to 1 (in this thesis, the scan range is from −60° to 60° azimuth and from −15° to 15° elevation).

3.2.1 Street and bus stop

With the goal of simulating a scenario where an antenna covers a street with a sidewalk parallel to the antenna's building, the street and bus stop scenarios are created. These follow the UDS shown in Figure 3.3. In these scenarios, a Dirac delta function is used to only allow users to be at the sidewalk's elevation - although this approach is not realistic, it yields an acceptable approximation to the desired simulation scenarios. The street scenario represents a uniformly distributed density of users over the azimuth at the sidewalk's elevation angle, as can be observed in Figure 3.4 and Figure 3.5. Its user probability density is described by

$$w(\psi) = \frac{3}{2\pi}\delta\left[\psi + \tan^{-1}\left(\frac{h_{a[\mathrm{m}]} + h_{b[\mathrm{m}]} - h_{user[\mathrm{m}]}}{d_{street[\mathrm{m}]}}\right)\right], \tag{3.1}$$

where

- ψ is the elevation angle;
- δ is the Dirac delta function;
- d_{street} is the street width;
- h_a is the antenna's height;
- h_b is the building's height;
- h_{user} is the user's height.

The bus stop scenario represents a cosine weighted distributed density of users over the azimuth at the sidewalk's elevation angle, mimicking a bus stop in the sidewalk, where users are more likely to be. It is also represented by Figure 3.4 and Figure 3.5, and its user probability density is described by

$$w(\psi, \phi) = \frac{3}{4}\cos\left(\frac{3\phi}{2}\right)\delta\left[\psi + \tan^{-1}\left(\frac{h_{a[\mathrm{m}]} + h_{b[\mathrm{m}]} - h_{user[\mathrm{m}]}}{d_{street[\mathrm{m}]}}\right)\right], \tag{3.2}$$

where ϕ is the azimuth angle.

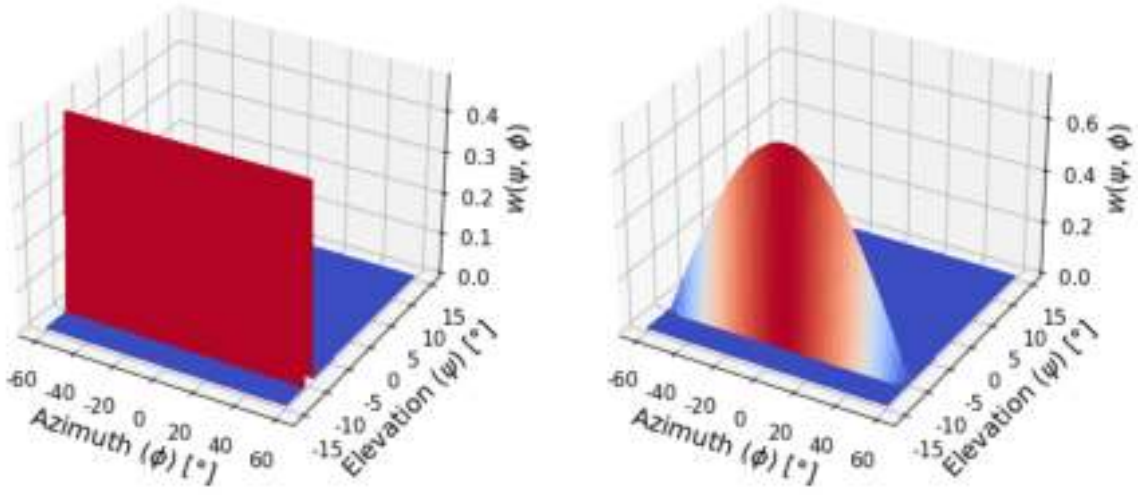

(a) Street scenario (uniform line). (b) Bus stop scenario (Gaussian line).

Figure 3.3: Plot examples of the UDS (adapted from [39]).

The users' distance to the antenna's perpendicular varies between d_{street} and d_{max}, with the latter being given by

$$d_{max[\mathrm{m}]} = \frac{d_{street[\mathrm{m}]}}{\cos(\phi_{max})}, \tag{3.3}$$

as represented in Figure 3.5 (the antenna's azimuth limits (ϕ_{max}) can be found in Annex C). The sidewalk length is considered to cover the entire azimuth range of the antenna, so that users can be present from the minimum azimuth value to its maximum. From Figure 3.4 and Figure 3.5, one can obtain the expression to calculate the distance from the antenna to the user in these scenarios:

$$d^{line}_{user[\mathrm{m}]} = \sqrt{\left(\frac{d_{street[\mathrm{m}]}}{\cos(\phi_{user})}\right)^2 + (h_{a[\mathrm{m}]} + h_{b[\mathrm{m}]} - h_{user[\mathrm{m}]})^2}. \tag{3.4}$$

As the users are always in LOS to the antenna, the only combinations of street width and building height that are evaluated are those that result in a user elevation in the antenna's elevation range. Figure 3.6 shows how the user elevation changes with respect to the street width, for various values of building height. From Figure 3.6, and by verifying the antenna's elevation range in Annex C, not all combinations of street width and building height result in a user elevation inside the antenna's range. The equation that describes Figure 3.6, accounting for the antenna's mechanical tilt, is

$$\psi^{line}_{user} = -\tan^{-1}\left(\frac{h_{a[\mathrm{m}]} + h_{b[\mathrm{m}]} - h_{user[\mathrm{m}]}}{d_{street[\mathrm{m}]}}\right) - \gamma. \tag{3.5}$$

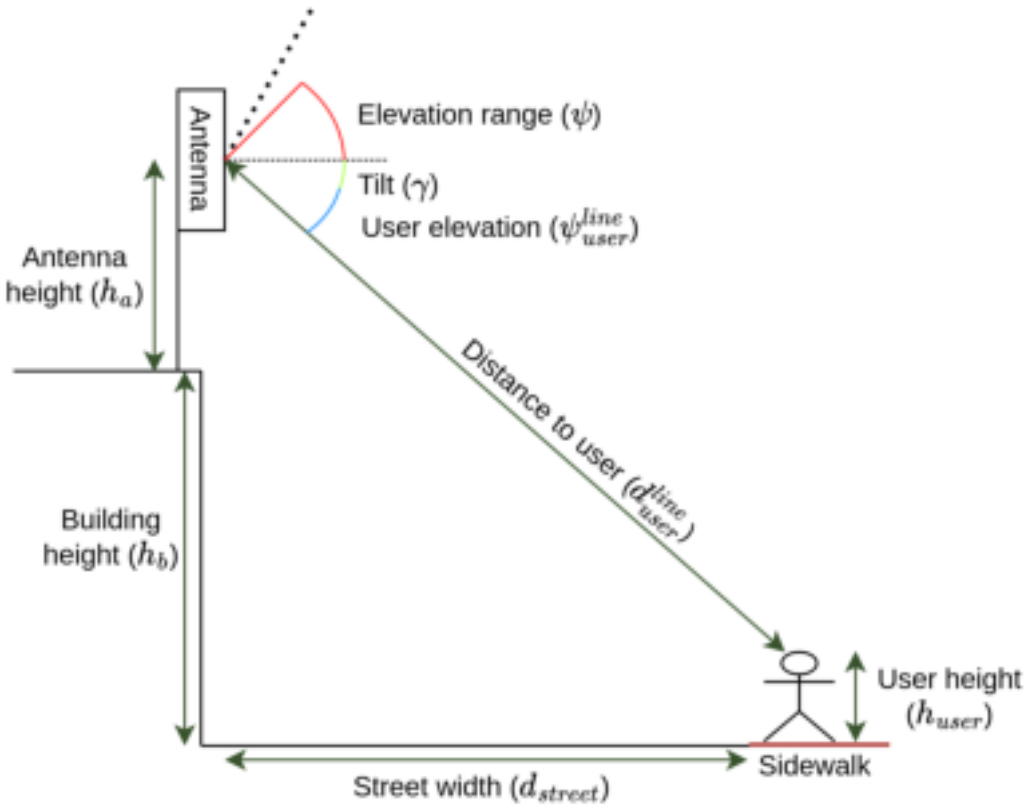

Figure 3.4: BS vertical sketch in the street and bus stop scenarios.

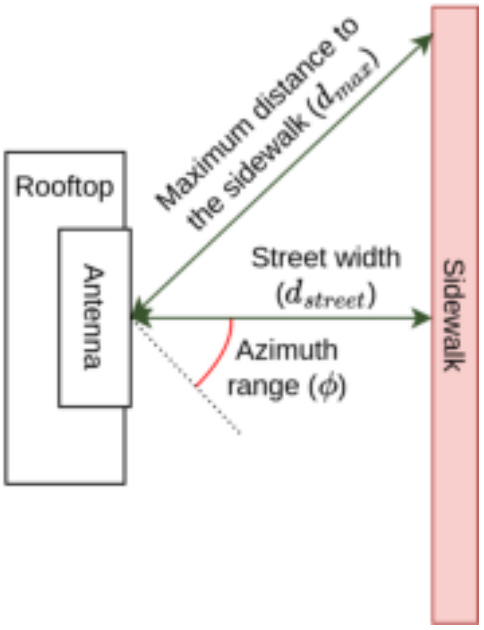

Figure 3.5: BS horizontal sketch in the street and bus stop scenarios.

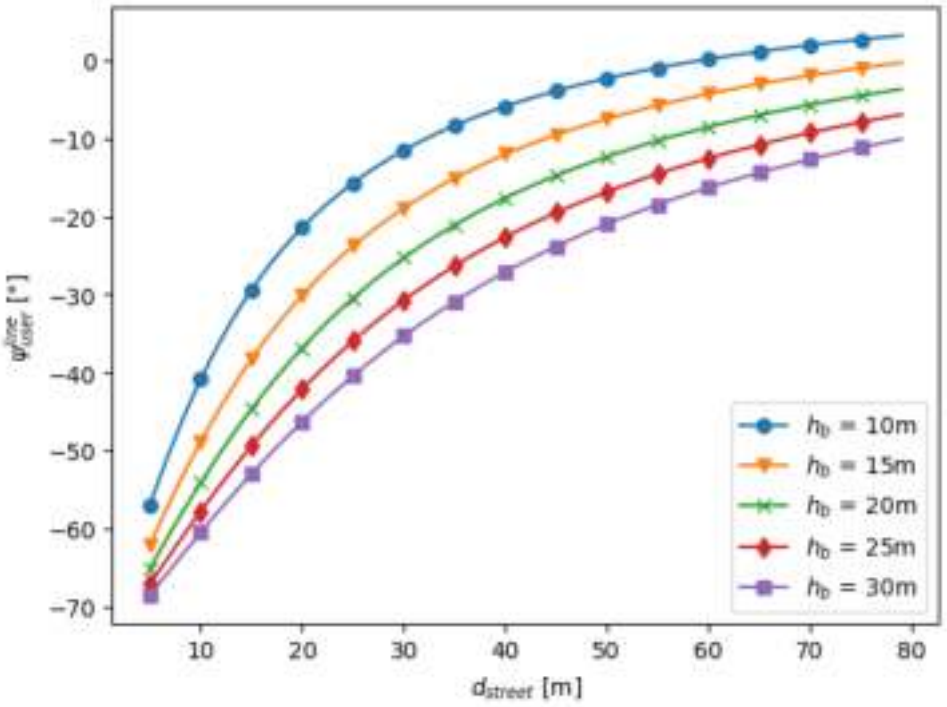

Figure 3.6: User elevation with respect to the street width, for various values of building height ($h_a = 5.5\,\text{m}, h_{user} = 1.8\,\text{m}, \gamma = -13°$).

3.2.2 Residential building

This scenario is designed to mimic a situation where a residential building exists in front of the building that hosts the BS. The users' spatial distribution follows the uniform plane UDS shown in Figure 3.7 - it has a uniformly distributed density of users over the azimuth and elevation, as described by

$$w = \frac{9}{\pi^2}. \tag{3.6}$$

In this scenario, users are present in the side of the residential building facing the BS, anywhere from a user's height up to the residential building's height, as is exemplified in Figure 3.8. There are multiple residential buildings, and besides all having the same height, they are considered to cover the entire azimuth range of the antenna, so that users can be present from the minimum to the maximum azimuth value (as can be observed in Figure 3.9).

The minimum elevation that a user can be is as shown in (3.5), as the minimum height that users can be present in this scenario is the same as in the street and bus stop scenarios. However, because the residential building can be taller than the BS, the elevation range in which a user can be is

$$-\tan^{-1}\left(\frac{h_{a[\text{m}]} + h_{b[\text{m}]} - h_{user[\text{m}]}}{d_{street[\text{m}]}}\right) - \gamma \leq \psi_{user}^{uni} \leq \tan^{-1}\left(\frac{h_{rb[\text{m}]} - h_{b[\text{m}]} - h_{a[\text{m}]}}{d_{street[\text{m}]}}\right) - \gamma, \tag{3.7}$$

keeping in mind that only situations where the user is in LOS are studied.

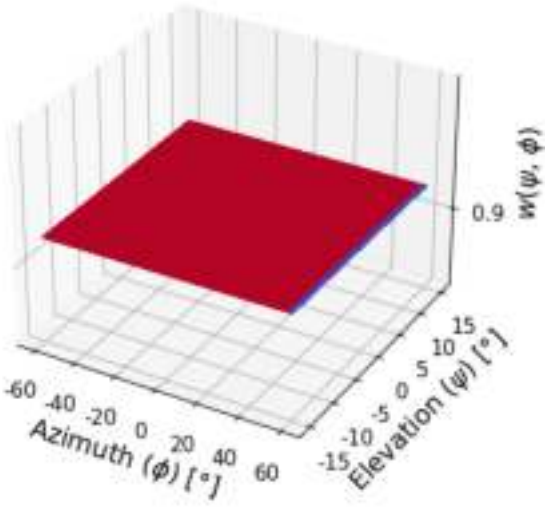

Figure 3.7: Residential building scenario (uniform plane).

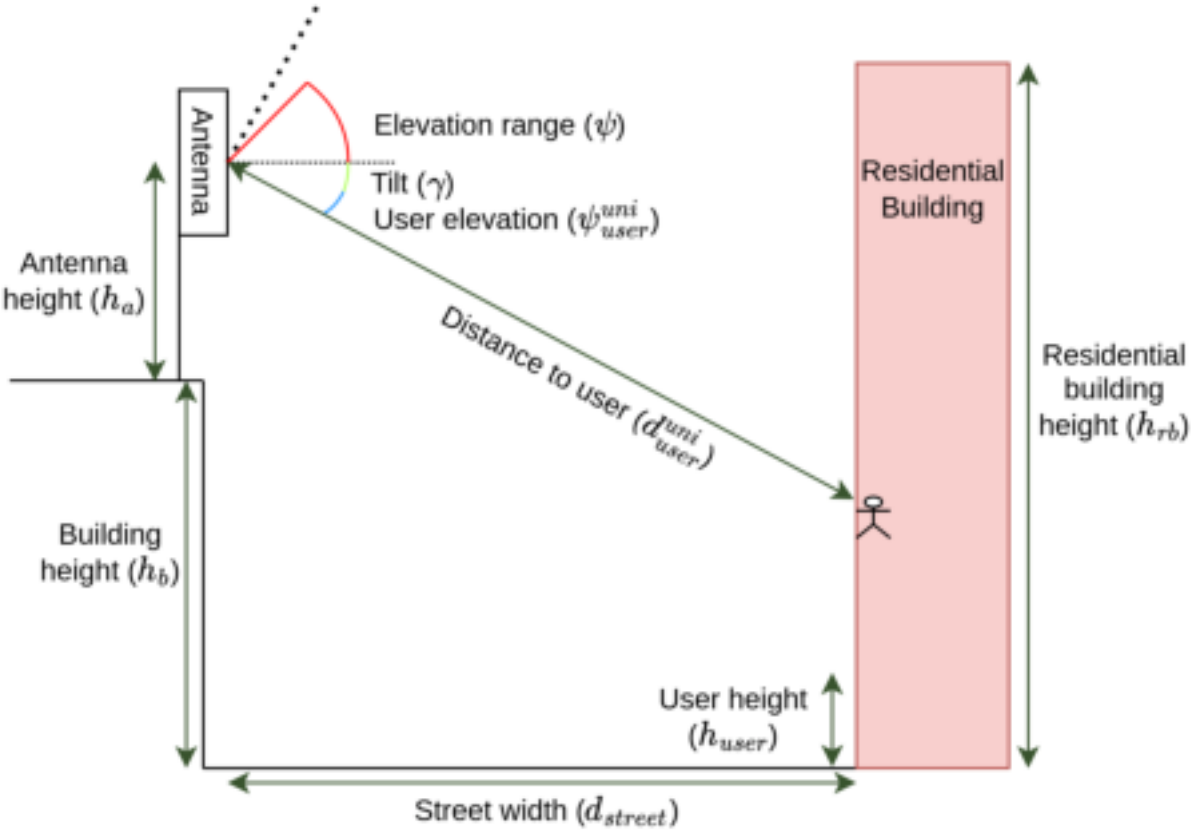

Figure 3.8: BS vertical sketch in the uniform plane scenario.

Any user's distance to the antenna's perpendicular varies between d_{street} and d_{max} (as given in (3.3)). Knowing this, and analysing Figure 3.8, it is possible to calculate the distance from the antenna to any user with

$$d_{user[\mathrm{m}]}^{uni} = \frac{d_{street[\mathrm{m}]}}{\cos(\phi_{user})\cos(\psi_{user}^{uni} + \gamma)}. \tag{3.8}$$

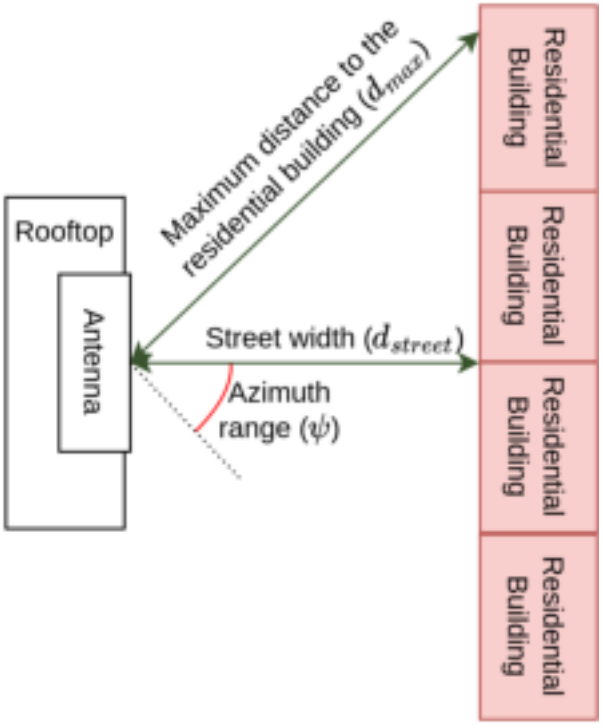

Figure 3.9: BS horizontal sketch in the uniform plane scenario.

3.2.3 Demonstration

This scenario is designed with the intent of replicating a high concentration of users at one point which gradually lowers along the elevation and azimuth, such as a demonstration of people on the street. It is based on the UDS shown in Figure 3.10; it has a cosine weighted distributed density of users over the azimuth and squared cosine weighted distribution over the elevation, as described in

$$w(\psi, \phi) = \frac{9}{\pi}\cos^2\left(6\psi + \tan^{-1}\left(\frac{h_{a[\mathrm{m}]} + h_{b[\mathrm{m}]} - h_{user[\mathrm{m}]}}{d_{fp[\mathrm{m}]}}\right)\right)\cos\left(\frac{3\phi}{2}\right), \tag{3.9}$$

where d_{fp} is the distance to the Gaussian waveform focal point. As in previous scenarios, users can be present from the minimum azimuth value to the maximum, as shown in Figure 3.11, and all users are at a user's height, as shown in Figure 3.12. The users' elevation range is

$$-\tan^{-1}\left(\frac{h_{a[\mathrm{m}]}+h_{b[\mathrm{m}]}-h_{user[\mathrm{m}]}}{d_{min}^{demo}{}_{[\mathrm{m}]}}\right)-\gamma\leq\psi_{user}^{demo}\leq-\tan^{-1}\left(\frac{h_{a[\mathrm{m}]}+h_{b[\mathrm{m}]}-h_{user[\mathrm{m}]}}{d_{max}^{demo}{}_{[\mathrm{m}]}}\right)-\gamma, \tag{3.10}$$

where

- d_{min}^{demo} is the minimum distance along the ground that a user can be;
- d_{max}^{demo} is the maximum distance along the ground that a user can be.

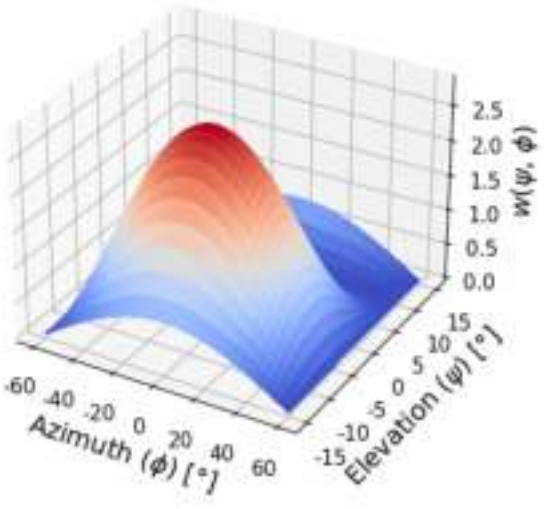

Figure 3.10: Demonstration scenario (Gaussian plane).

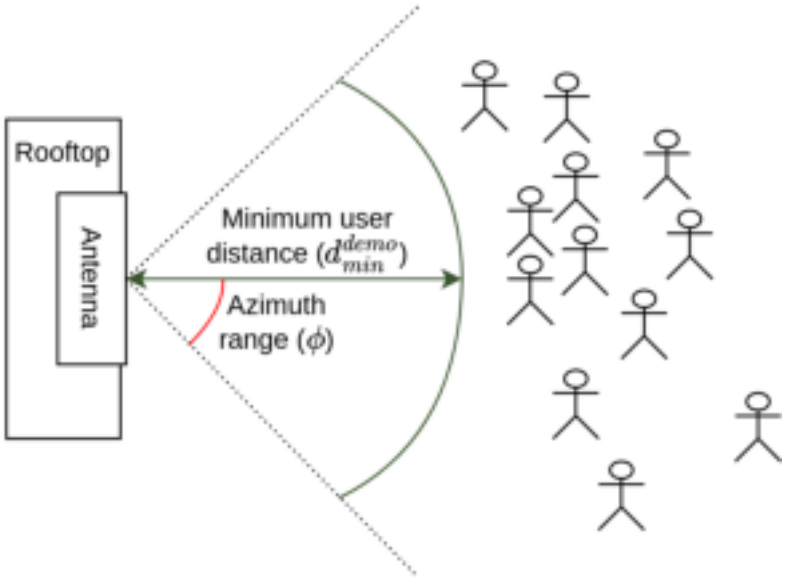

Figure 3.11: BS horizontal sketch in the uniform Gaussian scenario.

In this scenario, the distance from the antenna to any user is given by

$$d_{user}^{demo}{}_{[\mathrm{m}]} = \frac{h_{a[\mathrm{m}]} + h_{b[\mathrm{m}]} - h_{user[\mathrm{m}]}}{|\sin(\psi_{user}^{demo} + \gamma)|}. \tag{3.11}$$

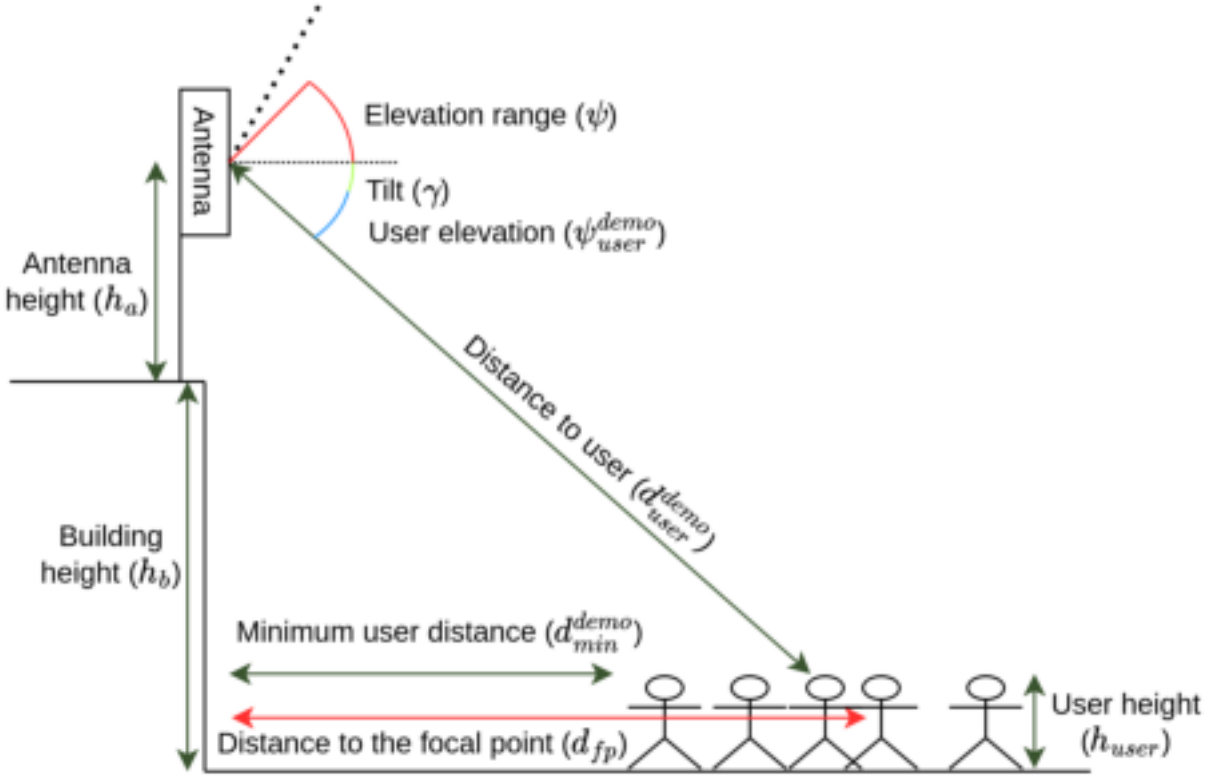

Figure 3.12: BS vertical sketch in the uniform Gaussian scenario.

3.3 Services description

As well as scenarios, services based on common daily usage of mobile telecommunications need to be created, as the transmission power (and therefore the EZ) is proportional to the required bandwidth. Table 3.1 shows each created service's minimum recommended throughput, and whether it is real-time or not (non real-time services are not exclusive, meaning several can be active in a given user at a time; real-time services are exclusive). Each non real-time service has its download size defined by a normal distribution [47], and so the average download size (together with its standard deviation) is shown in Table 3.1. Contrary to these, real-time services have their access time defined by an exponential distribution [48], with Table 3.1 showing the average access time for each service (more information can be found in Annex B). While the minimum recommended throughput can be used to calculate the transmission power from the antenna, access times and download sizes allow one to determine exposure time. Services are distributed among users according to a defined usage share for each scenario (Chapter 5), with each following that

$$\sum_{n=1}^{N_{serv}} S_n = 100\,\%, \tag{3.12}$$

where

- N_{serv} is the number of different services;
- S_n is the share of each service in each scenario.

Table 3.1: Created mobile services.

	Service	Download size (average, std. deviation) [MB]	Minimum recommended throughput [Mbit·s^{-1}]	Average access time [min]	References
Non real-time	Web browsing	(2, 1)	4.0	–	[49, 50, 51]
	Video download	(500, 400)	5.0	–	[50, 52]
	Large file download	(5000, 3500)	10.0	–	[50, 51]
	E-mail	(0.075, 0.010)	1.0	–	[53, 50]
	Online chat	(0.020, 0.005)	1.0	–	[54, 55, 50]
Real-time	Video conference	–	4.0	54	[50, 56, 57, 58]
	Gaming	–	7.0	60	[50, 59, 60]
	Video streaming	–	5.0	75	[61]
	Augmented / Virtual reality	–	50.0	38	[62, 63]
	Audio streaming	–	0.4	30	[50]

When making use of one or more services, users do not change their location and they remain in the simulation until their service is complete (which depends on the download size and user throughput for non real-time services or on the access time for real-time services). During simulation, new users are generated at a fixed period as detailed in Figure 3.13. First their services are randomly selected, making sure that each user only has one real-time service, then their location is also randomly selected, according to the UDS of the scenario that is being simulated. At last, the distance from the BS to the user is calculated as shown in Section 3.2.

To advance time in the simulation, the model calculates, for each value of t, how much time is left on every service for every user, while removing services that have ended and removing users with no services. Knowing this, the next value of t is the closest ending time for a service, unless that is greater than the period of new user generation (t_{user}). Each t_{user} seconds, new users are generated (up to a quarter of the difference between the maximum number and current number of users, arbitrarily). The model also assures that the number of users is always higher or equal than the minimum number of users, as reported in Figure 3.14.

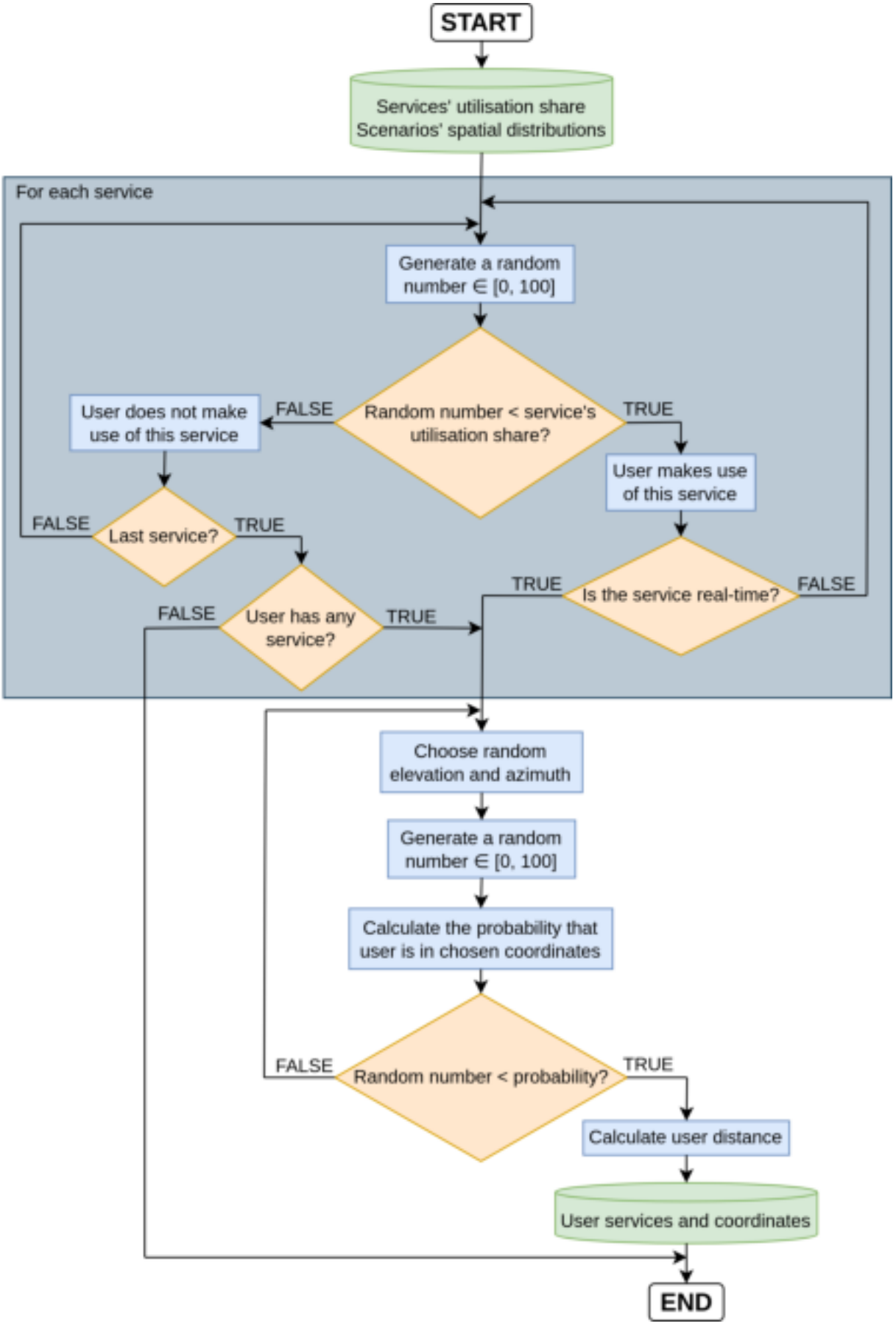

Figure 3.13: User generation.

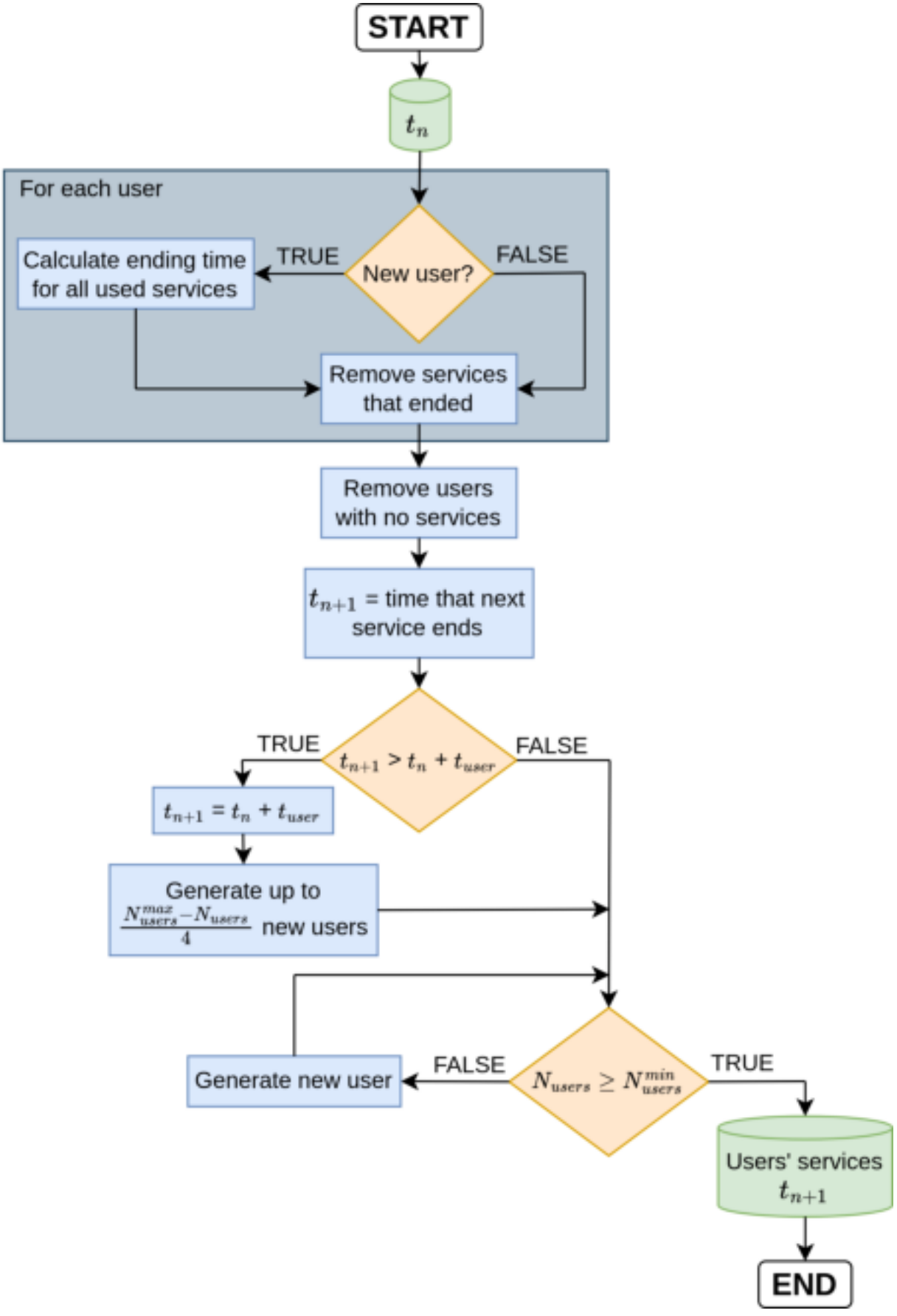

Figure 3.14: Temporal behaviour of the simulation.

3.4 Transmission power

As mentioned in [64], there are two types of beams: broadcast beams, for synchronisation and control, and service beams, for user data transmission. The latter presents a much higher transmission power than the former, and so, only service beams are considered in the EZ calculation.

In order to estimate an EZ around the BS, the transmission power of each beam must be determined. This analysis must be made on a per-beam basis, because beams are only active if there are users in it to be served, and they are independent of one another. As the studied antenna is an active antenna, a beamforming sub-model must be created in order to realistically simulate its MU beamforming behaviour. Beams are fixed in space, with only their transmission power varying [64, 65]. The coverage area of each beam is shown in Figure 3.15, with the centre of each beam's area being the point of maximum gain. In order to calculate a user's required transmission power, one must know the gain at the user's coordinates. According to [1], the general expression for the electric field strength over distance can be written as

$$E(P_{TX}, \phi, \psi, d)_{[\mathrm{V\cdot m^{-1}}]} = V_M(P_{TX})_{[\mathrm{V}]} f_{\phi\psi}(\phi, \psi) f_E(d)_{[\mathrm{m^{-1}}]}, \tag{3.13}$$

where V_M is the antenna maximum transmission voltage, described by

$$V_{M\,[\mathrm{V}]} = \sqrt{30 P_{TX\,[\mathrm{W}]} G_{TX}^{max}}, \tag{3.14}$$

where

- P_{TX} is the transmission power;
- G_{TX}^{max} is the maximum transmission gain (Annex C),

$f_{\phi\psi}$ is the normalised antenna radiation pattern at (ϕ, ψ), given by

$$f_{\phi\psi}(\phi, \psi) = \sqrt{\frac{G_{TX}(\phi, \psi)}{G_{TX}^{max}}}, \tag{3.15}$$

and f_E is the electric field strength behaviour with respect to distance, given by

$$f_{E[\mathrm{m^{-1}}]} = \frac{1}{d_{[\mathrm{m}]}},\ d_{[\mathrm{m}]} \geq d_{ff\,[\mathrm{m}]}, \tag{3.16}$$

where d_{ff} is given by (2.6). Still according to [1], in the far-field, the radiation pattern of a beam can be approximated by

$$E(P_{TX}, \phi, \psi, d)_{[\mathrm{V\cdot m^{-1}}]} = E_{max}(P_{TX}, \phi, \psi, d)_{[\mathrm{V\cdot m^{-1}}]} \cos^{c_\psi}(\psi_{[^\circ]} - \psi_{0[^\circ]}) \cos^{c_\phi}(\phi_{[^\circ]} - \phi_{0[^\circ]}), \tag{3.17}$$

where

$$\cos^{c_\psi}\left(\frac{\theta^v_{3dB}}{2}\right) = \frac{1}{\sqrt{2}} \equiv c_\psi = \frac{-\log_{10}(2)}{2\log_{10}\left[\cos\left(\frac{\theta^v_{3dB}}{2}\right)\right]} \tag{3.18}$$

and

$$\cos^{c_\phi}\left(\frac{\theta^h_{3dB}}{2}\right) = \frac{1}{\sqrt{2}} \equiv c_\phi = \frac{-\log_{10}(2)}{2\log_{10}\left[\cos\left(\frac{\theta^h_{3dB}}{2}\right)\right]}, \tag{3.19}$$

in which

- ϕ_0 is the azimuth angle of the centre of beam;
- ψ_0 is the elevation angle of the centre of beam;
- E_{max} is the value of the electric field at coordinates (ϕ_0, ψ_0);
- θ^v_{3dB} and θ^h_{3dB} are the vertical and horizontal beamwidths, respectively (Annex C).

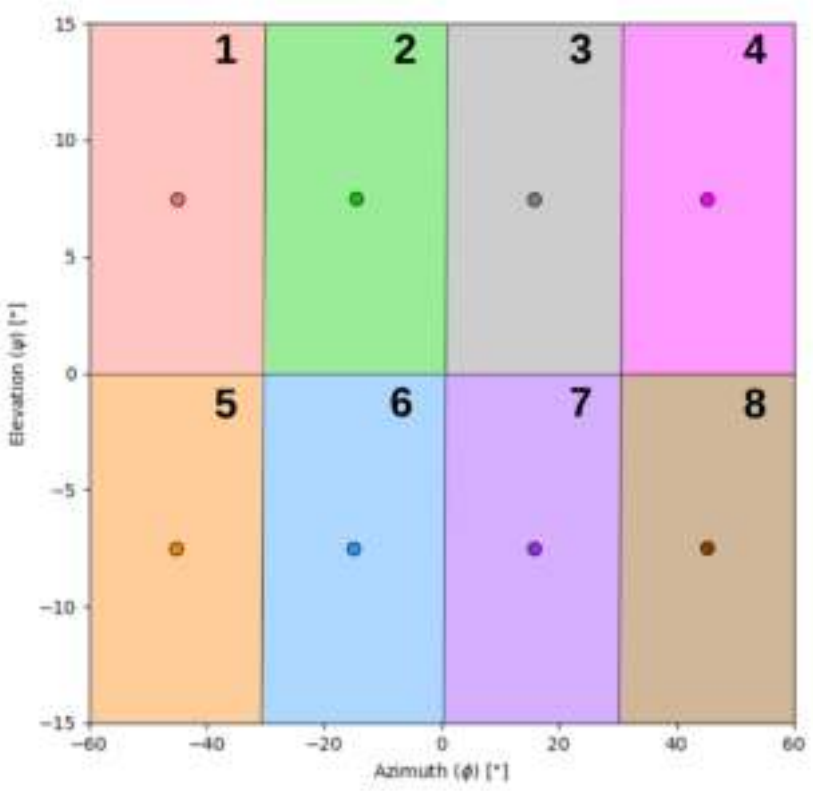

Figure 3.15: Beams' spatial location.

From (3.13) and (3.17), the transmission gain at each point in space is given by

$$G_{TX}(\phi, \psi) = G_{TX}^{max}\left[\cos^{c_\psi}(\psi_{[^\circ]} - \psi_{0[^\circ]})\cos^{c_\phi}(\phi_{[^\circ]} - \phi_{0[^\circ]})\right]^2. \tag{3.20}$$

As both beams and users (whilst making use of the BS) are fixed in space through time, users are aggregated into beams according to their coordinates, as shown in Figure 3.16.

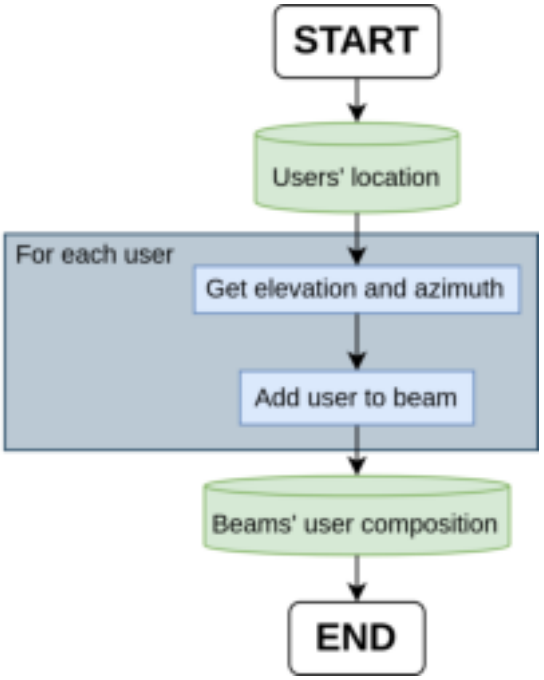

Figure 3.16: Flowchart representation of the creation of beams.

According to [1, 66], a relation between the received Signal to Noise Ratio (SNR) and the throughput per RB can be written for different modulation schemes, which allows one to calculate how many RBs are necessary for each user, given their required throughput and SNR. In this work, the SNR of one SC is assumed to be equal to the SNR of one RB. To calculate the SNR of a single SC received by the UE, one must follow

$$\rho_{N\,[\text{dB}]} = P_{RX}(\phi, \psi, d_{user}, f)_{[\text{dBm}]} - N_{[\text{dBm}]}, \tag{3.21}$$

where

- P_{RX} is the received power;
- N is the noise power.

To calculate the received power, one can use

$$P_{RX}(\phi, \psi, d_{user}, f)_{[\text{dBm}]} = P_{SC[\text{dBm}]} + G_{TX}(\phi, \psi)_{[\text{dBi}]} + G_{RX[\text{dBi}]} - L_{user[\text{dB}]} - L_{0[\text{dB}]}, \quad (3.22)$$

where

- P_{SC} is the transmission power per SC;
- G_{RX} is the reception gain;
- L_{user} are the user reception losses;
- L_0 is the path loss in free space propagation, given by (A.7).

The noise power, according to [1], is calculated with use of

$$N_{[\text{dBm}]} = -174 + 10\log_{10}(f_{\Delta[\text{Hz}]}) + F_{[\text{dB}]}, \quad (3.23)$$

where

- f_Δ is the frequency interval over which to measure noise, which in this case is equal to the SCS;
- F is the system's noise figure.

This thesis relies on the extrapolation of data done in [66]. The extrapolated expressions provide the best-fit curve to experimental values collected by 3GPP with the support of several manufacturers [67]. As these calculations do not take into account the inclusion of control and synchronisation data, the coding rate must be accounted for. This value depends on the quality of the channel, which is not controlled by neither the UE nor the BS, and so each modulation scheme is assigned the average coding rate value from among the possible ones in [68] - this information is shown in Table 3.2. Furthermore, it must be noted that the extrapolated expressions are determined for a 2x2 MIMO system with a numerology of 0, and as such, they must be adapted. The studied antenna has a system with a numerology of 1, and although it has an 8x8 MIMO system, common UE nowadays have a 4x4 or 2x2 MIMO system; 4x4 is considered in this thesis [69, 70].

Table 3.2: Average coding rate for each studied modulation scheme [68].

Modulation scheme	Average coding rate
QPSK	1 / 3
16-QAM	1 / 2
64-QAM	7 / 10
256-QAM	8 / 10

With this information it is possible to write the relation between the received SNR and the throughput per RB in different modulation schemes, taking into account the MIMO order, the SCS and the average coding rate. The equation that describes RB throughput with respect to the received SNR in 256-QAM is taken from [1], as the experimental values collected in [67] are not performed for this modulation. This relation can be written as, for different modulation schemes,

$$R_{RB}^{M-QAM}{}_{[\text{Mbit}\cdot\text{s}^{-1}]} = \begin{cases} \dfrac{9.36805}{14.0051 + e^{-0.577897\rho_{N\,[\text{dB}]}}} & , M = 4 \\ \dfrac{0.190453}{0.0926275 + e^{-0.29583\rho_{N\,[\text{dB}]}}} & , M = 16 \\ \dfrac{0.0985815}{0.0220186 + e^{-0.24491\rho_{N\,[\text{dB}]}}} & , M = 64 \\ \dfrac{0.121}{0.0179 + e^{-0.1989\rho_{N\,[\text{dB}]}}} & , M = 256 \end{cases} . \tag{3.24}$$

Knowing (3.24), it is possible to plot each modulation's throughput per RB over different values of SNR, as shown in Figure 3.17. For any given value of SNR, the system adjusts its modulation scheme to the one that yields the highest throughput per RB, which is also represented in Figure 3.17.

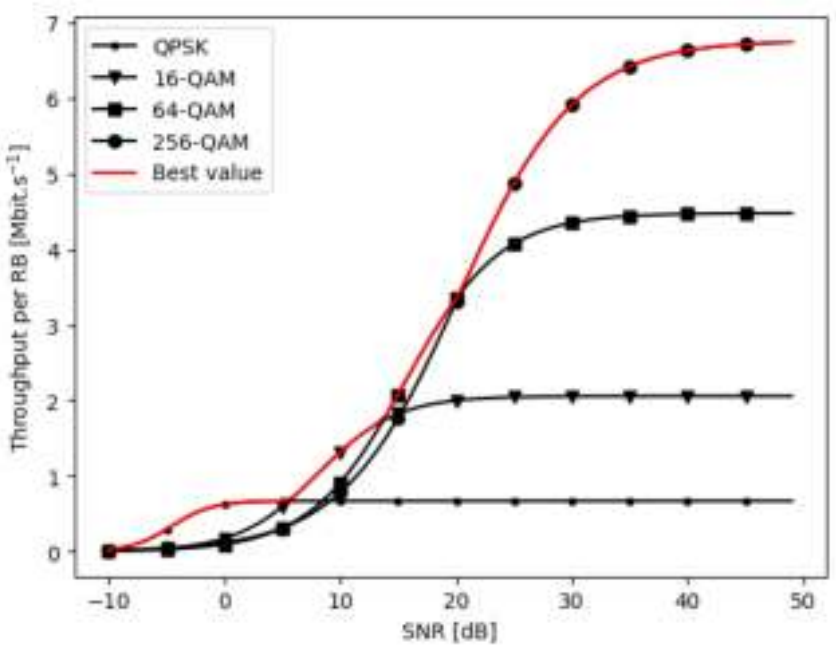

Figure 3.17: RB throughput as a function of SNR, for 4x4 MIMO and $\mu = 1$, with average coding rate values.

Each user's required transmission power is calculated by means of the sub-model presented in Figure 3.18, using their location relative to the antenna and their required throughput as inputs. The throughput required by each user is calculated by summing the minimum recommended throughput of each used service (Table 3.1). Knowing this and the throughput per RB allows one to calculate the number of required RBs for each user with

$$N_{RB} = \left\lceil \frac{R_{user\,[\text{Mbit}\cdot\text{s}^{-1}]}}{R_{RB}(\rho_N)_{[\text{Mbit}\cdot\text{s}^{-1}]}} \right\rceil, \tag{3.25}$$

where

- R_{user} is the user required throughput;
- R_{RB} is the highest throughput per RB at the user's SNR, given by

$$R_{RB[\text{Mbit}\cdot\text{s}^{-1}]} = \max\{R_{RB}^{QPSK}(\rho_N), R_{RB}^{16-QAM}(\rho_N), R_{RB}^{64-QAM}(\rho_N), R_{RB}^{256-QAM}(\rho_N)\}. \quad (3.26)$$

As explained in [1], the power to use in NR link budget calculations is the power transmitted per SC. In order to calculate a user's transmission power, at first, the maximum value for this is considered: the maximum antenna beam power in a single RB (which always has 12 SCs; Section 2.1.4). As this is the maximum possible power applied to a SC, it yields the maximum received power in (3.22), and consequently the maximum throughput per RB at the user's distance, which gives the minimum number of RBs for this user (taking into account the gain losses due to the user's position with (3.20) and due to the user absorption). After calculating the minimum number of required RBs, if the transmission throughput to the user (R_{TX}) surpasses the required one, the transmission power to the user (P_{user}) is lowered until the transmission throughput matches the required throughput or until the transmission power is equal to the power of one element (P_{ele}). As the studied antenna has 192 elements, the power per element is considered to be the antenna's maximum transmission power equally distributed over all elements (Annex C). When the transmission throughput is not higher than the required one, the same process is applied in reverse, comparing to see if the transmission throughput is lower than the required one, while not allowing for any user to require more power than the maximum power per beam (P_{beam}^{max}). This sub-model yields the transmission power to each user, along with their required number of RBs and their transmission throughput.

Knowing the beams' user composition and the power each user requires, it is possible to calculate each beam's transmission power, as it is the sum of the required power from all users that are in that beam. To prevent an unrealistic BS power usage, some physical layer verifications are performed, as shown in Figure 3.19. These stop users from using too many RBs and/or power, assuring that each beam does not exceed its maximum power and that the antenna is transmitting at least the minimum transmission power (P_{TX}^{min}) [71]. These verifications yield the transmission power of each beam and the number of required RBs per user.

3.5 Compliance distance and exclusion zone

Knowing each beam's transmission power over time, and in order to compare with the values shown in Figure 2.8, one must obtain an expression to find the power density over distance of each beam, and calculate, for each moment in time, at which distance its value equals the maximum defined by ICNIRP guidelines [10] - this is denominated as the compliance distance. As per [1], in the far-field, where the angular field distribution is known (Chapter 2), the electric field strength can be related to the power density level with

$$S_{[\text{W}\cdot\text{m}^{-2}]} = \frac{E^2_{[\text{V}\cdot\text{m}^{-1}]}}{Z_{0[\Omega]}}, \quad (3.27)$$

where $Z_0 = 120\pi$ is the free space impedance. Through use of (3.27), one can state that

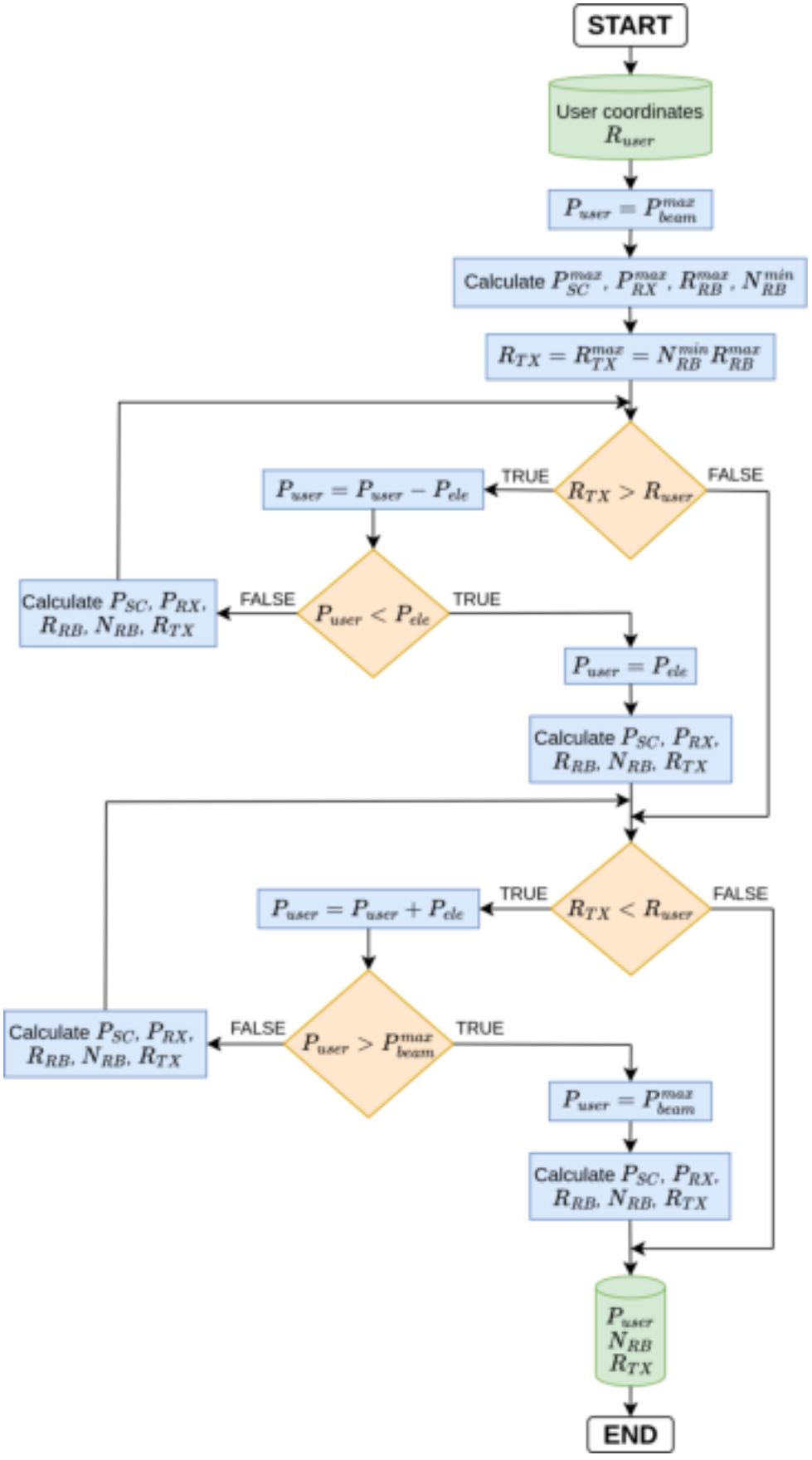

Figure 3.18: Flowchart representation of the steps to calculate any user's throughput, required RBs and power from the BS.

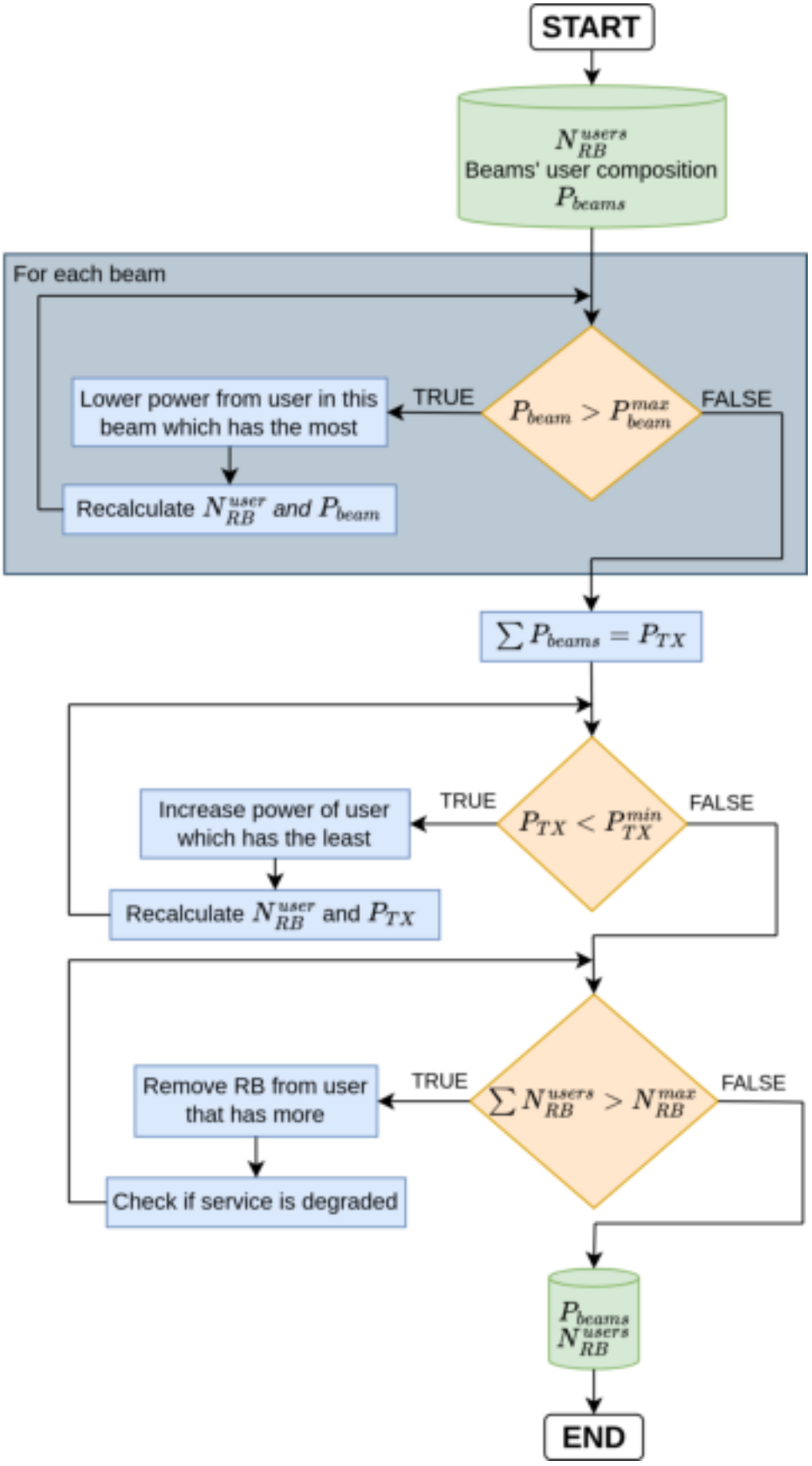

Figure 3.19: Flowchart of the physical layer verifications.

$$E_{lim[\mathrm{V\cdot m^{-1}}]} = \sqrt{S_{lim[\mathrm{W\cdot m^{-2}}]} Z_{0[\Omega]}}, \tag{3.28}$$

where S_{lim} is the maximum allowed power density value, and E_{lim} is taken from (3.13) by assuming

$$E_{lim} = E\big|_{d=d_{comp}}, \tag{3.29}$$

where d_{comp} is the compliance distance. This makes possible to write that, again using (3.13),

$$d_{comp}(\phi,\psi)_{[\mathrm{m}]} = \frac{V_M(P_{TX})_{[\mathrm{V}]}}{E_{lim[\mathrm{V\cdot m^{-1}}]}} f_{\phi\psi}(\phi,\psi). \tag{3.30}$$

Through analysis of (3.30), it can be observed that the compliance distance, for each elevation and azimuth value, is only dependent on the directivity ($f_{\phi\psi}(\phi,\psi)$) and on the transmission power (P_{TX}). As such, one is able to discover the maximum possible compliance distance with

$$d_{comp}^{max}(\phi,\psi)_{[\mathrm{m}]} = d_{comp}(\phi,\psi)_{[\mathrm{m}]}\big|_{P_{TX}=P_{TX}^{max},\, f_{\phi\psi}=1}. \tag{3.31}$$

In the near-field region, the angular field distribution is not known (Chapter 2), and therefore the electric field strength cannot be related to the power density as per (3.27). For this reason, the model only considers valid values of the compliance distance that are greater than the near-field radius given by (2.6). With (3.30) it is possible to know that the square of transmission power and the compliance distance are proportional to each other. As such, there is a transmission power limit below which the EZ cannot be calculated, but the latter must necessarily have a lower value than the EZ for the transmission power limit. As a conservative measure, the model states that the EZ is equal to the near-field radius when the transmission power is below this limit. Using (3.30) and (3.14), the transmission power limit can be found with

$$P_{TX}^{lim}(\phi,\psi)_{[\mathrm{W}]} = \left(\frac{E_{lim[\mathrm{V\cdot m^{-1}}]} d_{ff[\mathrm{m}]}}{f_{\phi\psi}(\phi,\psi)}\right)^2 \frac{1}{30 G_{TX}^{max}}. \tag{3.32}$$

Knowing the compliance distance over time makes it possible to estimate the value for the EZ. The model is run multiple times for the same scenario, and from each run it saves each beam's broadside compliance distance over time,

$$d_{comp}^{beams} = \{d_{comp,1}(t), d_{comp,2}(t), ..., d_{comp,n}(t)\}, \tag{3.33}$$

where n is the number of beams. From these, the model is able to calculate the absolute maximum broadside compliance distance,

$$d_{comp}^{abs} = \max\{d_{comp}^{beams}(t)\}, \tag{3.34}$$

which is the maximum value that any beam had at any given time, and the maximum average broadside compliance distance (the maximum average over time from among all beams in each run),

$$d_{comp}^{avg} = \max\{\overline{d_{comp,1}}, \overline{d_{comp,2}}, ..., \overline{d_{comp,n}}\}, \tag{3.35}$$

where $\overline{d_{comp,n}}$ indicates the average compliance distance value for beam n. This allows one to calculate the Probability Distribution Function (PDF) and the Cumulative Distribution Function (CDF) of these parameters, and to retrieve p-percentile values from the latter, which are used to define the EZ - this is summarised in Figure 3.20, and is further discussed in Chapter 5.

The computation of the EZ in this thesis assumes NR as the only active mobile telecommunications system in the BS. As such, multiband exposure is not addressed - a comparison of NR against previous technologies is made in [13].

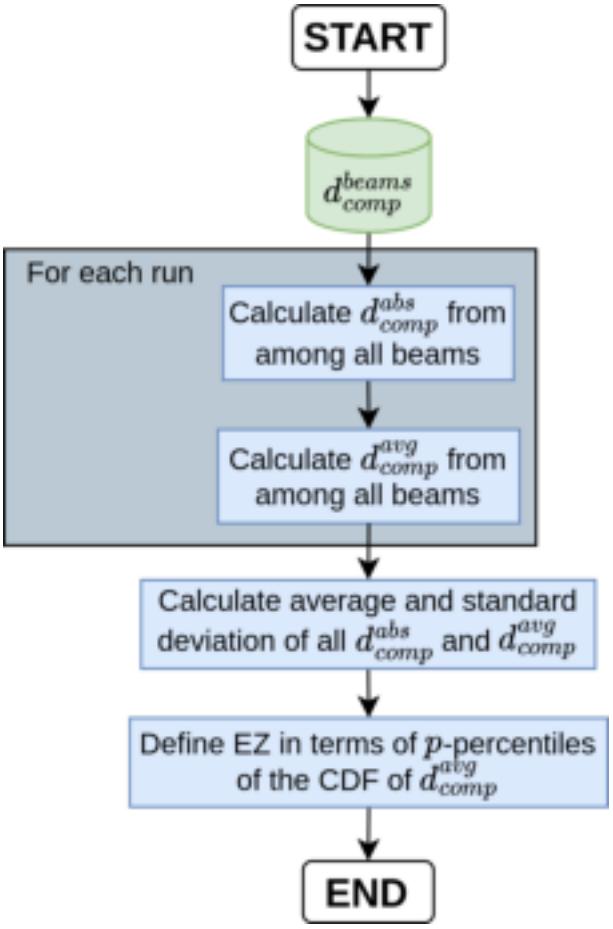

Figure 3.20: Flowchart representation of the EZ calculation.

3.6 Model assessment

In order to discover if the results yielded by the model are realistic, a set of empirical tests are designed, with their description shown in Table 3.3. These are designed to test unlikely but possible scenarios, such as an over usage situation (Test ID 1) or no usage at all (Test ID 2). A worst case situation is also tested in Test ID 3 and the physical properties of the model are tested in Test ID 4.

Table 3.3: Validation tests.

Test ID	Test description
1	Increase the average number of users by a factor of 3 and verify that the system behaves within its limits
2	Have no users making use of the system and verify that the BS does not transmit anything
3	Verify that the compliance distance increases with transmission power
4	Place the maximum number of users at the BS's maximum range, making use of the service with the highest throughput requirement (Table 3.1) and verify that the system behaves within its limits

By observing Figure 3.21, which represents the system in an over usage situation (Test ID 1), one can conclude that the system behaves within its limits in this situation, although all beams have the transmission power near the maximum and the RB allocation is close to 100 % (the number and colour of each beam is in accordance with Figure 3.15). Because of this, the compliance distance is also close to its maximum value in all beams. As an additional parameter, the number of serviced users can be seen to be less than their total number, as is expected in an over usage situation.

Test ID 2 completed with expected results - no users means no transmission power from the BS, which implies that there is no EZ, which is what the model states.

To execute Test ID 3, (3.30) is plotted for several values of transmission power (maintaining the directivity value). The resulting compliance distance can be seen in Figure 3.22, and as expected, it increases with transmission power.

Figure 3.23 shows the system under Test ID 4, a worst case situation (where again the number and colour of each beam is in accordance with Figure 3.15). In it, it can be seen that not all users are serviced - this is because each requires too many RBs (their allocation is near the maximum). In spite of this, beams are not at the maximum transmission power, they are only near it. This is because while each user requires a lot of RBs, the transmission power to them is not high - their throughput requirements are met nonetheless. The transmission power of the beams varies over time because when users have the same number of RBs and their sum is over 100 %, the model withdraws a RB from a random user, which deservices some users. There is no change in the number of users nor in the RB share because of the average access time of the service with the highest throughput requirement (Table 3.1).

These results validate the values presented by the model.

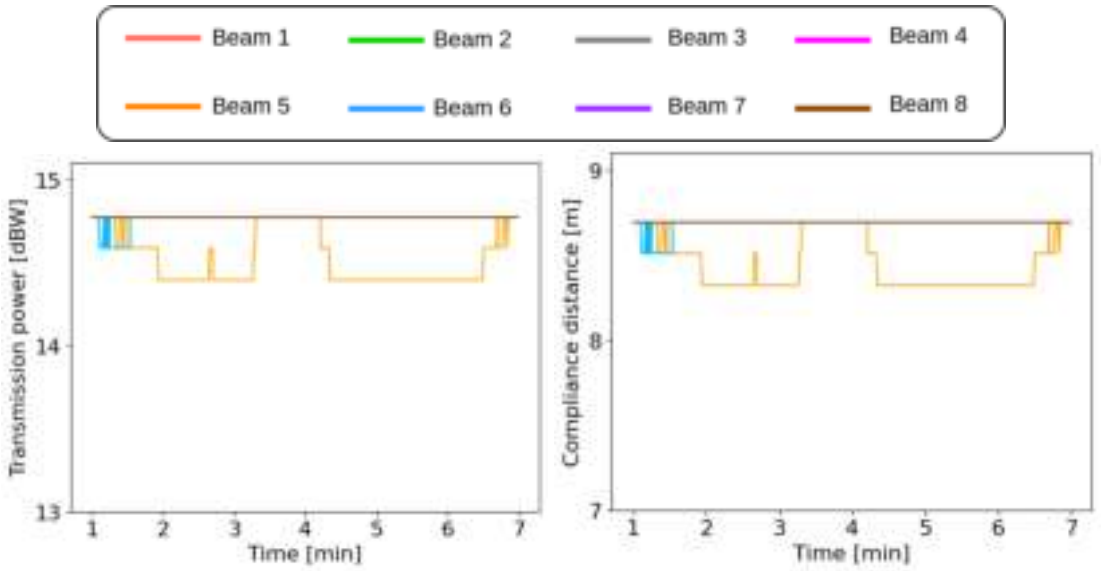

(a) Beam power over time.

(b) Compliance distance for each beam, over time.

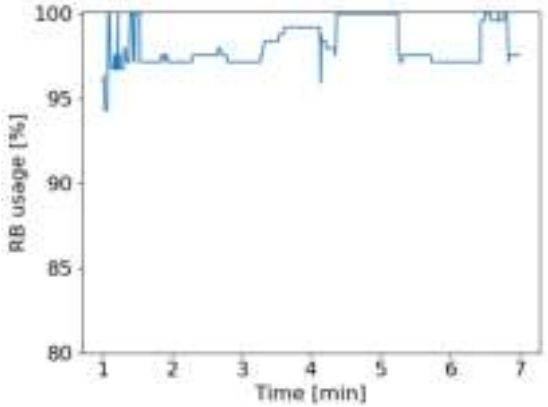

(c) Percentage of allocated RBs over time.

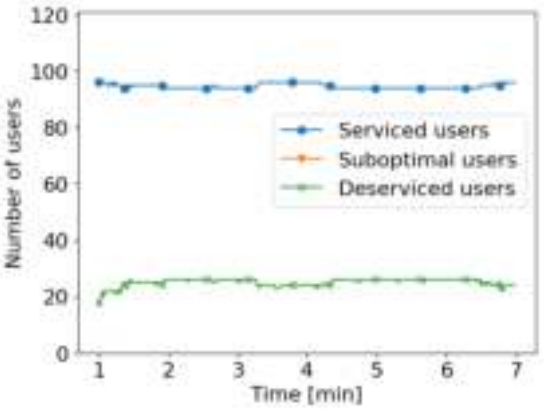

(d) Number of users over time.

Figure 3.21: System in an over usage situation.

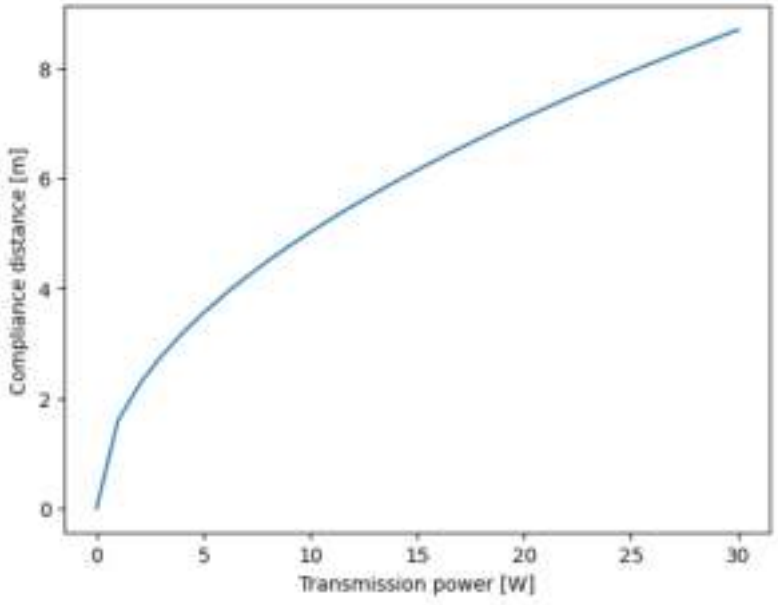

Figure 3.22: EZ distance with respect to the transmission power, along the direction of maximum gain.

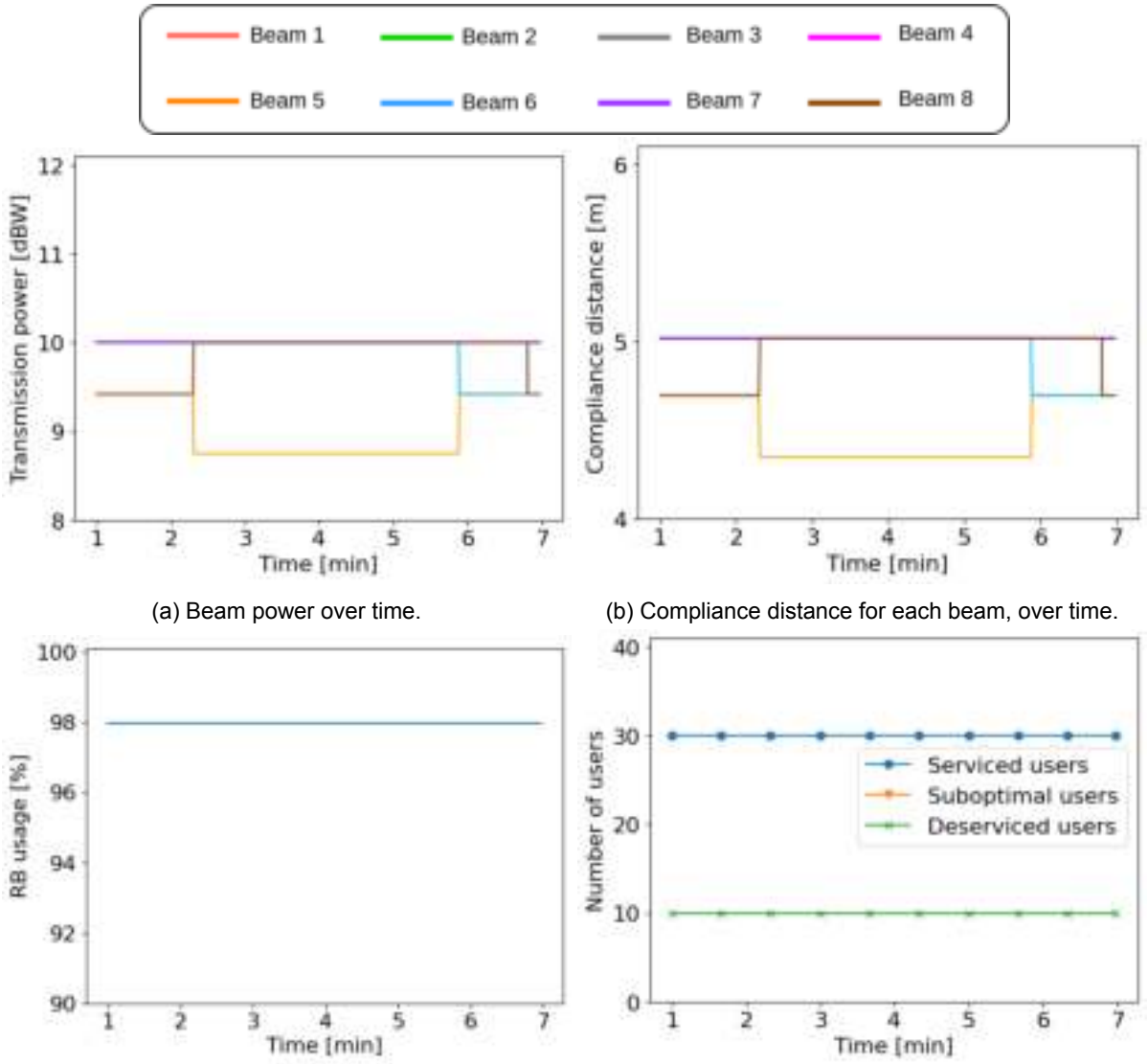

(a) Beam power over time.

(b) Compliance distance for each beam, over time.

(c) Percentage of allocated RBs over time.

(d) Number of users over time.

Figure 3.23: System in a worst case situation.

Chapter 4

On-site measurements

This chapter presents the analysis of the obtained on-site measurements, together with their procedure and a discussion on the obtained results. A comparison to previous work and to the developed model is made.

4.1 On-site measurements procedure

Besides developing the model to calculate the EZ around an active antenna, this thesis also has as an objective the analysis of the behaviour of the EMF around it, and determine if the simulation performed in [13] approximates reality. To do so, and to compare with the results from the developed model (Chapter 3), on-site measurements were performed. Two BSs around Lisbon were visited. Their description is presented in Annex D, and maps of the measurements made around them are shown in Figure 4.1 and Figure 4.2. The NOS Telecomunicações (NOS) BS is equipped with a NOKIA AirScalexxxx antenna [72] and the MEO Telecomunicações (MEO) BS is equipped with a Huawei AAUxxxx antenna [71]. As stated in Section 2.4.2, the near-field region surrounding an antenna has a limit distance given by (2.6). In the Huawei antenna, $D_L >= 0.086\lambda$, where D_L is the diagonal of a subarray (Annex C). The largest dimension of the NOKIA antenna is not known, although it should not be significantly different from Huawei's. In addition to this, it is known that the NOS BS is working in the frequency interval $[3.61, 3.71]$GHz and that the MEO BS is working in the frequency interval $[3.71, 3.8]$GHz. This information allows one to calculate the upper limit of this region for a single beam for the Huawei antenna: $d_{ff\text{Huawei}} \in [3.4, 3.6]$m; $d_{ff\text{NOKIA}}$ is assumed to be equal. This, together with Figure 4.1 and Figure 4.2, leads to the conclusion that every measured point is outside the near-field region of their respective antennas' beams. As in the near-field region the electric and magnetic fields are not necessarily in phase to each other, power density cannot be derived as per (3.27). For this reason, coupled with no knowledge at the time of measurement of what field the measurements were being done in, the electric field strength was measured, and not power density.

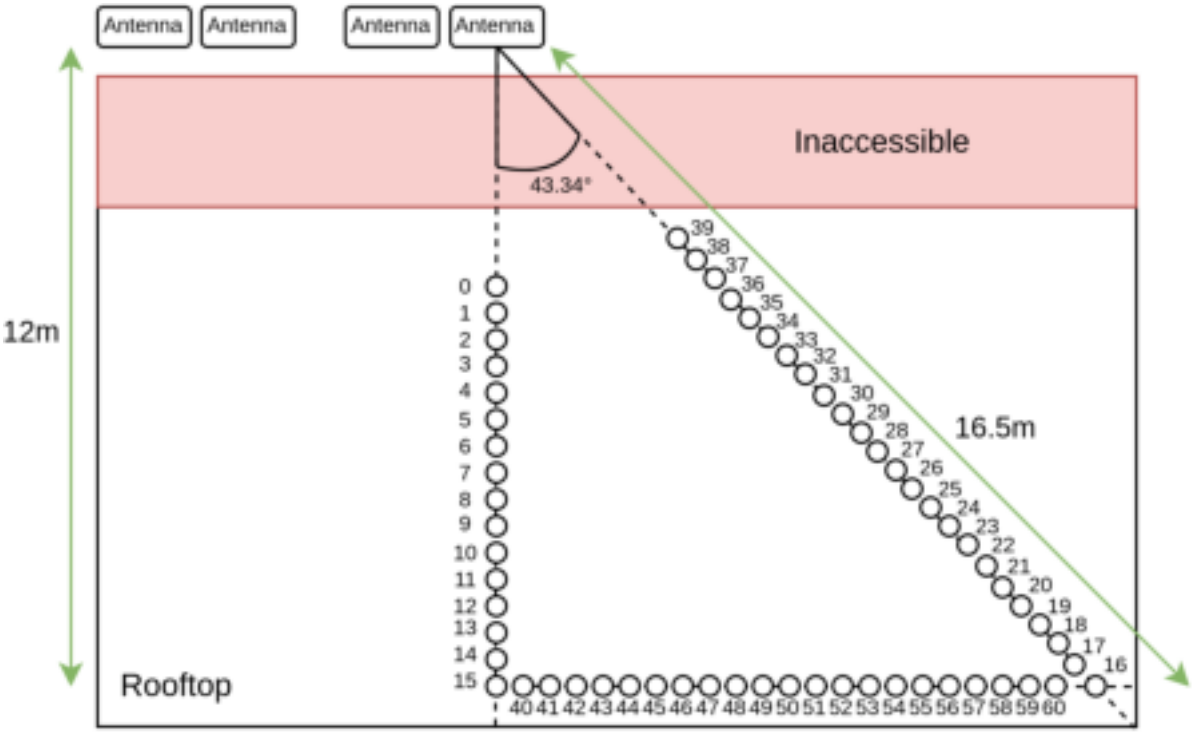

Figure 4.1: NOS BS horizontal sketch, along with the measurement points.

As the objective of the on-site measurements was to retrieve information in order to be able to describe

the EMF behaviour around the antenna, a channel with a time-constant, load-independent transmission power must be measured (otherwise, characterising the electric field strength over distance is impossible as the transmission power could vary in between measurements). For this reason, a static broadcast beam was measured: the Secondary Synchronisation Signal (SSS) in the Synchronisation Signal Block (SSB) [64]. These measurements were carried out only in the frequency of the SSB, which is defined for each individual system. In each measurement point, the electric field strength was measured for 1 min. Since these values are not to be compared with ICNIRP guidelines [10], it was not necessary to measure for 30 min. The equipment used for all on-site measurements was the Narda SRM-3006 field strength analyser [73] with a probe antenna capable of measuring EMF frequencies up to 6 GHz [74]. Details of the measurement procedure and guidelines can be found in [75, 76]. The probe is, at all times, 1.1 m from the ground.

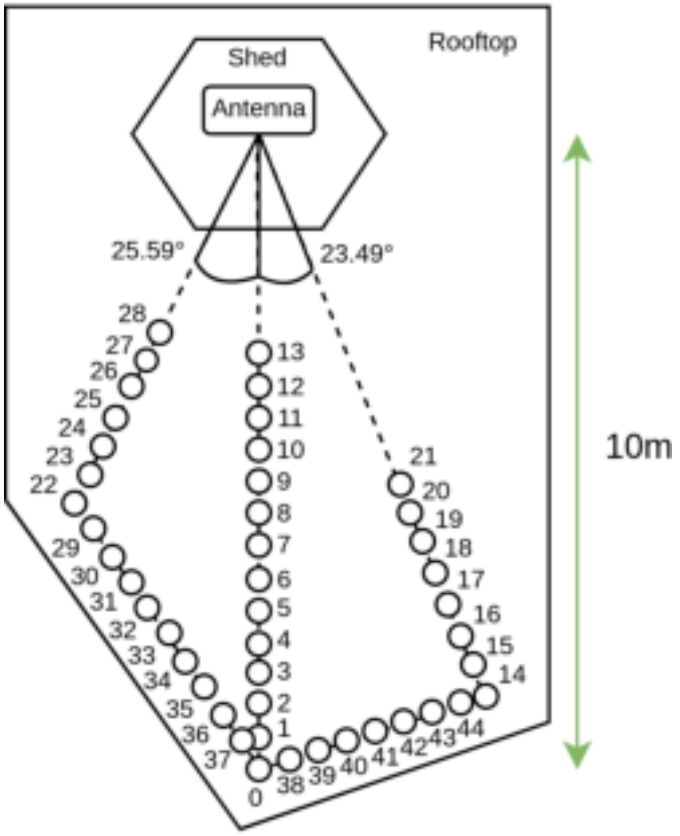

Figure 4.2: MEO BS horizontal sketch, along with the measurement points.

4.2 On-site measurements results and discussion

Computer simulations were made in [13] to simulate the behaviour of the EMF both in the far-field and in the near-field. However, the simulation produced results that were obtained by measuring along the direction of maximum gain of the antenna, which is very difficult to perform on-site, and cannot be done with measurements on the terrace of the BS. For this reason, the performed on-site measurements do

not suffice to prove or disprove the simulation performed in [13]. Furthermore, straight lines along the terrace of the BS may not be aligned with the direction of the any beam's maximum gain; along straight lines on the floor, several beams may be measured, as exemplified by Figure 4.3 and Figure 4.4 (which are exaggerated to better exemplify this). This shows that the performed on-site measurements are not adequate for comparison with results from the model either. One would need to measure the electric field strength along the direction of maximum gain of any single beam, which is difficult to perform on-site, in practise.

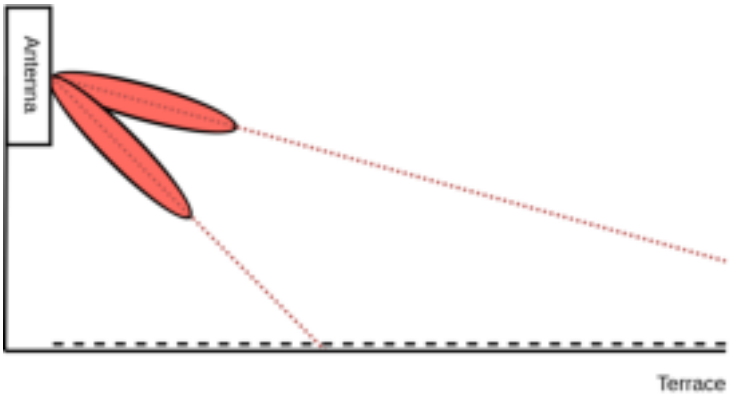

Figure 4.3: Vertical BS sketch with a straight line across the terrace.

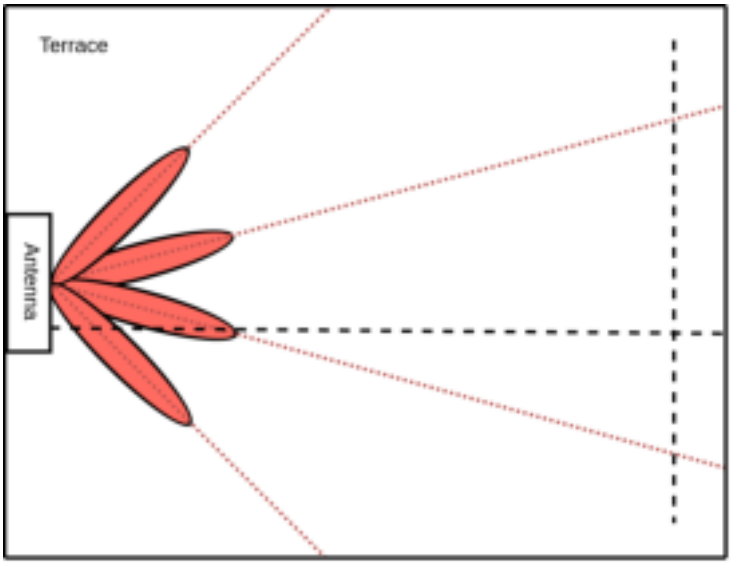

Figure 4.4: Horizontal BS sketch with straight lines across the terrace.

Nonetheless, the measurements can be useful to determine if there is any correlation between distance from the antenna and the electric field strength. Measurement point examples are shown in Figure 4.5, and from them it can be stated that the electric field strength is not continuous over time. This can be explained by the way the Huawei AAUxxxx antenna spatially distributes the SSB channel. As exemplified in Figure 4.6, this channel is periodically transmitted throughout the antenna's coverage range [64]. Because of this, any arbitrary point in space does not have a time-constant electric field strength, and so, the performed on-site measurements do not suffice to describe the behaviour of the EMF around the antenna; one would need to know the period of the SSB's spatial distribution and assure that no power control methods are in place.

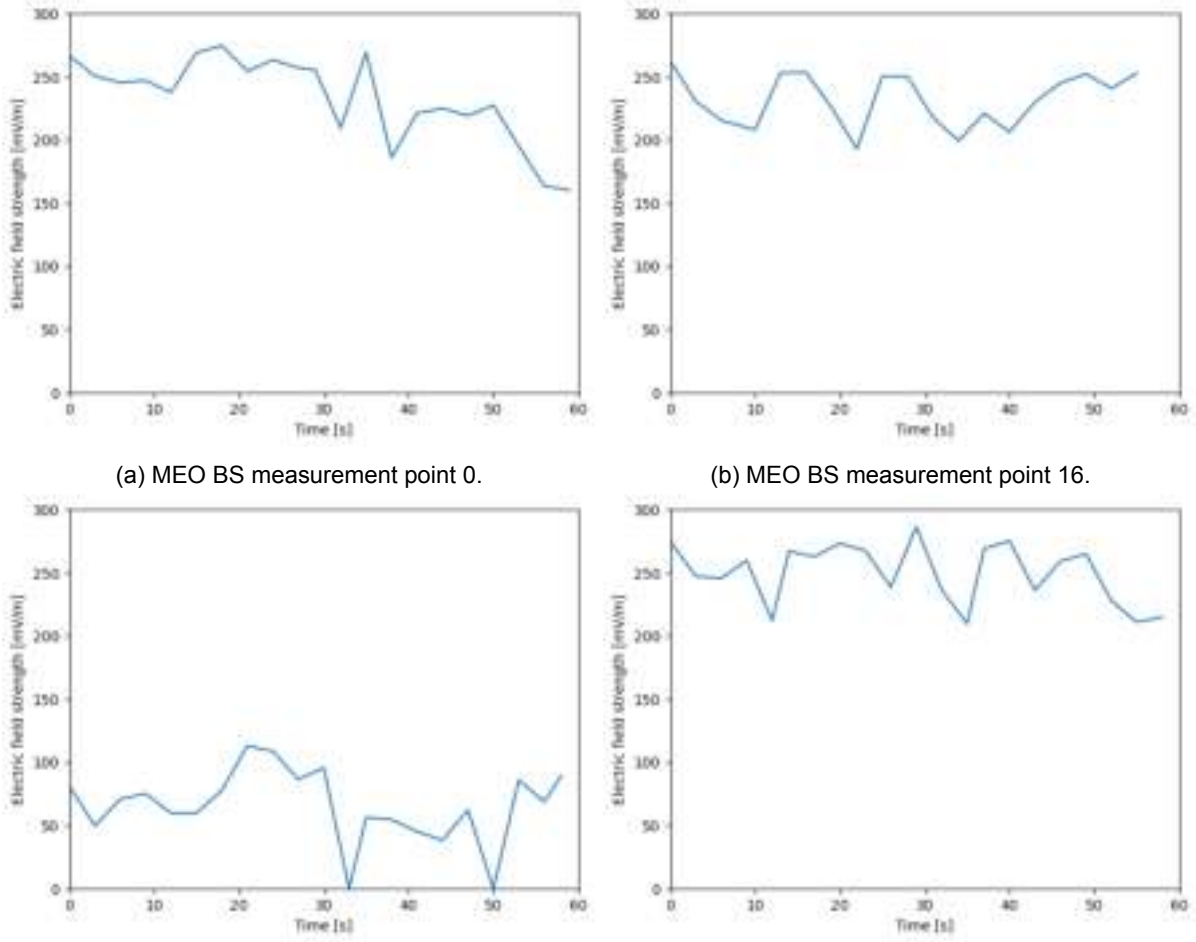

(a) MEO BS measurement point 0.

(b) MEO BS measurement point 16.

(c) NOS BS measurement point 7.

(d) NOS BS measurement point 21.

Figure 4.5: Measurement point examples.

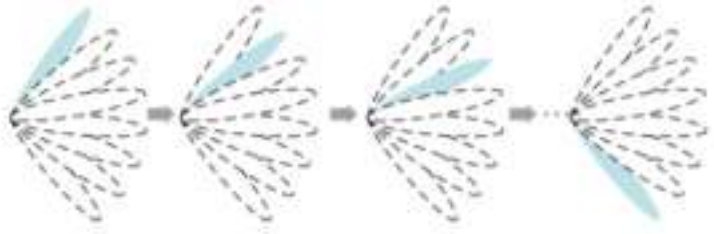

Figure 4.6: SSB beams spatial distribution (extracted from [64]).

However, even without knowing the spatial distribution of the SSB, one can average the obtained results along a straight line and check whether any pattern emerges. As several measurements are made along straight lines from the antennas (Figure 4.1 and Figure 4.2), it is possible to plot the electric field strength along them: from every point of measurement in the same straight line, the maximum, average and minimum values were recorded. Examples of these results are shown in Figure 4.7 and Figure 4.8, and these imply that there is not any obvious correlation between the strength of the electric field and the distance from the antenna. In Figure 4.7b the electric field strength seems to increase with distance, while in Figure 4.8c it seems to decrease with respect to it.

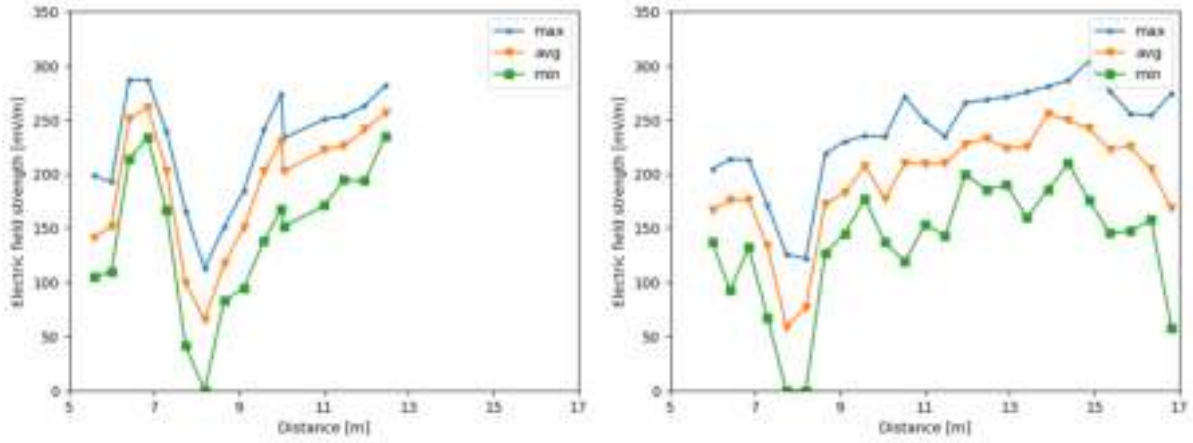

(a) 0° straight line.

(b) 43.34° straight line.

Figure 4.7: NOS BS electric field strength over distance.

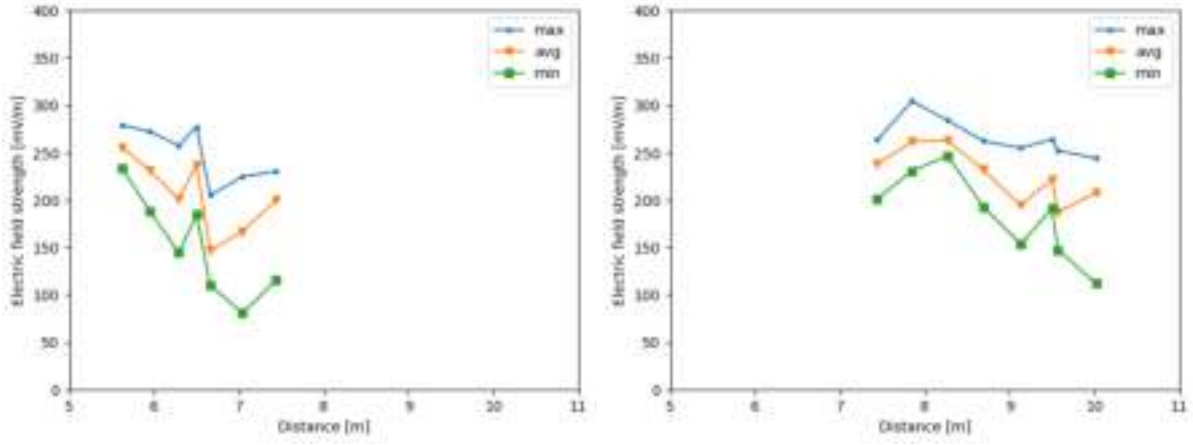

(a) −25.59° straight line.

(b) 23.49° straight line.

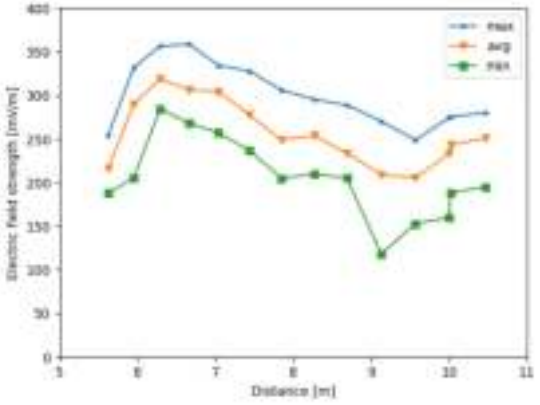

(c) 0° straight line.

Figure 4.8: MEO BS electric field strength over distance.

These measurements show that it is very difficult to analyse the behaviour of the EMF around a working production BS, whether due to the impossibility of measuring along any beam's maximum gain, or due to the nature of the site itself, or even due to the spatial distribution of the SSB. In order to retrieve any valid conclusion, these measurements should be conducted in a controlled environment.

Chapter 5

Model results

This chapter details the created scenarios in terms of input parameters to the model. The results from the model are shown and some conclusions are drawn up from them.

5.1 Scenarios' parameters

Real user statistics from antennas with the highest average RB usage were provided by Huawei [77]. From these, it is possible to obtain information about the number of active DL UEs over four days, which is presented in Table 5.1 (active users are those that are actively communicating with the BS, not just connected to it). As growth in 5G usage is expected to rise over the coming years [6], the maximum number of active UEs is considered as average in the simulation. The created services shown in Table 3.1 do not have the same usage share in all scenarios - that is shown in Table 5.2. The values are arbitrary and just serve to differenciate the scenarios further.

Table 5.1: Statistics on the number of active DL UEs in one sector of the BS, over four days [77].

	Day 1	**Day 2**	**Day 3**	**Day 4**
Maximum	39	36	33	32
Average	22	20	18	18
Minimum	1	2	1	1

Table 5.2: Services' utilisation share in different scenarios.

		Services' utilisation share [%]			
	Service	**Street**	**Bus stop**	**Residential building**	**Demonstration**
Non real-time	Web browsing	15	17	20	11
	Video download	5	5	5	5
	Large file download	2	1	5	1
	E-mail	4	7	15	7
	Online chat	30	30	9	30
Real-time	Video conference	2	1	15	2
	Gaming	7	9	2	15
	Video streaming	5	9	13	11
	Augmented / Virtual reality	5	6	9	6
	Audio streaming	25	15	7	12

In Chapter 3, realistic usage scenarios are defined. Each of them can be defined by a list of input parameters that are fed into the model. The default input parameters are shown in Table 5.3, and most can also be seen in Annex C, as they are tailored to replicate the studied antenna. Each scenario is based on a real location around Lisbon, as stated in Table 5.4, and each changes or adds some parameters in order to realistically represent itself. Regarding the demonstration scenario, as the number of people should be higher than usual, the minimum and maximum number of users is increased by a multiplier of 2.

Table 5.3: Default input parameters.

Parameter category	Parameter	Default value
Environmental	Antenna height (h_a) [m]	5.5
	Street width (d_{street}) [m]	Defined per scenario
	Building height (h_b) [m]	Defined per scenario
Operator	Elevation and azimuth range (ψ, ϕ) [°]	(± 15, ± 60)
	Mechanical tilt (γ) [°]	-13
	Numerology (μ)	1
	MIMO order (N_{MIMO})	4
	Transmit gain (G_{TX}) [dBi]	25
	Bandwidth (B_W) [MHz]	90
	Total number of elements and per beam (N_{ele}, N_{ele}^{beam})	(192, 24)
	Beamwidth (θ_{3dB}^{v}, θ_{3dB}^{h}) [°]	(20, 10)
	RB cutoff [%]	60
	DL time allocation [%]	75
	Power range (P_{TX}^{min}, P_{TX}^{max}) [W]	(15, 240)
User	Receiver gain (G_{RX}) [dBi]	0
	Number of users (N_{users}^{min}, N_{users}^{max})	(5, 40)
	New user period (t_{user}) [s]	1
	User height (h_{user}) [m]	1.8
	User losses (L_{user}) [dB]	3
	Noise figure (F) [dB]	5
	Services' average download size	Table 3.1
	Services' average access time	Table 3.1
	Services' minimum throughput	Table 3.1
	Services' utilisation share	Table 5.2

Table 5.4: Created scenarios and the real locations they simulate.

Created scenario	Real location	BS building height [m]	Added parameters
Street	Avenida Infante Dom Henrique	10	d_{street} = 68 m
Bus stop	Basílica da Estrela	15	d_{street} = 48 m
Residential building	Avenida Fontes Pereira de Melo	30	d_{street} = 23 m h_{rb} = 50 m
Demonstration	Jardim do Arco do Cego	18	d_{fp} = 54 m (d_{min}^{demo}, d_{max}^{demo}) = (10, 130) m (N_{users}^{min}, N_{users}^{max}) = (10, 80)

In order to compare with ICNIRP limits shown in Figure 2.8, a single run of the model, as detailed in Chapter 3, consisted of 6 min of nominal operation (besides the first minute, which is ignored for the model to reach nominal operation). While each run of the first two scenarios takes around 2 s to complete, each run of the residential building scenario takes around 7 min and each run of the demonstration scenario takes from 10 min to 45 min to complete. For this reason, the simulation of the street, bus stop and residential building scenarios consisted of 1000 runs, while the simulation of the demonstration scenarios consisted of 186 - this information is contained in Table 5.5. All plots in this chapter refering to the same scenario are of the same run.

Table 5.5: Number of runs and run duration in each scenario's simulation.

Scenario	Number of runs	Run duration [s]
Street	1000	2
Bus stop	1000	2
Residential building	1000	420
Demonstration	186	[600, 2700]

5.2 Beam transmission power over time

The beam transmission power over time in each scenario is shown in Figure 5.1, where the number and colour of each beam is in accordance with Figure 3.15. As seen in Figure 5.1, the street and bus stop scenarios only have 4 active beams - this is a consequence of the user distribution in these scenarios (Section 3.2). Furthermore, Figure 5.1 shows that beams from the same antenna can have very different levels of transmission power, and that they are rarely near their maximum value of 14.8 dB (all 24 elements in a beam radiating at maximum power). As an additional metric, Figure 5.1 also shows that, in any given 6 min period, it is likely that no beam is off - this is because the average access time of real-time services, shown in Table 3.1, is usually greater than the simulation run time; each beam fluctuates around a median value over the course of the run for the same reason. As the demonstration scenario has an higher minimum and maximum number of users, beams are closer to their maximum transmission power.

Knowing the transmission power of all beams, and each beam's user composition, it is possible to calculate the power density each user receives with the help of (3.13) and (3.27). Recalling Figure 2.8 and observing Figure 5.2 (where each line represents a different user), it can be stated that users are always subjected to a power density level under the imposed limit. It is also of note that the power density level received by each user does not fluctuate a lot - this is again because the average access time of real-time services, shown in Table 3.1, is usually greater than the simulation run time. Another point to retrieve from Figure 5.2 is that users are subjected to power density changes even if they do not alter their service; as beams serve multiple users, a change in one service in one user may impose a transmission power change in the beam, thereby affecting all users that are serviced by it. One further observation from Figure 5.2 is that the average power density received by users in the residential building scenario is greater than in other scenarios, in spite of having nominal beam transmission powers (Figure 5.1) and the same number of users as the street and bus stop scenarios (Figure 5.6). This can be explained by the users' distance distribution in this scenario; in fact, knowing (3.4), (3.8) and (3.11), and using the

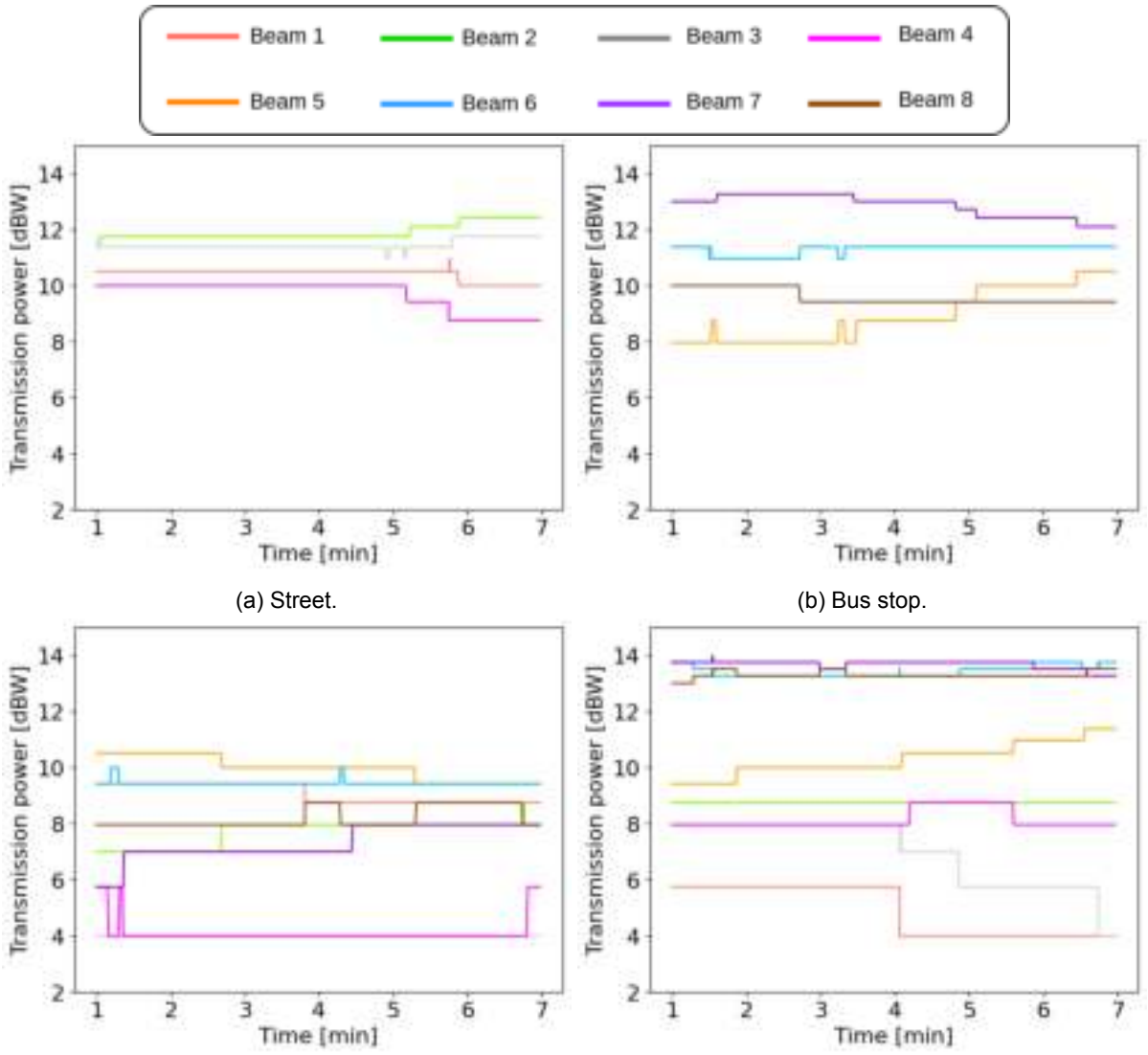

(a) Street.

(b) Bus stop.

(c) Residential building.

(d) Demonstration.

Figure 5.1: Beam transmission power over time in the different scenarios.

values shown in Table 5.4, it is possible to calculate the minimum and maximum user distance in each scenario, which is presented in Table 5.6. Figure 5.3 reveals how received power density decreases with an increase in user distance, for a few values of transmission power and a fixed directivity (making use of (3.13) and (3.27)). Table 5.6 and Figure 5.3 confirm that user distance in the residential building scenario is indeed lower than in other scenarios, and that this causes the noticed increase in the average received power density.

5.3 Service distribution, number of users and RB usage

It is possible to plot how services are being requested by users, recalling that the values shown in Table 5.2 are arbitrary. Real-time services of a run in each scenario are shown in Figure 5.4 and non real-time services are shown in Figure 5.5.

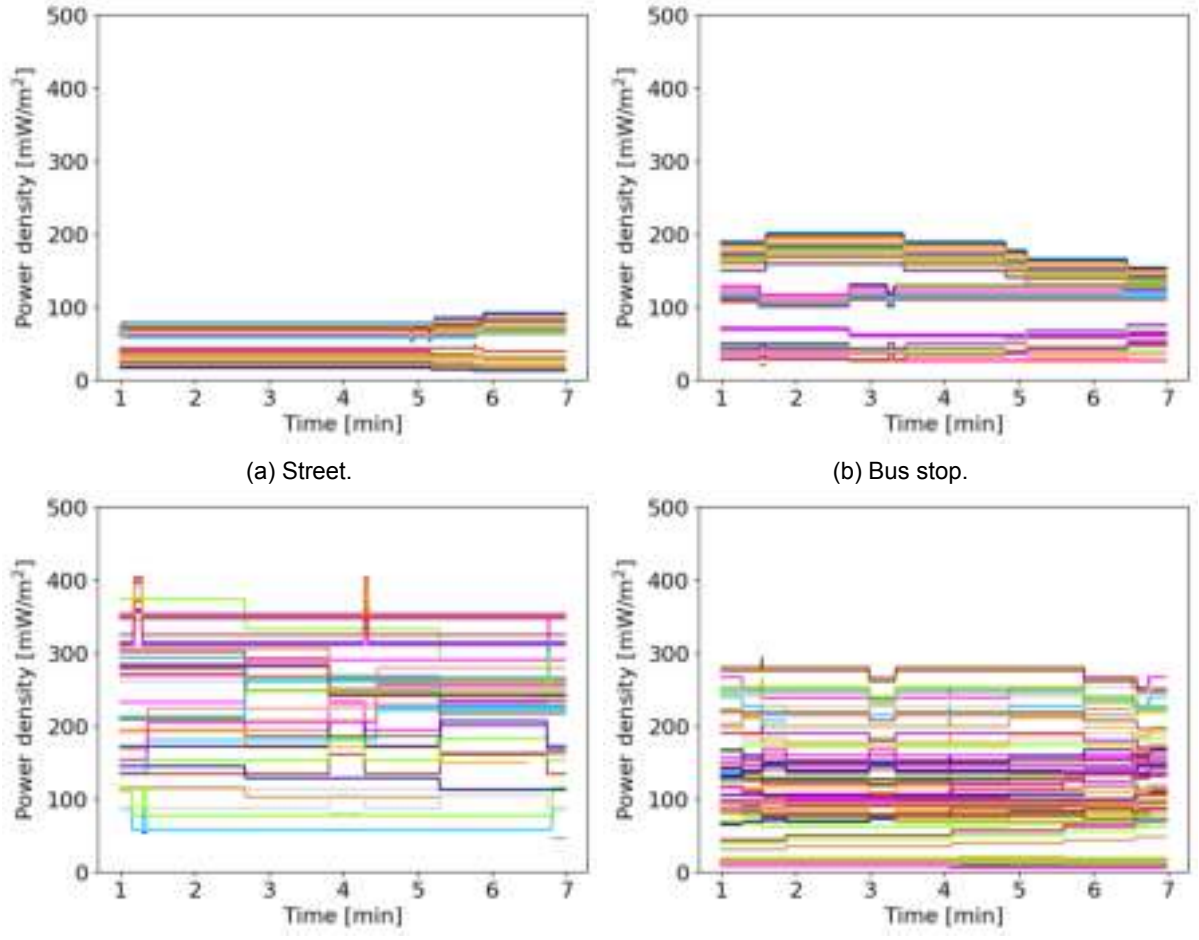

(a) Street.

(b) Bus stop.

(c) Residential building.

(d) Demonstration.

Figure 5.2: User received power density over time in the different scenarios.

Table 5.6: Minimum and maximum user distance to the BS in each scenario.

Scenario	Minimum user distance [m]	Maximum user distance [m]
Street	68.1	136.1
Bus stop	48.2	96.1
Residential building	23.0	47.6
Demonstration	46.2	131.8

Analysing Figure 5.4 reveals that almost every user makes use of a real-time service (their sum closely resembles the number of users, shown in Figure 5.6), and that once a user requests a real-time service, it is likely that its access time surpasses the simulation run time (the number of any real-time service tends to stay the same or increase). Increasing the simulation run time does not change this - as new users are constantly generated, the sum of real-time services tends to approach the number of users. This is why no beam is ever off and why their transmission power fluctuates around a median value (Figure 5.1).

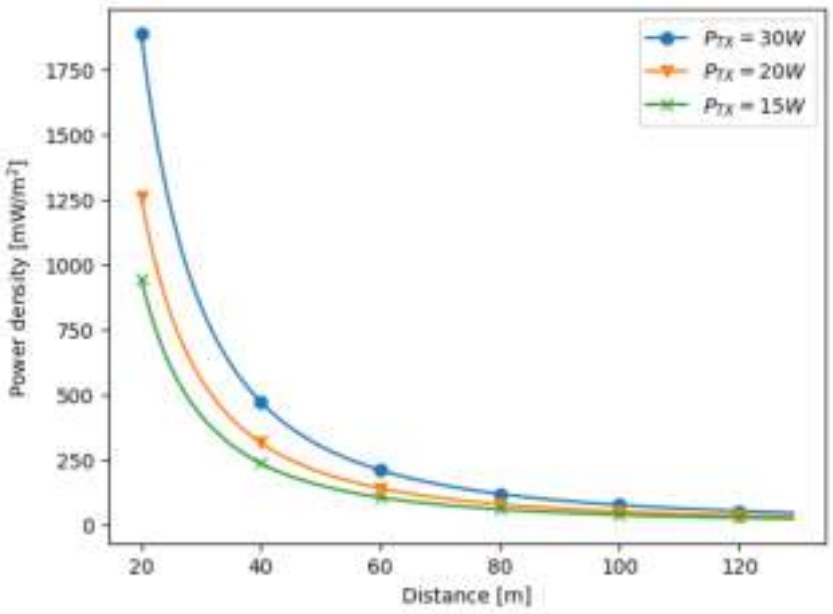

Figure 5.3: Power density with respect to distance, with $f_{\phi\psi} = 1$.

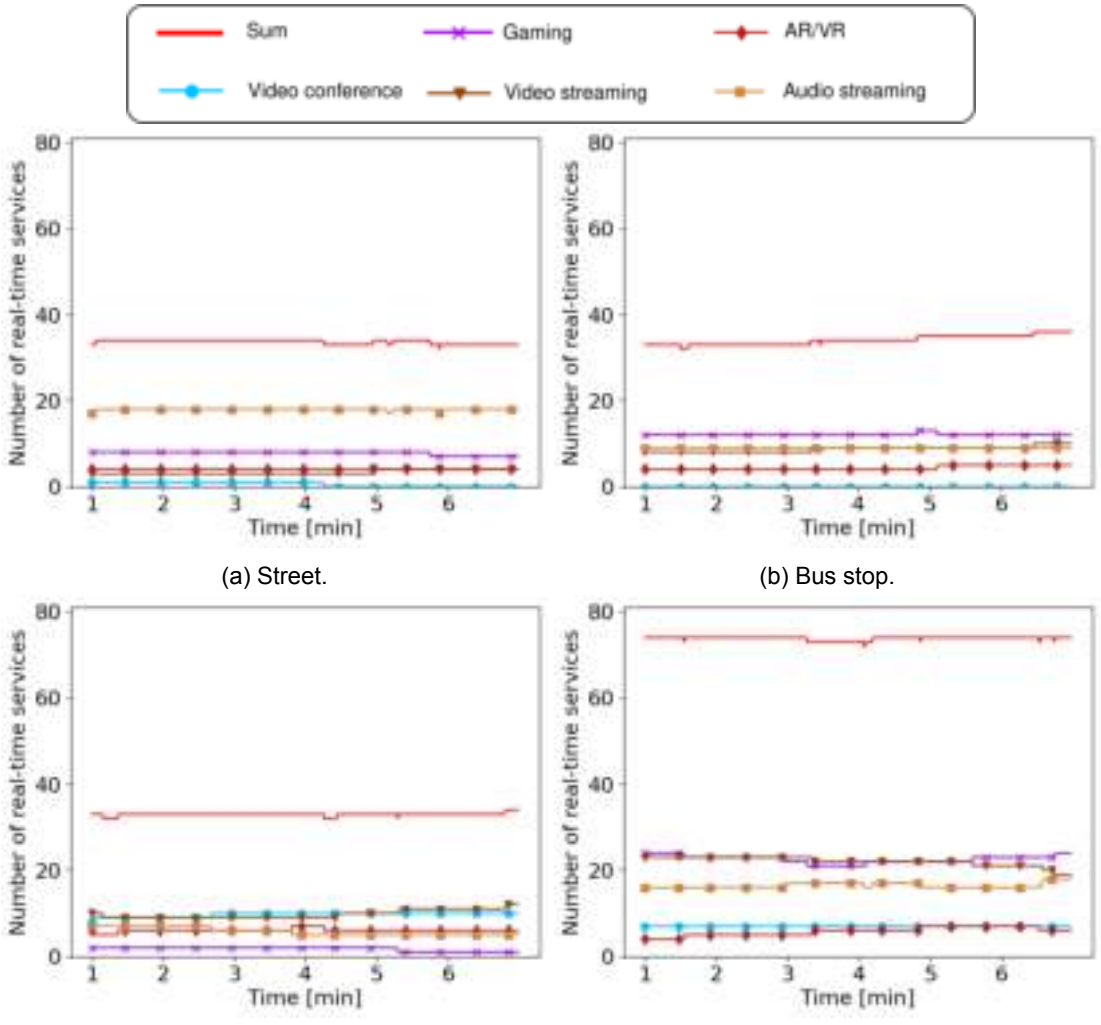

(a) Street.

(b) Bus stop.

(c) Residential building.

(d) Demonstration.

Figure 5.4: Number of real-time services over time in the different scenarios.

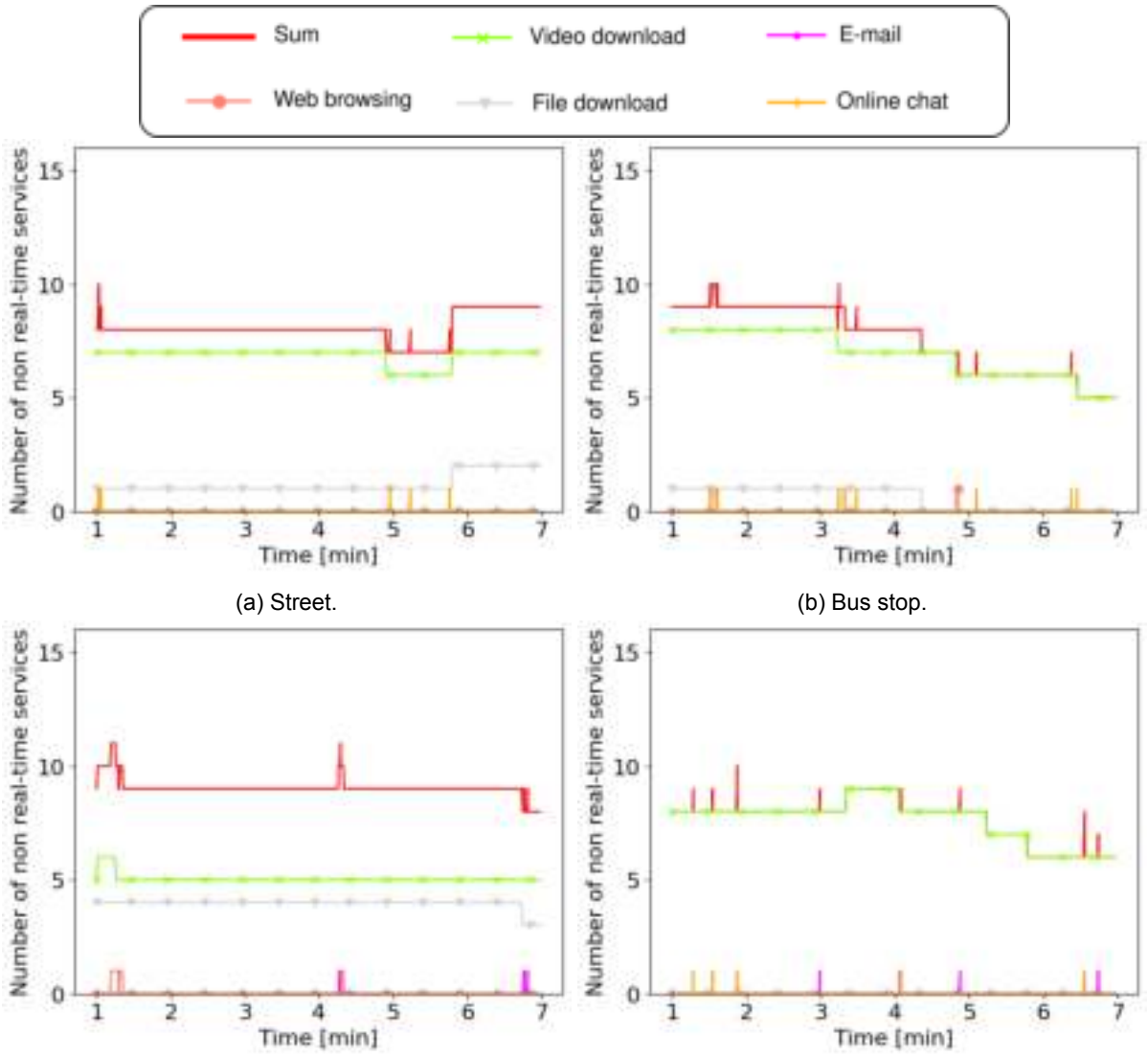

(a) Street.

(b) Bus stop.

(c) Residential building.

(d) Demonstration.

Figure 5.5: Number of non real-time services over time in the different scenarios.

Figure 5.5 showcases the fact that two of the non real-time services defined in Chapter 3 - file and video download - are the only services that always have more than one user simultaneously. This is because these two services possess download sizes much greater than the rest of the non real-time services. For this reason, they require more time to complete (depending on the throughput), and the user may continue using the service all throughout the run - this is more evidenced in Figure 5.5a and Figure 5.5c. On the other non real-time services, a different behaviour can be observed - these have smaller download sizes, so they are completed rapidly - they rarely have more than two users making use of it simultaneously. For this reason, these services only slightly alter the beam transmission power, as can be stated from a comparison with Figure 5.1.

Observing both Figure 5.4 and Figure 5.5 leads to the conclusion that real-time services affect the beam transmission power much more than non real-time services, because of their constant use of the BS.

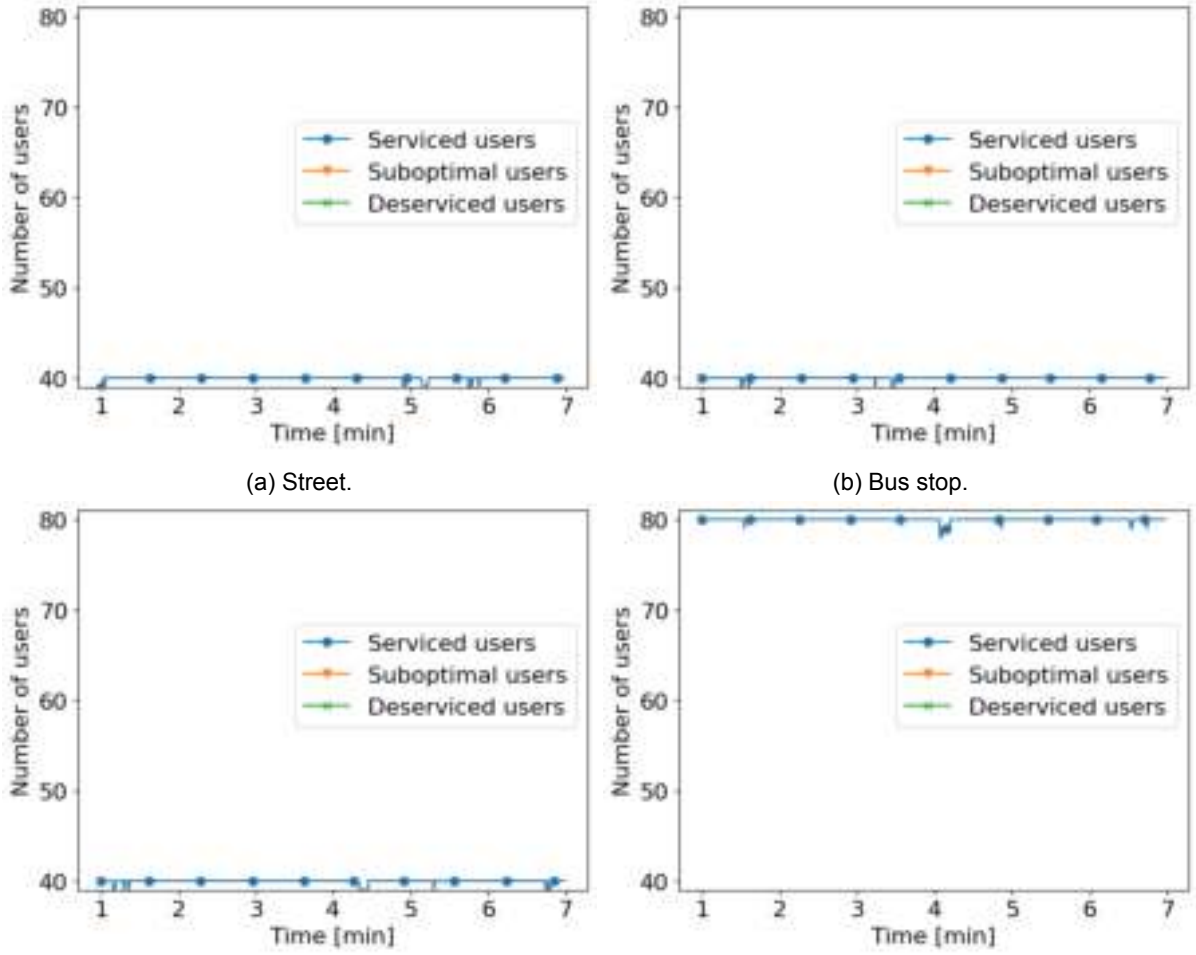

(a) Street.

(b) Bus stop.

(c) Residential building.

(d) Demonstration.

Figure 5.6: Number of users over time in the different scenarios.

Besides this, the amount of RBs used throughout the simulation run can be plotted, as shown in Figure 5.7. This reflects whether the BS nominal operation is near its maximum capacity or not, which depends on the scenario and service requests. While the street, bus stop and residential building scenarios have their nominal operation at around 40 % RB usage, the demonstration scenario presents a nominal operation close to 60 % - this is due to the increase in the number of users that is done in this scenario. These values show that the BSs have capacity to handle more users than what the simulation presents.

5.4 Broadside compliance distance over time

The broadside compliance distance, defined as the compliance distance in the direction of maximum gain of the beam, is retrieved from the beams' transmission power (as stated in Section 3.5). An example of the broadside compliance distance in each scenario is shown in Figure 5.8. As can be deduced from (3.30), the broadside compliance distance only depends on the transmission power (because ($f_{\phi\psi} = 1$)). As such, the broadside compliance distance curve and the beam transmission power curve are identical, only being shifted in the y-axis. In cases where the transmission power is lower than the limit power to

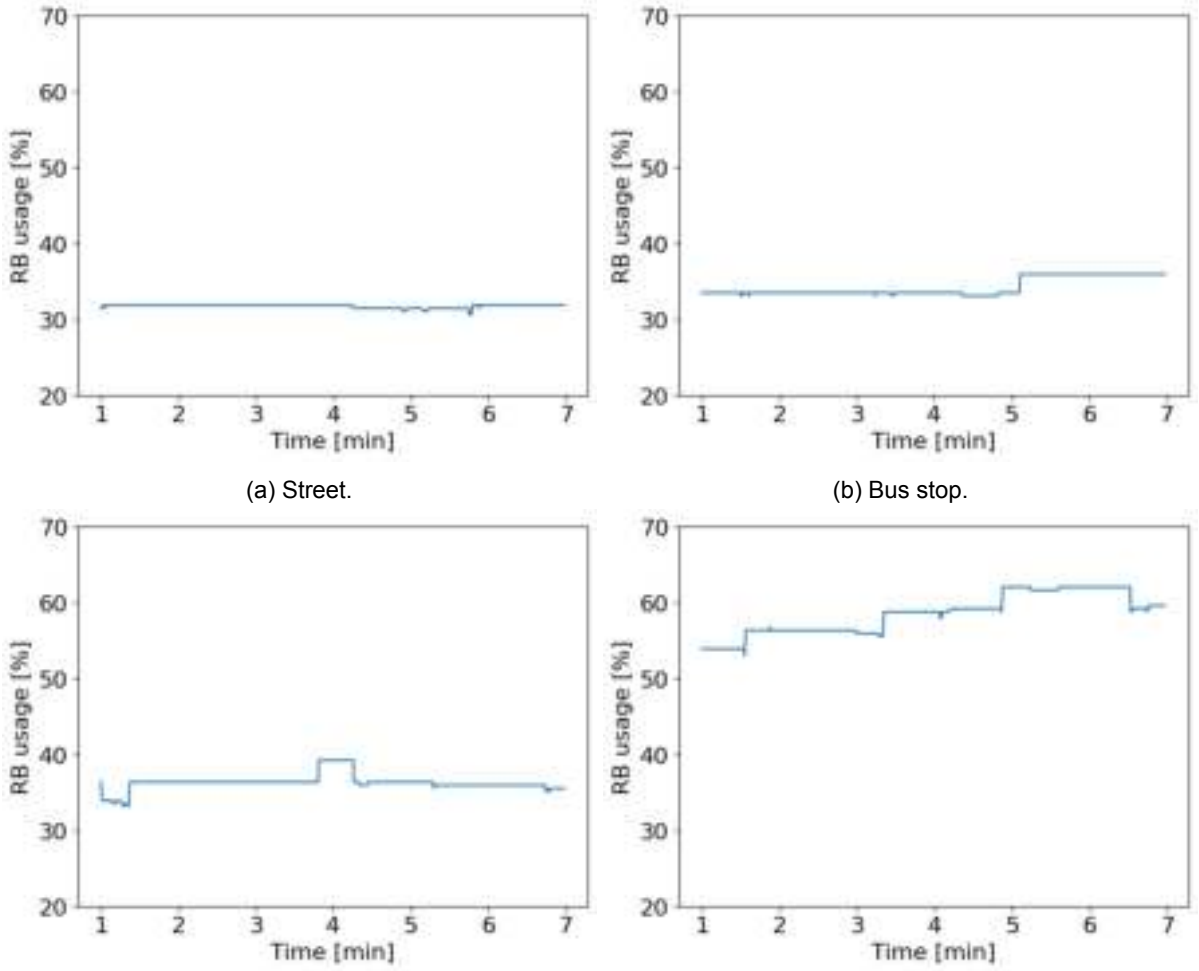

(a) Street.

(b) Bus stop.

(c) Residential building.

(d) Demonstration.

Figure 5.7: Used RB share over time in the different scenarios.

calculate a compliance distance (shown in (3.32) - this value is 5.15 W for the studied antenna), it is equal to the far-field radius of the beam (which is 3.6 m for the studied antenna, given by (2.6)). Through (3.31) it is possible to calculate that, for the studied antenna, the maximum broadside compliance distance is 8.69 m.

As expected, Figure 5.8 reveals that the demonstration scenario possesses beams whose broadside compliance distance is higher than the average found in other scenarios - this is again due to the increase in the number of users. It can also be stated that the beams in the residential scenario present a lower broadside compliance distance, compared with other scenarios. This is due to the proximity between users and the BS, as shown in Table 5.6, which implies a high SNR, and therefore less transmission power. As the beam transmission power fluctuates around a median value (Figure 5.1), so does the broadside compliance distance. Once again it can be seen that beams are independent of one another; they can have very different compliance distances.

To obtain the compliance distance for other directions other than broadside (sides, top, bottom and back of the antenna), the normalised antenna radiation patterns for these directions must be obtained. The gain for these directions can be extracted from the radiation patterns shown in Annex C, and it is possible

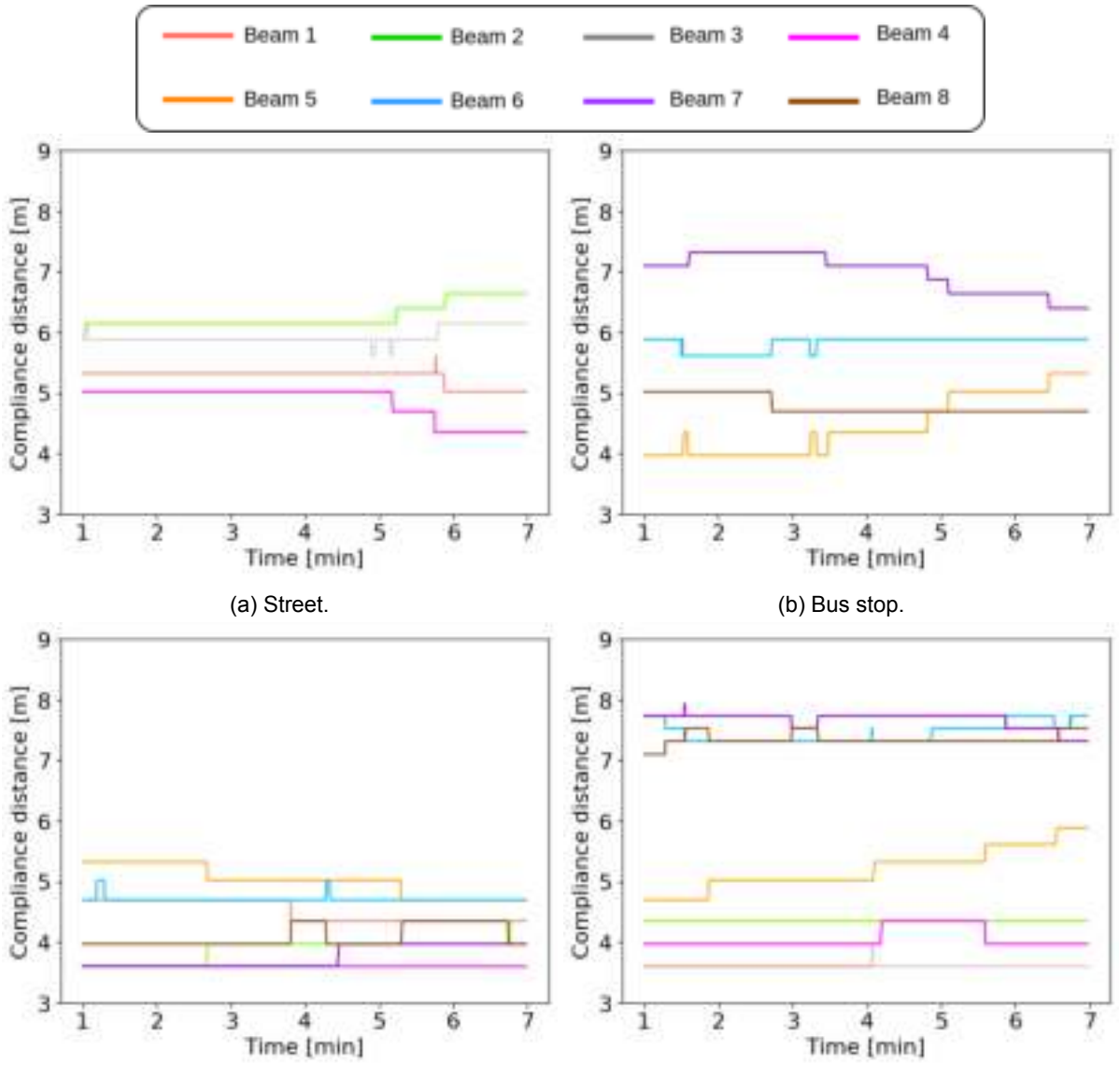

(a) Street.

(b) Bus stop.

(c) Residential building.

(d) Demonstration.

Figure 5.8: Broadside compliance distance over time in the different scenarios.

to calculate the normalised radiation pattern with the help of (3.15). However, the highest normalised antenna radiation pattern for these directions is just 1.4 % of the broadside compliance distance (in the case of the sides). As such, the analysis of these directions is not made in this thesis, on the grounds that their compliance distance is, at all times, much less than 1 m. Nonetheless, to observe the decline in the compliance distance as a user is gradually away from the broadside of a beam, the compliance distance over the entire scan range of a random beam at a random point in time is shown in Figure 5.9, making use of (3.20). As expected, the compliance distance rapidly drops to its minimum as the user is further away from the beam's broadside.

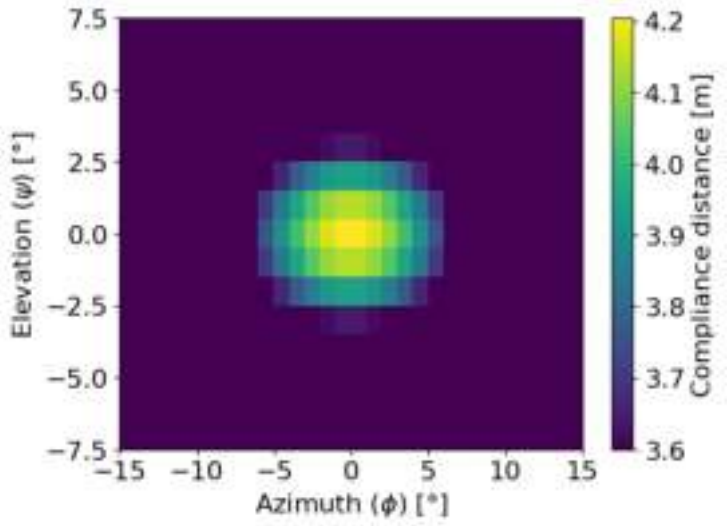

Figure 5.9: Compliance distance over an entire beam.

5.5 Exclusion zone distance

The results shown in Figure 5.8 assume that the BS has a continuous DL activity. Realistically, DL interchanges with UL to have two-way communication with the BS, although the DL time allocation is not standardised. In LTE, this can vary from 0.4 to 0.9. A reasonable value of DL time allocation is assumed to be 0.75 [39]. To simulate this, the results shown in Figure 5.8 are lowered by 25 %. The results in this subsection already take this into consideration.

Knowing the compliance distance of each beam over time (shown in Figure 5.8) allows one to define the value of the EZ around each scenario's BS, by proceding as explained in Section 3.5. At the end of each run of the model, it retrieves two parameters: the absolute maximum broadside compliance distance of any beam at any given time and, calculating the average broadside compliance distance over time for each beam, the maximum broadside compliance distance average. The average and standard deviation of the retrieved parameters are presented in Table 5.7, along with the relative difference between them. The PDF and CDF of these parameters for all runs in each scenario can be seen in Figure 5.10 and in Figure 5.11, respectively.

Table 5.7: Average and standard deviations of the absolute maximum and maximum average broadside compliance distance in the different scenarios, with their relative difference.

	Absolute maximum		**Maximum average**		
	Average [m]	**Standard deviation**	**Average [m]**	**Standard deviation**	**Relative difference [%]**
Street	5.01	0.28	4.83	0.28	3.59
Bus stop	4.98	0.27	4.80	0.27	3.61
Residential building	3.97	0.28	3.85	0.26	3.02
Demonstration	6.40	0.23	6.30	0.28	1.56

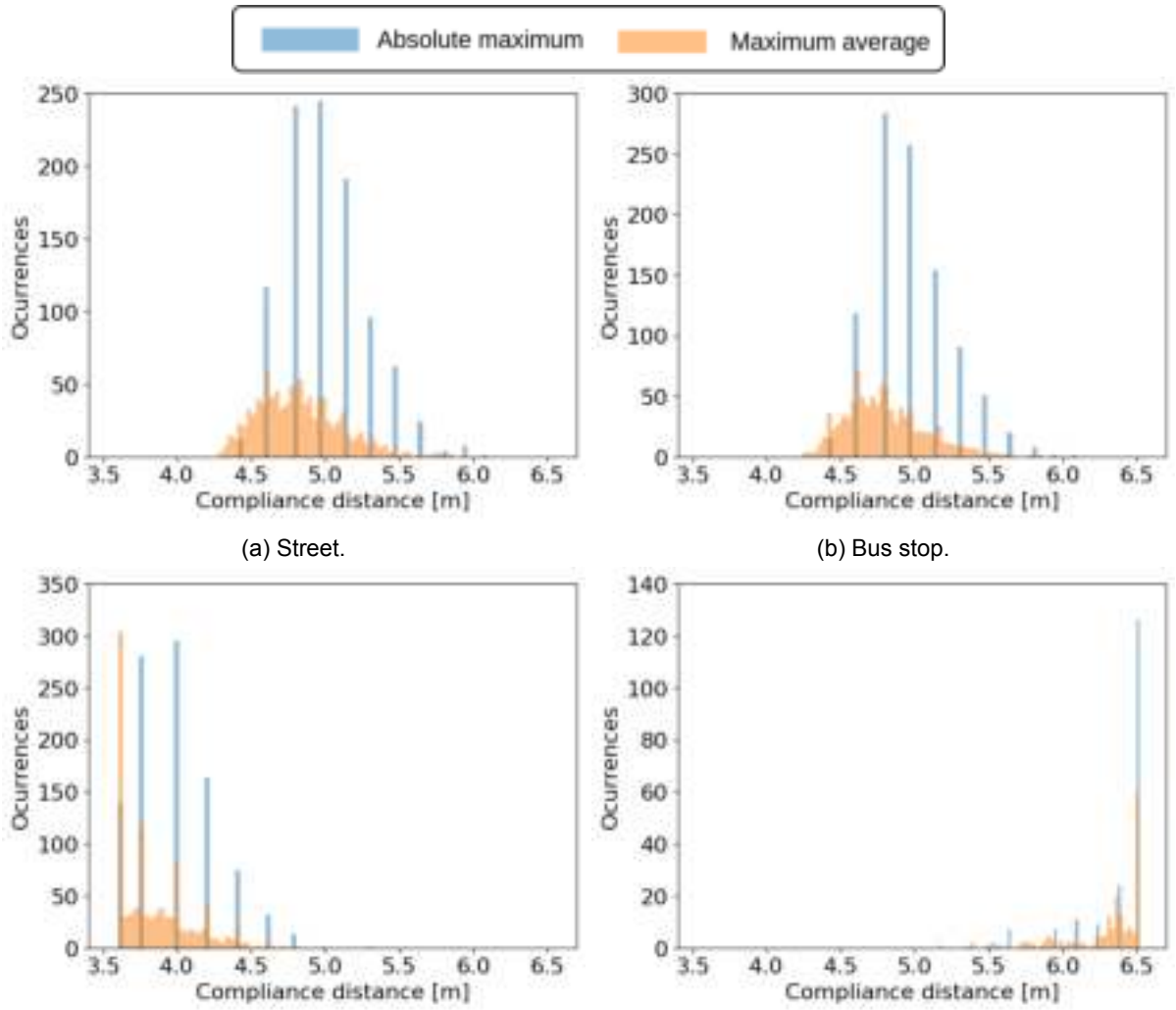

(a) Street.

(b) Bus stop.

(c) Residential building.

(d) Demonstration.

Figure 5.10: PDF of the absolute maximum and maximum average broadside compliance distance in the different scenarios.

The results from Table 5.7 suggest that the number of users and their spatial distribution are the defining factors in defining the EZ around the BS. In scenarios where users are more spread out (such as the residential building scenario), the EZ is shorter than scenarios where users are concentrated in fewer beams (street or bus stop scenarios) - this is because the user load is distributed across more beams; given the same number of users, spreading them throughout the antenna's range lowers the required power from each beam. Through (3.31), it is possible to calculate that the theoretical maximum broadside compliance distance for the studied antenna is 6.52 m (assuming a DL time allocation of 75 %). By observation of Table 5.7 one can conclude that the street and bus stop scenario present absolute maximum broadside compliance distances of around 77 % of the theoretical maximum; the residential building scenario presents values at around 61 % of it. In the demonstration scenario, which possesses a higher number of users, the absolute maximum broadside compliance distance is closer to the theoretical maximum, at around 98 % of it. All scenarios show a relative difference between the absolute maximum broadside compliance distance and the maximum average broadside compliance distance of around 3 %, except in the demonstration scenario, where this value is 1.4 % - this is due to beams often being at their maximum transmission power in this scenario, further evidencing that increasing the number of users is the defining factor in defining an EZ.

From Figure 5.10, one can deduce that the distribution of the maximum average broadside compliance distance approximates a Gaussian distribution (this is more noteceable in the street and bus stop scenarios). However, in the demonstration scenario, the maximum average compliance distance does not approximate a Gaussian distribution. This is because, in this scenario, the beam transmission power (and consequently the broadside compliance distance) is very close to its maximum in some beams, and often is at its maximum (Figure 5.1). The opposite happens in the residential building scenario, where the beam transmission power is sometimes lower than the limit to calculate an EZ, and as such its distribution is not similar to a Gaussian distribution as well. The absolute maximum broadside compliance distance is distributed in specific discrete values in all scenarios, although no reason to justify this can be stated with confidence.

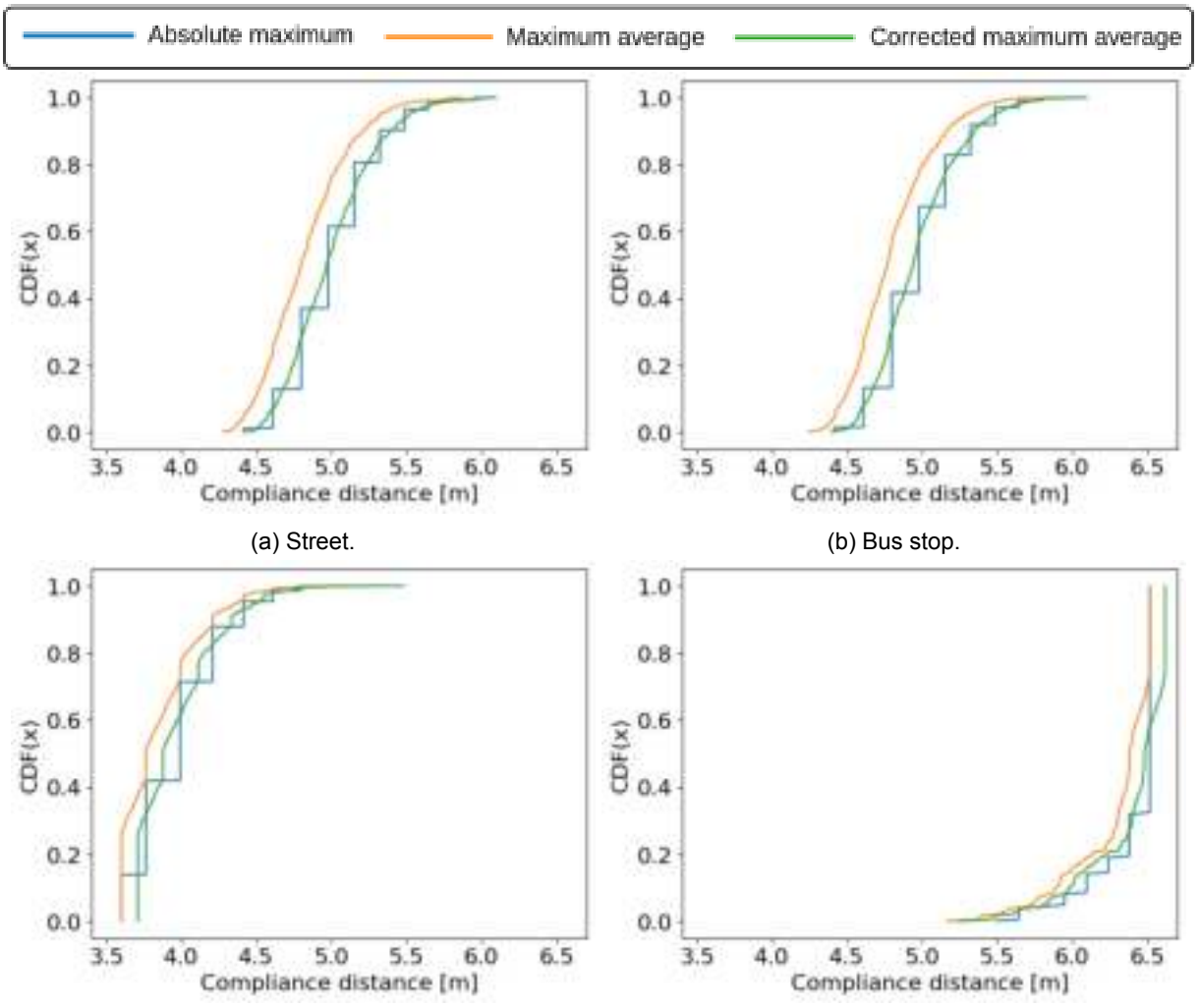

(a) Street.

(b) Bus stop.

(c) Residential building.

(d) Demonstration.

Figure 5.11: CDF of the absolute maximum and maximum average broadside compliance distance in the different scenarios.

The CDFs of both the residential building and the demonstration scenarios, shown in Figure 5.11, reveal once again that these often have broadside compliance distances equal to the minimum or maximum distance, respectively. This is due to the transmission power of the beams in these scenarios, as discussed previously. Through Figure 5.11 it is possible to retrieve several p-percentiles of the CDFs - these are

displayed in Table 5.8. As an additional security measure, a correction factor to the average broadside compliance distance can be applied; this is equal to the relative difference between the absolute maximum and the maximum average broadside compliance distances for each scenario, shown in Table 5.7.

Table 5.8: Various p-percentile of the obtained maximum average broadside compliance distance CDFs, in the different scenarios.

	Compliance distance [m]							
	Without correction				**With correction**			
	70 %	**80 %**	**90 %**	**95 %**	**70 %**	**80 %**	**90 %**	**95 %**
Street	4.96	5.05	5.21	5.33	5.14	5.23	5.39	5.52
Bus stop	4.91	5.01	5.16	5.29	5.09	5.20	5.35	5.48
Residential building	3.97	4.03	4.21	4.37	4.09	4.15	4.33	4.50
Demonstration	6.50	6.52	6.52	6.52	6.60	6.62	6.62	6.62

By observation of Table 5.8, one can see that from 70 % to 95 % of any CDF, the broadside compliance distance varies not more than 10 % in all scenarios, showing the system's stability. Furthermore, it is found that the demonstration scenario presents an 80-percentile equal to the theoretical maximum broadside compliance distance, which is as expected - beams are often at their maximum transmission power because of the increase in users. As further evidence, one can observe that other scenarios present 95-percentiles only 67 % to 82 % of this value. As in reality, one cannot predict the number and spatial distribution of users, the implemented EZ should be the maximum 95-percentile of the broadside compliance distance with the added correction present in Table 5.8, which in this case is the one found in the demonstration scenario - 6.62 m. Recalling the sketches of the created scenarios (Figures 3.4, 3.8 and 3.12), one can state that no user can be in the EZ of each respective BS, and thus this value is deemed safe in the created scenarios.

Chapter 6

Conclusions

This chapter summarises the information discussed in each chapter and presents their main conclusions. Key takeaways for future work are mentioned.

In this thesis, a statistical model capable of analysing the behaviour of the EMF around a 3.6 GHz band 5G active antenna and estimate its EZ is presented. As 5G must make use of active antennas in order to meet user throughput demands, the previously used methodology and procedures to monitor EMF in the vicinity of BSs and to estimate an EZ are no longer applicable.

This work is divided into 6 chapters, along with a set of annexes containing supplementary information and all the references used throughout it. In Chapter 1, a brief history of mobile communications, along with an overview of the work that is to be done on the thesis, is provided. The motivation for this work is laid out, stating its key differences with similar work done for the previous generations.

Chapter 2 presents the fundamental concepts related to the topic in study, namely the current radio interface in Portugal, new services and applications that use 5G, main concepts to be aware of when deciding on BS deployments and the use of active antennas in 5G, along with their comparison with passive antennas and their radiation behaviour. Furthermore, the EMF exposure restriction levels set by ICNIRP are provided, and a discussion on current models for determining an EZ is made. The state of the art, containing work done by other authors in this topic, is presented, along with their assumptions, results and conclusions. It can be said that the influence of the deployment of 5G in the EMF radiation is still unclear, as most of the literature is done on frequencies above 6 GHz and is focused on UE, not BSs. It can also be stated that the existing models for determining an EZ around a BS do not apply in this technology, and as such, suitable models for determining it are scarce.

In Chapter 3, the model created to determine the EZ of a 5G BS is presented, detailed and discussed. Its inputs and required outputs are indicated and described. The model is divided into further sub-models, which are throughouly explained. Four different UDSs are created - street, bus stop, residential building and demonstration - with the goal of simulating real locations with realistic usage. For this, realistic 5G telecommunications services are also created and described (in terms of download size, minimum recommended throughput and average access time). All the calculations the model does in order to determine the EZ, and how this relates to user behaviour and mobility, are presented. The model is put through some assessment tests to validate its results.

Chapter 4 showcases the performed on-site measurements together with their procedure and position around the BSs. Besides developing the previously mentioned model to estimate an EZ around an active antenna, this thesis also has as an objective the analysis of the behaviour of the EMF around the antenna. To do this, on-site measurements around BSs in Lisbon were performed, which are compared to the work made in [13] and to the model created in Chapter 3, reaching the conclusion that comparison is impossible in both cases, due to the fact that measuring as the simulations expect is very difficult to do on-site. Even so, the measurements results are presented and discussed. No correlation between electric field strength and distance from the antenna can be done - this is because the antenna spatially distributes the SSB. This leads to the conclusion that measuring active 5G BS is of no use to delimit an EZ, both because of the inability to make trustworthy electric field strength measurements and because it is impossible to measure along the direction of any beam's maximum gain. These measurements would need to be conducted in a controlled environment.

In Chapter 5, the created scenarios are described in terms of input parameters for the model. Each scenario is assigned a real location, the average number of users is taken from real BS data and the service share among users is set for every scenario. Several simulation parameters are shown, such as beam transmission power and broadside compliance distance over time. From these, it is possible

to estimate an EZ for each created scenario (assuming a DL time allocation of 75 %). It is found that the most meaningful variables in defining the EZ are the number of users and their spatial distribution. The demonstration scenario, which has more users that the other scenarios, possesses an 80-percentile equal to the theoretical compliance distance maximum. However, other scenarios present 95-percentiles only 67 % to 82 % of this value. It was also found that real-time services are the services that affect beam transmission power the most. As the adoption of these services, with high throughput requirements, is thought to increase over the coming years, special care will need to be administered.

There are some aspects of the model which could enhance the simulation's approximation to reality that are not addressed in this thesis, and they could reveal to be of some importance to the estimation of the EZ. As stated in Chapter 3, all users are in LOS to the antenna, which in reality does not always occur. Users in Non Line of Sight (NLOS) are serviced by an omnidirectional beam or by simultaneous transmission in multiple beams. Both of these beams present lower user exposure to the EMF, and it should lower the average transmission power of the BS - consequently, the EZ should lower as well. Although beamsteering is starting to be a feature in some active antennas [6], it is not explored in this thesis; this work only delves into beamforming. The performed on-site measurements show that it is very difficult to characterise the EMF behaviour around a working production BS, due to power limiters, SSB distribution and beam directivities. If these measurements were to be executed in a controlled environment - one where the SSB distribution is static or known, the beam directivities are known and there is no power limiter applied - some conclusion about the relation of distance and electric field strength might be drawn. Due to the BS building's height, and due to the fact that there is a minimum elevation to which the antenna can communicate, there is a portion of the ground in front of it that is not directly covered by the BS (this can be seen in Figure 3.4). This is true only if multipath propagation is ignored (and if the antenna is installed in the edge of the building). If multipath propagation were to be evaluated, users would be under the influence of a stronger power density level, but the EZ should not vary a lot from the one shown in this work.

This work reached the conclusion that BS deployments with active antennas in the created scenarios possess an adequate EZ, protecting the general public from harm. It was found that, for each individual beam, the EZ is never greater than 6.62 m (assuming a DL time allocation of 75 %). The results shown in this work corroborate previous work, such as [36, 37, 38], that state that traditional methods of estimating an EZ are not suitable for 5G, and they present over-conservative results. This work also indicates that, as beams are independent of one another, defining the EZ considering the entire array as a single beam is not realistic. It is of note to recall that this value considers NR as the sole active telecommunications technology, and that in NSA BSs (where NR will coexist with other telecommunications technologies), this value will be greater. This value is only deemed safe in the created scenarios; operators with 5G BSs should ensure that their EZs are greater than the value shown in this work.

Annex A

Supplementary equations

From [1], the maximum allowed path loss is given by

$$L_{max[\text{dB}]} = P_{EIRP[\text{dBm}]} + G_{RX[\text{dBi}]} - P_r^{min}{}_{[\text{dBm}]}, \tag{A.1}$$

where

- G_{RX} is the receiver antenna gain;
- P_r^{min} is the minimum accepted power level at the receiver antenna.

From [1], the average power decay with respect to distance is given by

$$L_{p[\text{dB}]} = L_{ref[\text{dB}]} + 10\alpha_{pd}\log_{10}(d_{[\text{km}]}), \tag{A.2}$$

where

- L_{ref} are the reference path losses (propagation model dependent);
- α_{pd} is the average power decay (propagation model dependent);
- d is the distance from the transmitter to the receiver.

From [1], the EIRP of an antenna is given by

$$P_{EIRP[\text{dBm}]} = P_{TX[\text{dBm}]} + G_{TX[\text{dBi}]} - L_{C[\text{dB}]}, \tag{A.3}$$

where

- P_{TX} is the transmitter output power;
- G_{TX} is the transmitter antenna gain;
- L_C are the cable losses between the transmitter and the antenna.

The number of available RBs per user is calculated with

$$N_{RB}^{user} = \left\lfloor \frac{N_{RB}}{N_{users}} \right\rfloor, \tag{A.4}$$

where

- N_{RB} is the number of available RBs;
- N_{users} is the number of users.

By [23], the number of symbols per OFDMA frame is given by

$$N_{symb}^{frame} = N_{symb}^{slot} N_{slot}^{SF} N_{SF}^{frame}, \tag{A.5}$$

where

- N_{symb}^{slot} is the number of symbols per slot (14 for normal CP or 12 for extended CP);
- N_{slot}^{SF} is the number of slots per subframe (2^{μ}, where μ is the numerology configuration integer);
- N_{SF}^{frame} is the number of subframes in an OFDMA frame (always 10).

Using [23], the theoretical throughput per user for a downlink OFDMA connection can be calculated:

$$R_{user[\text{bit}\cdot\text{s}^{-1}]} = \frac{N_{RB}^{user} N_{SC}^{RB} N_{symb}^{frame} N_{MIMO} \log_2 (M)_{[\text{bit}]}}{t_{frame[\text{s}]}}, \tag{A.6}$$

where

- N_{SC}^{RB} is the number of SCs per RB (always 12);
- M is the modulation order;
- N_{MIMO} is the MIMO order;
- t_{frame} is the OFDMA frame period (always 10 ms).

From [1], the path loss in free space propagation can be calculated with

$$L_{0[\text{dB}]} = 32.44 + 20 \log_{10}(d_{[\text{km}]}) + 20 \log_{10}(f_{[\text{MHz}]}), \tag{A.7}$$

where

- d is the distance to the BS;
- f is the frequency used for telecommunication with the BS.

Annex B

Download throughput and session duration for mobile streaming services

Table B.1: Required download throughput and average session duration for mobile streaming services.

Service	Specification	Average download size [MB]	Required download throughput [Mbit·s^{-1}]	References
Video download	480p	93.6	[0.584, 1.550]	[78, 79, 80, 50]
	720p	117.0	[0.667, 2.000]	[50, 81, 79, 52, 80]
	1080p	229.0	[1.55, 3.66]	[50, 81, 78, 52, 80]
	2K	390.0	[2.22, 6.67]	[50, 81, 79, 80]
	4K	995.0	[6.67, 16.00]	[50, 81, 79, 52, 80]
Video streaming	480p	–	[0.584, 1.550]	[78, 79, 80]
	720p	–	[0.667, 2.000]	[81, 79, 52, 80]
	1080p	–	[1.55, 3.66]	[81, 78, 52, 80]
	2K	–	[2.22, 6.67]	[81, 79, 80]
	4K	–	[6.67, 16.00]	[81, 79, 52, 80]
Audio streaming	Low	–	0.024	[82, 83, 50, 84]
	Normal	–	0.096	
	High	–	0.160	
	Very high	–	0.320	
Video conference	1:1	–	1.500	[50, 57, 56, 58]
	Group	–	6.000	[50, 56, 58]
Gaming	Local	–	3.000	[50, 59, 60]
	Cloud	–	10.000	

Annex C

Antennas description

C.1 Huawei AAUxxxx

The technical specifications of the Huawei AAUxxxx antenna [71], studied in the MEO BS, are shown in Table C.1. Its vertical and horizontal radiation patterns are displayed in Figure C.1.

Table C.1: Huawei AAUxxxx technical specifications [71, 64].

Parameter	Possible values
Frequency range [GHz]	[3.6, 3.8]
NR TDD gain [dBi]	25
TX/RX mode	64T64R
Supported bandwidth [MHz]	20, 30, 40, 50, 60, 70, 80, 90, 100
Maximum output power [W]	240
NR TDD horizontal beam sweeping range [°]	[-60, 60]
NR TDD vertical beam sweeping range [°]	[-15, 15]
Elevation tilt range [°]	[-13, 2]
Number of antenna elements	192 (96 dual-polarised elements)
Number of elements per TRX	3
Number of elements per beam	12
Array size	8 x 12
Antenna dimensions (h x W x D) [mm]	730 x 395 x 160
Beam dimensions (h x W x D) [mm]	182.500 x 49.375 x 160.000
Minimum power [W]	15

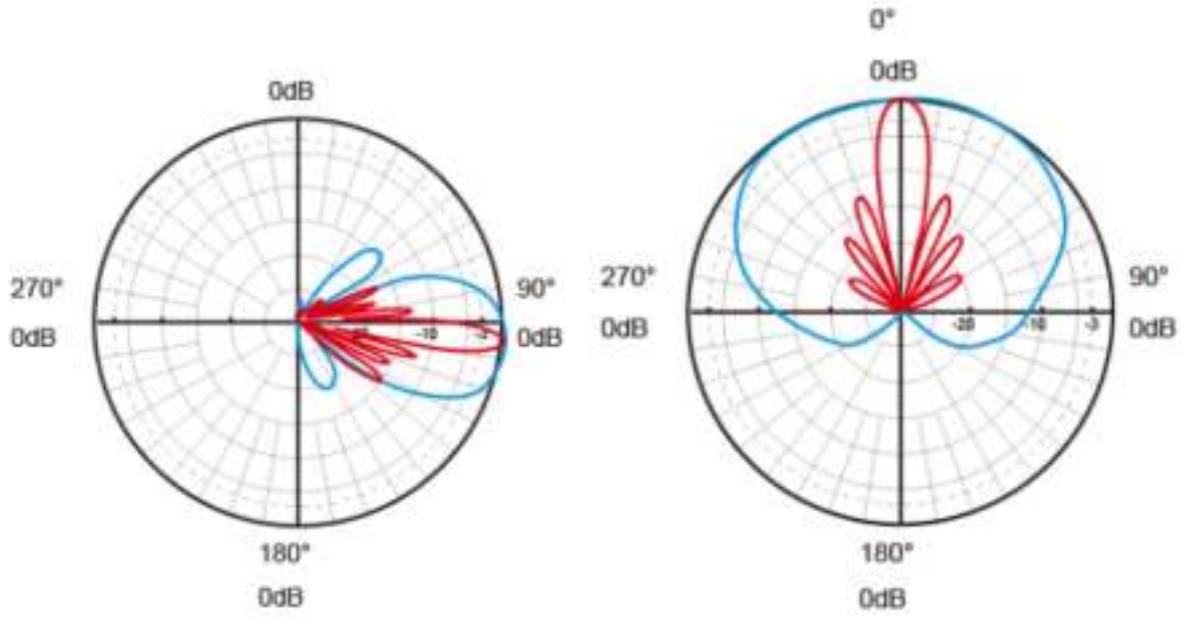

(a) Vertical radiation pattern.

(b) Horizontal radiation pattern.

Figure C.1: Huawei AAUxxxx radiation patterns (extracted from [71]).

C.2 NOKIA AirScalexxxx

The technical specifications of the NOKIA AirScalexxxx antenna [72], studied in the NOS BS, are shown in Table C.2.

Table C.2: NOKIA AirScalexxxx technical specifications [72].

Parameter	Possible values
Frequency range [GHz]	[3.42, 3.80]
NR TDD gain [dBi]	24 ±1
TX/RX mode	32T32R
Supported bandwidth [MHz]	20, 30, 40, 50, 60, 70, 80, 90, 100
Maximum output power [W]	200
NR TDD horizontal beam sweeping range [°]	[-60, 60]
NR TDD vertical beam sweeping range [°]	[-3, 15]
Number of antenna elements	192 (96 dual-polarised elements)
Array size	8 x 12
Dimensions (h x W x D) [mm]	730 x 403 x 185

Annex D

Description of base stations

D.1 NOS base station

This BS is located in a rooftop in Póvoa de Santo Adrião, Lisbon. In it, four active antennas are installed. However, only the rightmost in Figure D.1 was actively working (NOKIA AirScalexxxx [72] - Annex C), and so the measurements were made from it. Due to the spatial constraints of the rooftop, shown in Figure D.2, measurements were taken in two radial lines from the antenna, one at 0° and another at approximately 45°. Then, measurements parallel to the antenna were made, between these radial lines. A sketch of the BS and the measurement points can be seen in Figure 4.1. This antenna has a height of 4.4 m.

Figure D.1: NOS BS view of the measured sector (rightmost).

Figure D.2: NOS BS view of the rooftop in front of the measured sector.

D.2 MEO base station

This BS is located in a rooftop in Estrela, Lisbon. The measured sector, shown in Figure D.3, has the Huawei AAUxxxx antenna [71] (Annex C) installed, and has an unobstructed rooftop in front, shown in Figure D.4. As this rooftop did not present the same spatial constraints as the NOS BS, measurements were taken in three radial lines from the antenna, one at 0°, one at approximately 25° and another at approximately −23°. Then, measurements in straight lines from these radial lines were made, as can be seen in Figure 4.2. This antenna has a height of 5.5 m.

(a) Side view. (b) Frontal view.

Figure D.3: MEO BS views of the measured sector.

Figure D.4: MEO BS view of the rooftop in front of the measured sector.

References

[1] L. M. Correia, *Mobile Communications Systems Lecture Notes*, Instituto Superior Técnico, University of Lisbon, Lisbon, Portugal, 2020

[2] ETSI - 2nd Generation (GERAN), https://www.etsi.org/technologies/mobile/2g, Dec. 2022

[3] ETSI - 3rd Generation (UMTS), https://www.etsi.org/technologies/mobile/3g, Dec. 2022

[4] ETSI - 4th Generation (LTE), https://www.etsi.org/technologies/mobile/4G, Dec. 2022

[5] ETSI - 5G, https://www.etsi.org/technologies/mobile/5g, Dec. 2022

[6] Huawei, *New 5G, New Antenna*, Internal Report, Shenzhen, China, 2019 (https://carrier.huawei.com/~/media/CNBGV2/download/products/antenna/New-5G-New-Antenna-5G-Antenna-White-Paper-v2.pdf)

[7] ITU-R, *IMT Vision - Framework and overall objectives of the future development of IMT for 2020 and beyond*, Recommendation ITU-R M.2083-0, Geneva, Switzerland, Sep. 2015 (https://www.itu.int/dms_pubrec/itu-r/rec/m/R-REC-M.2083-0-201509-I!!PDF-E.pdf)

[8] European Parliamentary Research Service, *Health impact of 5G*, PE 690.012, Strasbourg, France, July 2021 (https://www.europarl.europa.eu/RegData/etudes/STUD/2021/690012/EPRS_STU(2021)690012_EN.pdf)

[9] I. Nasim, *Analysis of Human EMF Exposure in 5G Cellular Systems*, M.Sc. Thesis, Georgia Southern University, Statesboro, Georgia, United States of America, 2019 (https://digitalcommons.georgiasouthern.edu/cgi/viewcontent.cgi?article=3088&context=etd)

[10] ICNIRP, *ICNIRP Guidelines for Limiting Exposure to Electromagnetic Fields (100KHz to 300GHz)*, Internal Report, Berlin, Germany, 2020 (https://www.icnirp.org/cms/upload/publications/ICNIRPrfgdl2020.pdf)

[11] R. Pawlak, P. Krawiec and J. Żurek, "On Measuring Electromagnetic Fields in 5G Technology", *IEEE Access*, Vol. 7, Mar. 2019, pp. 29826-29835 (https://ieeexplore.ieee.org/stamp/stamp.jsp?arnumber=8660395)

[12] Huawei - Main page, https://www.huawei.com/en/, Jan. 2023

[13] S. Patrício, *Influence of Active Antennas on EMF Restrictions in 5G Base Stations Deployment*, M.Sc. Thesis, Instituto Superior Técnico, University of Lisbon, Lisbon, Portugal, 2021 (https://grow.tecnico.ulisboa.pt/wp-content/uploads/2022/03/Thesis_SofiaP_vfinal.pdf)

[14] ETSI, *Digital cellular telecommunications system (Phase 2+) (GSM); GSM/EDGE Modulation*, Technical Specification, TS 45.004, Ver. 17.0.0, Sophia Antipolis, France, May 2022 (https://www.etsi.org/deliver/etsi_ts/145000_145099/145004/17.00.00_60/ts_145004v170000p.pdf)

[15] ANACOM, *Frequency band distribution by Portuguese telecommunications operators* (in Portuguese), Internal Report, Lisbon, Portugal, Aug. 2015 (https://www.anacom.pt/render.jsp?categoryId=382989)

[16] ANACOM, *Spectrum Strategic Plan* (in Portuguese), Internal Report, Lisbon, Portugal, May 2016 (https://www.anacom.pt/streaming/PlanoEstrategicoEspectroMaio2016.pdf?contentId=1385398&field=ATTACHED_FILE)

[17] ETSI, *Digital cellular telecommunications system (Phase 2+) (GSM); GSM/EDGE Radio transmission and reception*, Technical Specification, TS 45.005, Ver. 17.0.0, Sophia Antipolis, France, May 2022 (https://www.etsi.org/deliver/etsi_ts/145000_145099/145005/17.00.00_60/ts_145005v170000p.pdf)

[18] ETSI, *Universal Mobile Telecommunications System (UMTS); Spreading and modulation (FDD)*, Technical Specification, TS 25.213, Ver. 17.0.0, Sophia Antipolis, France, May 2022 (https://www.etsi.org/deliver/etsi_ts/125200_125299/125213/17.00.00_60/ts_125213v170000p.pdf)

[19] ETSI, *Universal Mobile Telecommunications System (UMTS); Base Station (BS) radio transmission and reception (FDD)*, Technical Specification, TS 25.104, Ver. 17.0.0, Sophia Antipolis, France, Apr. 2022 (https://www.etsi.org/deliver/etsi_ts/125100_125199/125104/17.00.00_60/ts_125104v170000p.pdf)

[20] ETSI, *LTE; Evolved Universal Terrestrial Radio Access (E-UTRA); Physical channels and modulation*, Technical Specification, TS 36.211, Ver. 17.2.0, Sophia Antipolis, France, Aug. 2022 (https://www.etsi.org/deliver/etsi_ts/136200_136299/136211/17.02.00_60/ts_136211v170200p.pdf)

[21] ETSI, *LTE; Evolved Universal Terrestrial Radio Access (E-UTRA); Base Station (BS) radio transmission and reception*, Technical Specification, TS 36.104, Ver. 17.7.0, Sophia Antipolis, France, Oct. 2022 (https://www.etsi.org/deliver/etsi_ts/136100_136199/136104/17.07.00_60/ts_136104v170700p.pdf)

[22] M. Enescu, *5G New radio - A Beam-based Air Interface*, Wiley, West Sussex, United Kingdom, 2020

[23] ETSI, *5G; NR; Physical channels and modulation*, Technical Specification, TS 38.211, Ver. 17.3.0, Sophia Antipolis, France, Sep. 2022 (https://www.etsi.org/deliver/etsi_ts/138200_138299/138211/17.03.00_60/ts_138211v170300p.pdf)

[24] ETSI, *5G; NR; Base Station (BS) radio transmission and reception*, Technical Specification, TS 38.104, Ver. 17.7.0, Sophia Antipolis, France, Oct. 2022 (https://www.etsi.org/deliver/etsi_ts/138100_138199/138104/17.07.00_60/ts_138104v170700p.pdf)

[25] ANACOM, *Auction for the Attribution of Rights for the Usage of Frequencies in the 700MHz, 900MHz, 1800MHz, 2.1GHz, 2.6GHz and 3.6GHz bands - Final Auction Report* (in Portuguese), Internal Report, Lisbon, Portugal, Nov. 2021 (https://www.anacom.pt/streaming/Relatorio_Final_Leilao.pdf?contentId=1710784&field=ATTACHED_FILE)

[26] S. Sbit, M. B. Dadi and B. C. Rhaimi, ”Interference Analysis: from 2G to 4G”, in *Proc. of International Conference on Advanced Systems and Electric Technologies*, Hammamet, Tunisia, Jan. 2017 (https://ieeexplore.ieee.org/stamp/stamp.jsp?tp=&arnumber=7983681)

[27] J. A. Aldihaibani, A. Yahya, R. B. Ahmab, A. S. Md Zain, M. K. Salman and R. Edan, ”On Coverage Analysis for LTE-A Cellular Networks”, *International Journal of Engineering and Technology*, Vol. 5, Feb. 2013 (https://www.enggjournals.com/ijet/docs/IJET13-05-01-033.pdf)

[28] S. S. Phule and A. Y. Kazi, ”MIMO Antenna system for LTE (4G)”, in *Proc. of International Conference on Emerging Technology Trends in Electronics, Communication and Networking*, Surat, India, Dec. 2012 (https://ieeexplore.ieee.org/stamp/stamp.jsp?tp=&arnumber=6470110)

[29] A. Mandhyan, *4G and 5G Capacity solutions - comparative study*, Internal Report, Hickory, North Carolina, United States, July 2019 (https://www.commscope.com/globalassets/digizuite/2154-capacity-solutions-comparative-study-wp-113400-en.pdf?r=1)

[30] C. A. Balanis, *Antenna Theory: Analysis and Design*, Wiley, New Jersey, United Stated of America, 2016

[31] WHO - The International EMF Project, https://www.who.int/initiatives/the-international-emf-project, Dec. 2022

[32] IEEE, *IEEE Standard for Safety Levels with Respect to Human Exposure to Electric, Magnetic, and Electromagnetic Fields, 0 Hz to 300 GHz*, Internal Report, Piscataway, New Jersey, United States, Oct. 2019 (https://ieeexplore.ieee.org/document/8859679)

[33] D. Sebastião, D. Ladeira, M. Antunes, C. Oliveira and L. M. Correia, ”Estimation of Base Stations Exclusion Zones”, in *Proc. of 72nd IEEE Vehicular Technology Conference*, Ottawa, Canada, Sep. 2010 (https://www.researchgate.net/publication/221640285_Estimation_of_Base_Stations_Exclusion_Zones)

[34] ITU - *5G technology and human exposure to radiofrequency electromagnetic fields*, Internal Report, Geneva, Switzerland, May 2019 (https://www.itu.int/rec/T-REC-K.Sup9-201905-I/en)

[35] V. Jevremovic, *EMF Radiation in Mobile Networks: A Closer Look at Emission Limits & Safe Distances*, White Paper, iBwave, Montreal, Quebec, Canada, June 2020 (https://www.ibwave.com/storage/app/media/pdf/white-papers/EMF-radiation-in-mobile-wireless-networks-pt1.pdf)

[36] P. Baracca, A. Weber, T. Wild and C. Grangeat, ”A Statistical Approach for RF Exposure Compliance Boundary Assessment in Massive MIMO Systems”, in *Proc. of WSA 2018; 22nd International ITG Workshop on Smart Antennas*, Bochum, Germany, Mar. 2018 (https://ieeexplore.ieee.org/abstract/document/8385449)

[37] D. Colombi, P. Joshi, R. Pereira, D. Thomas, D. Shleifman, B. Tootoonchi, B. Xu and C. Törnevik, ”Assessment of Actual Maximum RF EMF Exposure from Radio Base Stations with Massive MIMO Antennas”, in *Proc. of 2019 Photonics & Electromagnetics Research Symposium - Spring (PIERS-*

Spring), Rome, Italy, June 2019 (https://ieeexplore.ieee.org/document/9017343)

[38] D. Colombi, P. Joshi, B. Xu, F. Ghasemifard, V. Narasaraju and C. Törnevik, "Analysis of the Actual Power and EMF Exposure from Base Stations in a Commercial 5G Network", *Applied Sciences*, Vol. 10, No. 15, July 2020, pp. 5280 (https://www.mdpi.com/2076-3417/10/15/5280)

[39] B. Thors, A. Furuskär, D. Colombi and C. Törnevik, "Time-Averaged Realistic Maximum Power Levels for the Assessment of Radio Frequency Exposure for 5G Radio Base Stations Using Massive MIMO", *IEEE Access*, Vol. 5, Sep. 2017, pp. 19711-19719 (https://ieeexplore.ieee.org/document/8039290)

[40] L. Chiaraviglio, A. S. Cacciapuoti, G. Di Martino, M. Fiore, M. Montesano, D. Trucchi and N. B. Melazzi, "Planning 5G Networks Under EMF Constraints: State of the Art and Vision", *IEEE Access*, Vol. 6, Oct. 2018, pp. 51021-51037 (https://ieeexplore.ieee.org/document/8453791)

[41] B. Thors, D. Colombi, Z. Ying, T. Bolin and C. Törnevik, "Exposure to RF EMF From Array Antennas in 5G Mobile Communication Equipment", *IEEE Access*, Vol. 4, Aug. 2016, pp. 7469-7478 (https://ieeexplore.ieee.org/document/7546896)

[42] B. Xu, M. Gustafsson, S. Shi, Z. Ying and S. He, "Upper Bound Study of 5G RF EMF Exposure", in *Proc. of 2018 IEEE International Symposium on Antennas and Propagation & USNC/URSI National Radio Science Meeting*, Boston, Massachusetts, United States of America, July 2018 (https://ieeexplore.ieee.org/document/8609310)

[43] B. Xu, K. Zhao, B. Thors, D. Colombi, O. Lundberg, Z. Ying and S. He, "Power Density Measurements at 15 GHz for RF EMF Compliance Assessments of 5G User Equipment", *IEEE Transactions on Antennas and Propagation*, Vol. 65, No. 12, Dec. 2017, pp. 6584-6595 (https://ieeexplore.ieee.org/abstract/document/7942093)

[44] M. Nesterova, S. Nicol and Y. Nesterova, "Evaluating Power Density for 5G Applications", in *Proc. of 2018 IEEE 5G World Forum (5GWF)*, Santa Clara, California, United States of America, July 2018 (https://ieeexplore.ieee.org/document/8517003)

[45] P. Noren, L. J. Foged, L. Scialacqua and A. Scannavini, "Measurement and Diagnostics of Millimeter Waves 5G Enabled Devices", in *Proc. of 2018 IEEE Conference on Antenna Measurements & Applications (CAMA)*, Västerås, Sweden, Sep. 2018 (https://ieeexplore.ieee.org/document/8530472)

[46] F. Moura, *Analysis of the Impact of EMF Restrictions on 5G Base Stations Deployment in Existing Networks*, M.Sc. Thesis, Instituto Superior Técnico, University of Lisbon, Lisbon, Portugal, 2020 (https://grow.tecnico.ulisboa.pt/wp-content/uploads/2021/02/Thesis_FredericoMoura.pdf)

[47] Wikipedia, *Normal distribution*, https://en.wikipedia.org/wiki/Normal_distribution, Apr. 2024

[48] Wikipedia, *Exponential distribution*, https://en.wikipedia.org/wiki/Exponential_

distribution, Apr. 2024

[49] HTTP Archive, *Page Weight*, https://httparchive.org/reports/page-weight#bytesTotal, Mar. 2023

[50] FCC, *Broadband Speed Guide*, Public Report, Washington DC, United States of America, July 2022 (https://www.fcc.gov/consumers/guides/broadband-speed-guide)

[51] FCC, *Household Broadband Guide*, Public Report, Washington DC, United States of America, July 2022 (https://www.fcc.gov/consumers/guides/household-broadband-guide)

[52] Netflix, *Internet connection speed recommendations*, https://help.netflix.com/en/node/306, Mar. 2023

[53] Lifewire, *Why Are Email Files so Large?*, https://www.lifewire.com/what-is-the-average-size-of-an-email-message-1171208, May 2024

[54] ITGeared, *How Much Data Does WhatsApp Use?*, https://www.itgeared.com/how-much-data-does-whatsapp-use/, May 2024

[55] ITGeared, *How Much Data Does Facebook Messenger Use?*, https://www.itgeared.com/how-much-data-does-facebook-messenger-use/, May 2024

[56] Skype, *How much bandwidth does Skype need?*, https://support.skype.com/en/faq/FA1417/how-much-bandwidth-does-skype-need, May 2024

[57] Zoom, *Zoom system requirements: Windows, macOS, Linux*, https://support.zoom.com/hc/en/article?id=zm_kb&sysparm_article=KB0060748, May 2024

[58] Zoom, *Here's How You Zoomed Over the Past Year*, Public Report, San Jose, California, United States of America, Apr. 2022 (https://blog.zoom.us/how-you-zoomed-over-the-past-year-2021/)

[59] High Speed Internet, *What Is a Good Internet Speed for Gaming?*, https://www.highspeedinternet.com/resources/how-much-speed-do-i-need-for-online-gaming. May 2024

[60] Statista, *Average gaming session length among desktop PC gamers in the United States as of August 2022*, https://www.statista.com/statistics/1339296/us-pc-gaming-session-length/, May 2024

[61] Twitch, *Broadcasting Guidelines*, https://stream.twitch.tv/encoding, Mar. 2023

[62] M. Mahbub and B. Barua, "Optimal Coverage and Bandwidth-Aware Transmission Planning for Augmented Reality/Virtual Reality", in *Proc. of 2021 International Conference on Information Technology*, Amman, Jordan, July 2021 (https://ieeexplore.ieee.org/document/9491124)

[63] Statista, *Virtual reality and augmented reality (VR and AR) devices average session time in the United States as of 2018*, https://www.statista.com/statistics/831819/us-virtual-augmented-reality-device-average-session-time/, May 2024

[64] Huawei, *Beam Management Feature Parameter Description*, Internal Report, Shenzhen, China, 2023

[65] Huawei, *Output Power per NR TDD Carrier*, Internal Report, Shenzhen, China, 2023

[66] A. Alcobia, *LTE radio network deployment design in urban environments under different traffic scenarios*, M.Sc. Thesis, Instituto Superior Técnico, University of Lisbon, Lisbon, Portugal, 2017 (https://grow.tecnico.ulisboa.pt/wp-content/uploads/2017/07/Thesis_AntonioA_70070_vFinal.pdf)

[67] 3GPP, *R4-112308: Summary of the simulation results of PDSCH demodulation performance requirements on eDL-MIMO*, Internal Report, Apr. 2011 (https://www.3gpp.org/ftp/tsg_ran/WG4_Radio/TSGR4_58AH/Docs/R4-112308.zip)

[68] ETSI, *5G; NR; Physical layer procedures for data*, Technical Specification, TS 38.214, Ver. 17.6.0, Sophia Antipolis, France, July 2023 (https://www.etsi.org/deliver/etsi_ts/138200_138299/138214/17.06.00_60/ts_138214v170600p.pdf)

[69] Apple, *iPhone 14*, https://www.apple.com/iphone-14/specs/, Sep. 2023

[70] Huawei, *Huawei P60 Pro*, https://consumer.huawei.com/en/phones/p60-pro/specs/, Sep. 2023

[71] Huawei, *AAUxxxx Technical Specifications*, Internal Report, Shenzhen, China, 2022

[72] NOKIA, *AirScalexxxx Technical Specifications*, Internal Report, Espoo, Finland, 2023

[73] NARDA - SRM-3006 field strength analyzer, https://www.narda-sts.com/en/selective-emf/srm-3006-field-strength-analyzer/, Sep. 2023

[74] NARDA - SRM-3006 probe, https://www.narda-sts.com/en/selective-emf/srm-3006-field-strength-analyzer/antenna-e-field-up-to-6-ghz-three-axis-srm/, Sep. 2023

[75] NARDA, *SRM-3006 5G NR Code Selective Measurement*, Internal Report, Pfullingen, Germany, 2023 (https://www.narda-sts.com/fileadmin/Produktliteratur_BAs_Software/5G/5G_code_selective_measurement_with_SRM.pdf)

[76] ANACOM, *Monitoring and measurement of the EMF intensity levels originating in telecommunications base stations* (in Portuguese), Internal Report, Lisbon, Portugal, May 2007

[77] Huawei, *PRB Usage*, Internal Report, Shenzhen, China, 2023

[78] NBN, *How much data does streaming video, movies and TV use? (2018 edition)*, https://www.nbnco.com.au/blog/entertainment/how-much-data-does-streaming-video-movies-and-tv-use, May 2024

[79] Android Central, *How much mobile data does streaming media use?*, https://www.androidcentral.com/how-much-data-does-streaming-media-use, May 2024

[80] Statista, *Average YouTube video length as of December 2018, by category*, https://www.statista.com/statistics/1026923/youtube-video-category-average-length/, May 2024

[81] Netflix, *How to control how much data Netflix uses*, https://help.netflix.com/en/node/87, Mar. 2023

[82] WhistleOut, *How Much Data Does Spotify Use?*, https://www.whistleout.ca/CellPhones/Guides/How-Much-Data-Does-Spotify-Use-Canada, May 2024

[83] Android Authority, *How much data does Spotify use? Probably less than you think*, https://www.androidauthority.com/spotify-data-usage-918265/, May 2024

[84] UCLA DataRes, *Spotify Trends Analysis*, https://ucladatares.medium.com/spotify-trends-analysis-129c8a31cf04, May 2024